UNIVERSITY OF OKLAHOMA

GRADUATE COLLEGE

ADAPTIVE GRID BASED FINITE DIFFERENCE METHODS FOR SOLUTION OF HYPERBOLIC PDES: APPLICATION TO COMPUTATIONAL MECHANICS AND UNCERTAINTY QUANTIFICATION

A DISSERTATION

SUBMITTED TO THE GRADUATE FACULTY

in partial fulfilment of the requirement for the

Degree of

DOCTOR OF PHILOSOPHY

By

MANI RAZI

Norman, Oklahoma

2015

ADAPTIVE GRID BASED FINITE DIFFERENCE METHODS FOR SOLUTION OF HYPERBOLIC PDES: APPLICATION TO COMPUTATIONAL MECHANICS AND UNCERTAINTY QUANTIFICATION

A DISSERTATION APPROVED FOR THE
SCHOOL OF AEROSPACE AND MECHANICAL ENGINEERING

BY

Dr. Peter Attar, Chair

Dr. Prakash Vedula, Co-Chair

Dr. Cengiz Altan

Dr. Ramkumar Parthasarathy

Dr. Dimitrios Papavassiliou

To my parents for their unconditional love and support:

Mohammad (father)

Nasrin (Mother)

Acknowledgements

This work was supported partly by subcontracts with Advanced Dynamics Inc. and Ohio Aerospace Institute and also by the National Science Foundation. I wish to express my sincere gratitude to Dr. Attar and Dr. Vedula for providing me with an excellent academic support during these past 6 years and helping me to obtain better understanding of research especially in the broad area of computational mechanics and uncertainty quantification. Moreover, I would like to thank Dr. Altan and Dr. Parthasarathy as my teachers and committee members in this period and Dr. Papavassiliou as the outside committee member for their valuable comments and feedback. Also, particularly, I would like to thank my parents and all my family for their unconditional love and support throughout my life. Finally, I would like to acknowledge the University of Oklahoma Supercomputing Center (OSCER) which provided supercomputing time to me enabling me in the completion of this work.

Table of Contents

List of Figures

Abstract

Novel finite-difference based numerical methods for solution of linear and nonlinear hyperbolic partial differential equations (PDEs) using adaptive grids are proposed in this dissertation. The overall goal of this research is to improve the accuracy and/or computational efficiency of numerical solutions via the use of adaptive grids and suitable modifications of a given low-order order finite-difference scheme. These methods can be grouped in two broad categories. The first category of adaptive FD methods proposed in the dissertation attempt to reduce the truncation error and/or enhance the accuracy of the underlying numerical schemes via grid distribution alone. Some approaches for grid distribution considered include those based on (i) a moving uniform mesh/domain, (ii) adaptive gradient based refinement (AGBR) and (iii) unit local Courant-Freidrich-Lewy (CFL) number. The improvement in the accuracy which is obtained using these adaptive methods is limited by the underlying scheme formal order of accuracy. In the second category, the CFL based approach proposed in the first category was extended further using defect correction in order to improve the formal order of accuracy and computational efficiency significantly (i.e. by at least one order or higher). The proposed methods in this category are constructed based upon the analysis of the leading order error terms in the modified differential equation associated with the underlying partial differential equation and finite difference scheme. The error terms corresponding to regular and irregular perturbations are identified and the leading order error terms associated with regular perturbations are eliminated using a non-iterative defect correction approach while the error terms associated with irregular perturbations are eliminated using grid adaptation. In the second category of methods involving defect correction (or reduction of leading order terms of truncation error), we explored two different

approaches for selection of adaptive grids. These are based on (i) optimal grid distribution and (ii) remapping with monotonicity preserving interpolation. While the first category of methods may be preferred in view of ease of implementation and lower computational complexity, the second category of methods may be preferred in view of greater accuracy and computational efficiency. The two broad categories of methods, which have been applied to problems involving both bounded and unbounded domains, were also extended to multidimensional cases using a dimensional splitting approaches.

The performance of these methods was demonstrated using several example problems in computational uncertainty quantification (CUQ) and computational mechanics. The results of the application of the proposed approaches all indicate improvement in both the accuracy and computational efficiency (by about three orders of magnitude in some selected cases) of underlying schemes. In the context of CUQ, all three proposed adaptive finite different solvers are combined with the Gauss-quadrature sampling technique in excitation space to obtain statistical quantities of interest for dynamical systems with parametric uncertainties from the solution of Liouville equation, which is a linear hyperbolic PDE. The numerical results for four canonical UQ problems show both enhanced computational efficiency and improved accuracy of the proposed adaptive FD solution of the Liouville equation compared to its standard/fixed domain FD solutions. Moreover, the results for canonical test problems in computational mechanics indicate that the proposed approach for increasing the formal order of the underlying FD scheme can be easily implemented in multidimensional spaces and gives an oscillation-free numerical solution with a desired order of accuracy in a reasonable computational time. This approach is shown to provide a better computational time compared to both the underlying scheme (by about three orders of magnitude) and standard FD methods of the same order of accuracy.

CHAPTER 1

Introduction

1.1 Motivation

The numerical solution of multidimensional hyperbolic partial differential equations (PDE) is one of the most challenging and interesting subjects of research in the area of numerical methods/analyses. Hyperbolic PDEs are relevant to many problems in the engineering and science, including computational uncertainty quantification [1, 2], fluid dynamics [3, 4, 5, 6], acoustics [7, 8], electromagnetics [9], heat transfer [10]. Hence, there is a need for efficient methods for improvement of the accuracy of numerical solutions. As analytical solutions exist only for rare cases, available numerical methods have become a valuable asset toward the goal of better understanding the solution of these PDEs. While much research has been conducted in this area, achieving a numerical method for multidimensional problems which is accurate, easily implemented and computationally efficient (low computational time for a given accuracy) is still a major challenge, which serves as the major motivation for the research conducted in this dissertation.

1.2 Finite Difference Solutions of Partial Differential Equations

Amongst the many methods which exist for the numerical solution of partial differential equations, including the popular finite element [11] and finite volume methods [12, 13], due to their conceptual simplicity, and ease of implementation, finite

difference (FD) schemes [14, 15, 16, 17, 18, 19] are commonly used to obtain numerical solutions of linear and nonlinear partial differential equations. The process of constructing a numerical solution through a finite difference method is conceptually very simple and involves choosing i) a discrete representation of the continuous solution domain (grid) and ii) finite difference approximations for the partial derivatives contained in the partial differential equation. The finite difference approximations can be developed in a number of ways including the use of Taylor series expansions, Padé approximation and polynomial interpolation. The construction of a quality grid is in itself a complex subject [20], in particular when the solution domain can be considered complex. As the problem domains considered in this work are simple, this general subject will not be discussed outside of any grid modifications which are used to enhance solution accuracy.

As discussed in Section 1.1, in this dissertation we are interested in the development of finite difference solutions for hyperbolic equations, which can be considered a type of propagation problem. There are four properties of finite difference schemes which are typically considered when analyzing a particular finite difference method for propagation problems: consistency, order, stability and convergence [17]. While convergence is in general difficult to prove, the analysis of consistency, order and (to a lesser extent) stability is typically possible for any newly developed finite difference scheme. Consistency of a scheme implies that as grid sizes (in space and time) approach zero, the difference between the finite difference equation and the partial differential equation which it is approximating, goes to zero. Consistency of a scheme can be shown using the modified equation approach, which will be discussed later in this dissertation. Stability of a scheme implies that the numerical solution will remain bounded if the exact solution remains bounded. Stability comes in two flavors, conditional stability, whereby stability depends upon the grid (space and time) spacing, and unconditional stability. While not necessary, all of the methods

developed in this work will be conditionally stable. Finally the order of a given finite difference scheme relates to the rate at which the global error approaches zero as the grid spacing approach zero. The higher the order the scheme, the faster the rate of decrease in error for a given grid refinement. In this dissertation, in the second class of methods which we will present (Chapters 3 and 5), our goal is to formally improve the order of an underlying low(er)-order scheme.

To simplify things, the research paths regarding the development of finite difference methods for improving the accuracy of numerical solutions of hyperbolic equations can generally be broken down into two classes. First there are efforts which attempt to develop computationally efficient schemes which are (provably) high order, stable and free of non-physical oscillations [21, 22, 23, 24, 25]. These methods typically rely on high order finite difference approximations for the partial derivatives on either standard or compact [26] stencils. As high-order finite difference schemes are often more complicated to develop and implement, when compared to lower-order schemes, the second class of methodologies involves enhancing the accuracy of an underlying low-order scheme. Such methods may also be thought to be advantageous from the standpoint of modification of existing (widely used) low order codes to obtain higher order of accuracy. Modifying low order codes to use traditional high order finite difference approximations typically requires extensive modification of data structures and the writing of new code modules. Methods in this class include those based upon adaptive grid refinement [27, 28], Richardson extrapolation [29], defect correction [30, 31, 32] and optimal time-step selection combined with non-iterative defect correction (OTS-NIDC) [33].

Of course the above discussion on finite difference solutions of partial differential equations is just a basic overview and much more detail can be found in almost all textbooks on numerical methods [17, 34] and in particular numerical methods for fluid dynamics [35, 13, 16]. The remainder of this chapter is organized as follows.

In Section 1.3, literature review will be given for some commonly used high-order schemes for numerical solution of hyperbolic equations. In general these methods are required to be nonlinear schemes due to limitations implied by the Godunov order barrier theorem. In Sections 1.4- 1.6, discussion and literature review of the abovementioned approaches for enhancing the error of an underlying low-order scheme will be presented. In section 1.7, one particular application of the numerical solution of hyperbolic equations, namely computational uncertainty quantification, will be discussed. Finally, in Section 1.8, the dissertation objectives are given along with the scope of the work which is used to achieve these objectives.

1.3 High Order Finite Difference Schemes

As mentioned above, using a high (formal) order of accuracy finite difference scheme is one way of achieving high fidelity numerical solutions of PDEs. Unfortunately, for linear finite difference schemes Godunov's order barrier theorem [36] limits monotonicity preservation [35] to first order schemes and therefore high order linear schemes typically produce results which contain non-physical (spatial) oscillations. On the other hand high order nonlinear schemes, many of which have been designed to be monotonicity preserving/total variation diminishing [35], have been shown to be very effective in producing highly accurate solutions free from non-physical oscillation [37]. Some of these high order nonlinear schemes include Total Variation Diminishing (TVD), Piecewise Hyperbolic method (PHM), Piecewise Parabolic Method (PPM), Essentially Non-Oscillatory (ENO) and Weighted Essentially Non-Oscillatory (WENO).

TVD schemes as developed by Harten [38] are designed to obtain high order of accuracy while avoiding the spurious oscillations. However, as a direct consequence of application of flux/slope limiters in this type of approach, the accuracy essentially degenerates to first order near local extrema. Moreover, linear interpolation

is often used near discontinuities to avoid Gibbs phenomena. To address this latter limitation regarding interpolation order, PHM [39] and PPM [40] were developed to use higher order of interpolation for better representation of discontinuities, as well as to increase the accuracy of the numerical solution to third order. These methods use fixed stencils for piecewise hyperbolic or parabolic interpolation to approximate the numerically averaged flux and, as a result, the extension of these methods to higher dimensions is very complicated. Moreover, numerical results still indicate accuracy degeneration near local extrema [39, 40].

In order to obtain better accuracy even near local extrema, ENO (essentially non-oscillatory) schemes were developed [5, 41, 42]. In contrast with other approaches, ENO schemes are designed such that the smoothest grid-point stencil for interpolation is chosen among other possible choices based on the values of divided differences. The approximation of the flux in this approach is through construction of a polynomial interpolant from a local adaptive stencil. However, using this free adaptation of the stencil is not necessarily required throughout the whole domain of computation and hence can result in reduced computationally efficiency of the numerical simulation. WENO (weighted essentially non-oscillatory) schemes [43, 37, 44] resolve the issue by applying a weighted combination of candidate stencils to construct the numerical flux interpolant. These schemes have been shown to be at least twice as fast as ENO methods and perform better in a high performance computing environment [37].

1.4 Adaptive Grid Refinement/redistribution (AGR) Methods

As the truncation error of a finite difference scheme is a function of spatial and temporal increments [17], refining the spatial grid (e.g. making the spatial grid spacing

smaller) can directly enhance the accuracy of the numerical solution. Adaptive grid refinement/redistribution (AGR) methods effectively modify a computational grid in order to maximize the effect on solution accuracy. Using this technique, a mesh is refined only in those regions of the computational domain where high resolution is most needed in terms of solution accuracy. This technique can be tailored based upon the type of partial differential equation to be solved. For numerical solution of PDEs with large variability in spatial gradients, it would appear desirable to employ a non-uniform mesh which adapts in time such that fine grid resolution is used in regions with large gradients and a more coarse resolution is used in smooth regions. The problem of mesh redistribution for hyperbolic partial differential equations has been addressed extensively in the literature starting with the work of Harten and Hyman[45] who employed a static regridding procedure, and more recently in the work of Stockie et al.[46], who used a semi-implicit approach which coupled moving mesh equations based upon the equidistribution principle to a high-resolution Godunov-type scheme for the physical PDE. As shown in [47], a grid point distribution is asymptotically optimal if some error measure is equally distributed over the field. This concept is the motivation for the use of the equidistribution, over the solution domain, of some monitor function (or its integral) to determine a mesh. In the moving mesh literature this is known as the equidistribution principle. Typical monitor functions which are used are the arclength and local curvature of the solution [48, 49].

While the adaptive mesh approach based upon equidistribution attempts to minimize the error in regions of strong gradients and local extrema, another possibility in reducing numerical error is to attempt to find a mesh distribution which equidistributes or minimizes the local truncation error or its estimate [50, 51, 52, 53, 54]. Using this principle Carey and Dinh [55] introduced an optimal grading function in various norms and semi-norms for two-point boundary-value problems. This ap-

proach improves the accuracy of a numerical solution for a given number of grid points through adaptive mesh redistribution in high gradient regions. While in order to apply equidistribution based methods, no prior knowledge is needed about the truncation error expression of the underlying numerical scheme, such information is necessary for approaches which are developed based upon the minimization of the local truncation error [51]. The application of these truncation error AGR techniques can result in an increase in the global (formal) order of accuracy of finite difference computations. However, non-uniformity of grids may introduce an additional source of error (due to the use of approximate grid metrics). Moreover, as shown by Yamaleev [54], it is impossible to increase the global (formal) order of accuracy for first order finite difference schemes using only a spatial grid distribution. Thus, these techniques can not benefit from the computational simplicity of first order schemes to develop a higher order method. Moreover the algorithms are often not easily extendable to multiple dimensions. In addition, the resultant enhancement does not have any impact on the temporal order of accuracy and the numerical stability of the computations is often affected by the refinement of the grid in critical regions of the domain leading to a smaller time-step selection requirement and subsequent longer computational time.

1.5 Richardson Extrapolation

Another popular approach for increasing the accuracy of lower order schemes is through the use of Richardson extrapolation [56, 57, 58]. This method improves the spatial order of accuracy by considering successive finite difference computations on increasingly refined, equally spaced, meshes, followed by linear extrapolation on the computed results. However, this approach requires function evaluations at refined locations and prior truncation error analysis to obtain the linear extrapolation. Although this method can be applied to enhance both temporal and spatial orders

of accuracy [29], the numerical stability on the finer grid is not guaranteed and due to its significant computer memory usage and high volume of computations, the cost of additional finite difference computations on several meshes is high and therefore this approach has rarely been applied to multidimensional problems.

1.6 Defect/Deferred Correction Methods

Defect correction is another commonly used approach for improving the order of accuracy of difference schemes [59]. These methods are developed based upon either truncation error analysis or through the use of a higher order finite difference scheme in addition to the lower order base scheme. The former type of defect correction approaches can be classified into two major groups including high-order compact and iterative defect correction methods.

The derivation of the modified differential equation for a given finite difference scheme gives the expression for the truncation error of the difference scheme [60, 61, 62]. Using this expression, one can either develop high-order compact schemes or gradually in an iterative process increase the order of accuracy of a finite difference scheme to the desired level. In high-order compact approaches [63, 64], first the stationary part of the differential equation is considered and a compact high-order scheme is derived using the truncation error analysis based upon the modified differential equation approach. Next, the temporal derivative is added to the compact discretized equation as a source term. As such, this approach is implicit. Moreover, it only reduces the spatial discretization error and the temporal accuracy is unaffected and given by the order of temporal discretization of the underlying low-order scheme [33].

Numerical methods based upon the concept of deferred correction are defect correction methods which use an iterative subtraction of local truncation error from the original low-order accurate discretized equation [59]. In this regard, Jones [65]

evaluated these terms in the stationary condition and enhanced the numerical stability and accuracy of difference schemes by applying them in the original low-order discretized equation. Alternatively, using an iterative procedure in defect correction process provides a highly accurate numerical scheme with improved stability properties. An example of this iterative approach is given in the work of Christleib et al. [66], who applied a spectral differed correction approach by predicting the residual error and then correcting the numerical solution in an iterative process. Implementing their approach to solve ordinary differential equations (ODE), they could obtain numerical results with superior stability properties and high accuracy. The iterative differed correction strategy has typically been applied to an underlying low-order implicit finite difference solution to enhance its formal order of accuracy [30, 32]. This iterative subtraction of local error estimates at the current time-step ensures the numerical stability of the solution [30]. Deferred correction methods have often been used to enhance either spatial or temporal order of accuracy. When used to improve both, domain decomposition must be used which makes the approach computationally more complicated and more difficult to extend to higher dimensions [31].

Another form of defect correction methods can be developed by first solving the PDE with a low-order finite difference scheme and then applying a higher order scheme in an iterative procedure to increase the numerical solution accuracy [35]. This approach is typically designed to be used with implicit schemes where in each iteration, a system of equations with matrix coefficients governed by the lower order scheme is solved. These matrix solutions are often very efficient which, when combined with the increased order of accuracy, typically leads to a more computational efficient scheme despite the need for iteration. However, the numerical stability of this approach is highly dependent upon the underlying higher order finite difference scheme and application of this approach to explicit schemes typically does not pro-

vide any computational benefits. Thus, the major drawback of this approach is its lack of computational benefit for explicit difference schemes.

Defect correction without iteration can lead to an unstable numerical solution [30]. Klopfer and McRae applied such an approach by only eliminating the dominant leading term of the truncation error [67]. Using prior truncation error analysis for the Lax-Wendroff scheme, they removed the dominant nonlinear term and obtained a defect corrected discretization which gives a significant improvement in the accuracy. When the method was used to solve a one-dimensional shock tube problem, some spurious oscillations were observed near the shock [67]. Moreover, such a method was shown to be incapable of enhancing the accuracy of first order schemes.

Combining defect correction with optimal time-step selection, Chu recently proposed a new approach (OTS-NIDC) for improving the order of accuracy in finite difference schemes [33]. His methodology is based upon distinguishing irregular perturbations (singularities) in the modified differential equation from the regular ones. Using OTS-NIDC, irregular perturbations are automatically removed by the selection of the optimal time-step. On the other hand, regular perturbations are eliminated by a non-iterative defect correction. The optimal time-step is determined by solving an equation derived from the truncation error analysis of the original difference scheme. Unfortunately, if the expression obtained for the optimal time-step selection is not constant this approach is not feasible in the framework of standard finite difference computations as it would require a time-step which is spatially dependent. Since such a constant value can not be found for most nonlinear and linear PDEs with non-constant coefficients, application of OTS-NIDC is unable to enhance the order of accuracy for these types of problems. Moreover, the resultant difference scheme is not always necessarily monotonicity preserving. As such, spurious oscillations may occur in the numerical solution.

1.7 Example Application of Numerical Solution of Hyperbolic Equations: Computational Uncertainty Quantification

Uncertainty quantification (UQ) generally involves determining the effects of uncertainty in system input parameters on system output variables. In the design of engineering systems, the information produced from uncertainty quantification can be used as a tool for enabling quantitative risk analysis [68]. Computational uncertainty quantification (CUQ) involves determination of the effect of uncertainty in the input parameters of a computational model on the statistics of the underlying output/state variables. The results produced by such an analysis play a crucial role in the quantitative reliability assessment of the system. These statistics can then be used to determine the probability of undesirable events (outputs) which in turn can be used to assess the reliability of the physical system which is being modeled. Computational uncertainty quantification is used in a wide variety of engineering applications such as computational fluid dynamics [69], chemical systems [70], scientific computing [71], structural mechanics [72], fracture mechanics [73] and aerospace system analysis [74, 75, 76, 77, 78].

According to the classification proposed by Melchers [79, 80] there are three types of uncertainties: aleatory uncertainty, epistemic uncertainty and uncertainty due to human error. In this dissertation only aleatory uncertainty is considered. Unlike epistemic uncertainty, which is due to the lack of knowledge about the true physics of the system being modeled, aleatory or irreducible uncertainty is concerned with inherent randomness in the system parameters. Common computational uncertainty quantification approaches that deal with aleatory uncertainty can be classified into two major groups, intrusive [81, 82] or non-intrusive [83, 84] methods, where here the word intrusive refers to a modification of the underlying computer program used

in a deterministic simulation.

Non-intrusive methods are characterized by the "black box" treatment of deterministic computations and as a result do not require modification of existing simulation codes. This is the main advantage of using non-intrusive methods. On the other hand intrusive methods, by definition, generally require modification of the original deterministic simulation code. This modification involves altering the implementation of the system of governing equations. Most intrusive methods in computational uncertainty quantification can be viewed as weighted residual methods whereby a new system of governing equations is obtained through the expansion of the (random) response variable as a finite series of basis function and then enforcing the error of such an approximation to be orthogonal to the test functional space [85]. Other intrusive approaches which are based upon the solution of the Fokker-Planck equation, which consider the effects of stochastic forcing [86] as well as parametric uncertainty, are also possible.

Monte Carlo simulation is the most popular approach among non-intrusive methods due to the simplicity of its implementation. Unfortunately Monte Carlo simulation has a poor convergence rate ($\mathcal{O}(N^{-\frac{1}{2}})$ for the mean, where N denotes the number of samples) [87]. In order to improve the convergence rate of the statistical moments, projection based methods such as the generalized polynomial chaos (gPC) method [88], a generalization of the classical polynomial chaos [89], have been developed for use in both the intrusive and non-intrusive frameworks [90, 91, 92, 93]. Intrusive methods, while more difficult to implement than non-intrusive methods, are often more efficient for a given level of accuracy [94].

A major area of concern in CUQ, involves the accurate simulation of random processes as they evolve in time. Standard intrusive and non-intrusive projection-based methods, such as polynomial chaos [95, 96] and generalized polynomial chaos (gPC) [85, 97, 88], expand the random variables corresponding to system states

in a finite series of fixed basis functions. As was first discussed by Orszag [98] in the context of using a truncated Wiener-Hermite expansion for stochastic processes in turbulence, and reiterated by Gerritsma et al. [99] for CUQ applications, such expansions are unable to accurately describe time-dependent random processes. In their work Gerritsma et al. [99] proposed a method which used time-dependent basis functions as a means of overcoming the abovementioned problem of accurately determining the long-time statistical behavior of (random) response variables or system states in CUQ. In this dissertation we attempt to alleviate this issue with long-time integration of statistics using a high fidelity solution of the Liouville equation (see Chapters 2 and 4).

An additional difficulty encountered in standard projection-based CUQ methods that employ global basis functions involves the accurate determination of the time-dependent statistical properties for problems with deterministic solutions which contain bifurcations. A good example of such a problem can be found in the context of aeroelastic instability and limit cycle oscillations (LCO). In such cases, projection-based methods with global basis, such as standard gPC, are often unable to accurately predict the statistical behavior of the response [100, 101]. Even if a sufficient number of basis functions are used Gibbs phenomena can be expected to negatively affect solution accuracy. Other methods which are based upon Fourier chaos expansions [102] and normal form equations [101] have been used for these problems, as have methods which employ basis functions with local (compact) support [103, 100, 104]. As the location of the discontinuity (bifurcation point) is often unknown, methods [104, 105] which adapt the basis/grid to the solution seem particularly well-suited for such problems.

Despite the rapid enhancement in computational resources (CPU speed, memory, etc.), uncertainty quantification of high dimensional dynamical systems has remained as a major challenge and active area of research in the UQ community.

The difficulty is particularly due to the tensor product nature of multidimensional interpolation used in many intrusive and non-intrusive methods to approximate the system response. This problem has, to some extent, been addressed by applying some advanced non-intrusive approaches such as Smolyak Clenshaw-Curtis sparse grids algorithm combined with multi-element probabilistic collocation method (MEPCM) [106], MEPCM with analysis of variance (ANOVA) functional decomposition [107] and intrusive approaches such as approximate solution of the Liouville equation with truncated BBGKY hierarchies [108, 109]. An additional approach to reduce computational costs in large-scale stochastic simulations was introduced in [110] where the authors used non-standard stochastic sensitivity analysis to rank the importance of all inputs.

An important outcome of uncertainty quantification in the field of engineering is the determination of the likelihood of fulfilling the systems' design requirements, often denoted as the system reliability and expressed mathematically in terms of a failure probability. This failure probability can in turn be expressed as an integral over the probability space, bounded by a limit function defining the "safe" operation of the system, of the joint probability density function involving the uncertain system inputs and outputs [89, 111].

Errors in the estimation of the joint probability density function can lead to inaccurate reliability estimates in the direct reliability approach. As such, a number of approximate methods for reliability assessment have been proposed. Two common approximate reliability measures are the reliability index [112] and Hasofer and Lind index [113], both of which are computed using lower order moments such as mean and variance. Unfortunately these simple approaches are typically not suitable for problems in which the limit states are nonlinear or when the joint probability density is non-Gaussian. For such problems higher order moments become more important, in particular for systems which require high reliability, and methods which address

the reliability assessment problem directly in terms of the accurate determination the probability density are often necessary. Of course given a sufficient number of samples, Monte Carlo analysis or other non-intrusive methods can provide an accurate, direct measure of the required density. However as mentioned above, either their convergence with respect to the number of samples is slow or they are dealing with long-time results inaccuracy, particularly in the tails of the density.

One effective approach could be developing a method based upon the formulation of UQ problems in terms of a Liouville equation for (random) response variables conditional density [114, 115] to accurately predict the long-time statistics of multi-state dynamical systems. The solution of the resultant Liouville equation, which is a linear multidimensional hyperbolic partial differential equation (PDE), provides the conditional probability density function of random variables at a given time. While analytical solutions of multidimensional PDEs such as the Liouville equation are rare, numerical solutions of such PDEs typically involve large computational costs. Standard finite difference approaches have been developed by several authors to obtain probability density function evolution [1, 116, 117, 118, 119, 2]. However, the high computational cost of such approaches for solving the multidimensional Liouville equation highlights the need for development of new methods and algorithms for solving the Liouville equation at reasonably low computational cost (at least for moderately high dimensional problems).

1.8 Objective and Scope of Dissertation Research

In the context of finite difference solution of multidimensional hyperbolic PDEs, our primary research objective in this dissertation is to develop and analyze methods which give high fidelity, computationally efficient numerical solutions of PDEs but which still benefit from the computational simplicity of a low-order finite difference scheme. A secondary objective of the dissertation involves demonstrating that CUQ

can be accomplished accurately and efficiently through numerical solution of the Liouville equation governing the evolution of conditional density for the system states.

In the dissertation, two categories of methods are developed in order to address the abovementioned objectives. The first class, which is detailed in Chapter 2 and extended to multidimensional problems in Chapter 4, enhances the accuracy of numerical solutions of hyperbolic PDEs through modification of the grid distribution/domain. Within this class two novel concepts are introduced. First for problems in unbounded domains, methods are developed to allow adaptation of domain boundaries thus allowing for higher fidelity solution. Second, a grid distribution method is developed which is based upon satisfying a local CFL=1 condition everywhere in the domain of computation. Numerical results, and truncation error analysis, of this latter idea show that accuracy is significantly enhanced due to reduction of numerical diffusion and dispersion.

While the methods in the first category developed show significant improvement over more standard approaches (e.g. fixed domain, uniform mesh), in particular for unbounded domains (e.g. CUQ problems addressed using numerical solution of the Liouville equation), the improvement is limited by the underlying accuracy of the base finite difference scheme used. As such, in the second category of methods, which are detailed in Chapter 3, and extended to multidimensional problems in Chapter 5, the formal order of accuracy of an underlying finite difference scheme is increased through application of mesh redistribution and defect correction. Within this category two separate types of methods are developed. The first determines the mesh distribution through solution of a constrained minimization problem, with the objective function consisting of the irregular perturbative term in the modified differential equation. In the second method, mesh distribution is once again determined using the irregular perturbative term in the modified differential equation.

However in this case this is accomplished using a remap procedure, whereby data is transferred between uniform and non-uniform meshes using a monotonicity preserving interpolation. This latter method allows for simple extension to bounded and multidimensional domains. Numerical results indicate that the desired, designed, increase in formal order of accuracy is indeed achieved using the methods in this category. In addition the results indicate that, in general, the methods are more computationally efficient (less computational time for a given accuracy) than standard methods and the method based upon monotonicity preserving interpolation appears to provide numerical solutions which are free from non-physical oscillation.

Regarding the application of efficient numerical solution of hyperbolic equations to CUQ, e.g. the secondary objective of this work, each chapter in the dissertation contains example problems pertaining to solution of the Liouville equation. In particular, in Chapters 2 and 4, the abovementioned finite difference methods are combined with numerical quadrature in the (uncertain) parameter space to provide accurate and efficient solution to various problems in CUQ. The numerical results in these chapters compare favorably with analytical solutions and Monte Carlo simulation.

CHAPTER 2

Selected Strategies for Adaptive Grid Based Numerical Solution of PDEs

In this chapter, we consider time-dependent numerical solutions of hyperbolic PDEs with one independent state (or response) variable based on various grid/domain adaptation strategies, with an overall goal of improving the accuracy and/or computational efficiency. In particular, we focus on seeking numerical solutions of a class of PDEs represented by the Liouville equation. The Liouville equation is important in the context of computational uncertainty quantification as it can give the evolution of the joint probability of the state and parameter variables from which relevant statistics of the state (or response) variables can be obtained. Here, we specifically consider three different methods to determine a time-dependent mesh in the space of response variables.

In each of these methods the computational domain is time-dependent, with the location of the boundary determined through the use of predefined values of the (random) response. The first method is based upon the principle of equidistribution of the gradients of the conditional density. This grid adaptation approach increases the resolution of grid points in high gradient regions of the conditional density and consequently enhances the accuracy of the finite difference scheme by reducing the truncation error. The second method relies on determination of a mesh distribution which results in local Courant-Friedrichs-Lewy (CFL) equal to 1. A truncation error analysis of the finite difference scheme will show that imposing the local CFL=1 condition results in an order of magnitude reduction in both the dispersion and

diffusion errors. In the third approach, after determining the new boundaries in each time-step, the interior grid points are distributed uniformly within the newly found bounds. The enhancement in the accuracy of the finite difference solution obtained from the application of these proposed grid adaptation approaches results, when compared to a standard fixed mesh/domain solution, in the use of significantly fewer number of grid points in order to solve Liouville equations with an acceptable level of accuracy (less than 10 percent error). Thus, computational costs are reduced considerably.

Here, in order to study the impact of the proposed methodology in one-dimensional spaces, we investigate a finite difference based solution of a Liouville equation that describes the evolution of a conditional probability density function depending on state variables and model input parameters. The efficiency of the numerical solution is enhanced through (i) a quadrature-based sampling of random variables corresponding to model input parameters and (ii) time-adaptive methods for determining the computational grid in the space of state or response variables. As the results will demonstrate, the methodology allows for the accurate computation of the response conditional density and resulting statistical moments. Two example problems with analytical solutions, a simple decay model and a problem which has nonlinear deterministic dynamics with multiple equilibrium points, will be used to illustrate the methodology. Also, in order to show the efficiency of the proposed grid adaptation techniques in reducing the computational costs, comparisons are made between the numerical solutions of Liouville equation obtained by these methods and those computed by applying the finite difference scheme directly on a fixed uniform grid.

2.1 Theory: Liouville equation and conditional density evolution

We define the probability space for the problem as $(\Omega, \mathcal{F}, \mathcal{P})$ where Ω is the sample space, $\mathcal{F} \subset 2^{\Omega}$ its σ-algebra of events and $\mathcal{P}$ the associated probability measure. In addition we let $T \subset \Re$ be a certain temporal domain and refer to $\mathbf{x}(t, \omega) = (x_1, x_2, ..., x_M) : T \times \Omega \rightarrow \Re^M$ as an M-dimensional vector of stochastic processes where ω represents an element in the sample space Ω. Here we assume that the probability space can be described by a finite number of random variables $\xi_1, \xi_2, ..., \xi_N : \Omega \rightarrow \Re$, such that the random process can now be written as $\mathbf{x}(t, \boldsymbol{\xi}) : T \times \Re^N \rightarrow \Re^M$ where $\boldsymbol{\xi} = (\xi_1, \xi_2, ..., \xi_N)$ is an N-dimensional vector of random variables. We further assume that there is no stochastic excitation and write the differential equations describing the flow of $\mathbf{x}$ as:

$$\dot{\mathbf{x}}(t, \boldsymbol{\xi}) = \mathbf{h}(\mathbf{x}, \boldsymbol{\xi}, t) \quad , \tag{2.1}$$

where it should be noted that Eq. 2.1 could be the result of a semi-discretization in physical space of a partial differential equation with a stochastic operator.

We are interested in determining a partial differential equation describing the evolution of the initial joint probability density function (JPDF), $f_{\mathbf{x},\boldsymbol{\xi}}(\mathbf{X}; \boldsymbol{\xi}, t = 0)$ with

$$\int_{\Re^{\mathbf{M}}} \int_{\Re^{\mathbf{N}}} f_{\mathbf{x},\boldsymbol{\xi}}(\mathbf{X}; \boldsymbol{\xi}, t = 0) d\boldsymbol{\xi} d\mathbf{x} = 1 \quad . \tag{2.2}$$

Under the condition that the marginal density of $\boldsymbol{\xi}$, $f_{\boldsymbol{\xi}}(\mathbf{Y})$, is time-invariant it can be shown (see Appendix A) that this evolution can be written in terms of a Liouville

equation for the conditional probability density of $\mathbf{x}$ given $\boldsymbol{\xi} = \mathbf{Y}$, $f_{\mathbf{x}|\boldsymbol{\xi}}(\mathbf{X}|\boldsymbol{\xi} = \mathbf{Y}, t)$:

$$\frac{\partial f_{\mathbf{x}|\boldsymbol{\xi}}}{\partial t} = \sum_{i=1}^{M} -\frac{\partial}{\partial x_i}[h_i(\mathbf{x}, \mathbf{Y}, t) f_{\mathbf{x}|\boldsymbol{\xi}}] \quad , \tag{2.3}$$

where the h_i are elements of $\mathbf{h}$. It should be noted that the evolution equation for the JPDF associated with flow in the presence of Wiener processes (stochastic forcing) would be governed by the associated Fokker-Planck equation. Also the CUQ approach outlined in this chapter could be used to evolve, directly, the Liouville equation for the JPDF if this is required. In this case the Gauss-quadrature sampling, to be outlined in the next paragraph, would not be needed.

Here, the values $\boldsymbol{\xi} = \mathbf{Y}$, on which $f_{\mathbf{x}|\boldsymbol{\xi}}$ is conditioned, are numerical (Gauss) quadrature sampling points. Given a marginal density for $\boldsymbol{\xi}$ these sampling points would correspond to the Gauss quadrature which has a weighting function which is equal to the marginal density. This allows for an accurate determination of the statistical moments of the random processes with a limited number of conditioning variables $\mathbf{Y}$:

$$< x_i^n > = \int_{\Re^{\mathbf{N}}} \int_{\Re^{\mathbf{M}}} x_i^n f_{\mathbf{x}|\boldsymbol{\xi}} \left(\prod_{k=1}^{N} f_{\xi_k} \right) d\mathbf{x} d\boldsymbol{\xi} \tag{2.4}$$

$$\approx \prod_{k=1}^{N} \left(\sum_{j_k=1}^{N_{p_k}} w_{j_k} \left(\int_{\Re^{\mathbf{M}}} x_i^n f_{\mathbf{x}|\boldsymbol{\xi}}(\mathbf{x}, Y_{j_1}, Y_{j_2}, ..., Y_{j_M}, t) d\mathbf{x} \right) f_{\xi}(Y_{j_k}) \right) \quad , \tag{2.5}$$

where the product of $f_{\mathbf{x}|\boldsymbol{\xi}}$ and $\left(\prod_{k=1}^{N} f_{\xi_k} \right)$ represents the joint probability density function. Equations 2.4 and 2.5 are, respectively, expressions for the exact and approximate nth raw moment of the random variable x_i. In Eq. 2.5 symbols w_{j_k} and Y_{j_k} are, respectively, the quadrature weights and abscissas. In Chapter 2 and 4 numerical integration over the support of x, $\Re^{\mathbf{M}}$, is accomplished using the quadrature developed in Ref. [120] for non-uniform meshes and composite trapezoidal rule [17],

respectively.

2.2 Numerical methods

2.2.1 Rezoning approach to numerical solutions on time-varying meshes

We will approximate the solution to Eq. 2.3 using a finite difference solution on a (possibly) nonuniform, time-varying mesh. In the sections to follow the specific finite difference scheme, and the manner in which the mesh is adapted in time, will be discussed. In this section we will only describe the general rezoning approach [121, 122] for numerical solution on time-varying meshes.

Consider a sequence of times t^n for $n = 0, 1, ..$, where the time-steps $\Delta t^{n+1} = t^{n+1} - t^n$ need not be equal. We define a time-varying partition (mesh) of $\mathbf{x}$ as $\Gamma(t)$ and allow for the possibility that the boundary of $\Gamma(t)$, $S_\Gamma(t)$, is also time-varying. In the rezoning approach, $\Gamma(t)$ is considered to vary only at discrete time instants $t = t^n$ and as such the time-derivative in Eq. 2.3 need not be transformed.

In the rezoning method a new mesh $\Gamma(t^{n+1})$ is first generated for time-step t^{n+1}. Following the generation of this new mesh the PDE is integrated for the current step with the mesh held fixed. This time integration requires the approximate numerical solution for $f_{\mathbf{x}|\boldsymbol{\xi}}$ at time-step t^n, denoted as $\mathbf{F}^n = \{f_1^n, f_2^n, ...\}$, to be known on $\Gamma(t^{n+1})$. However since this solution is only known on $\Gamma(t^n)$, an interpolated solution $\tilde{\mathbf{F}}^n = \{\tilde{f}_1^n, \tilde{f}_2^n, ...\}$ must be found on $\Gamma(t^{n+1})$. A monotonicity preserving cubic Hermite interpolation [123] is used to determine $\tilde{\mathbf{F}}^n$.

2.2.2 Finite difference solution

A second order accurate, MacCormack finite difference method with flux limiting [124], is used to numerically solve Eq. 2.3. To demonstrate, we consider the following differential equation for a problem with one response variable x and (ran-

dom) parameters $\boldsymbol{\xi}$:

$$\dot{x}(t,\boldsymbol{\xi}) = h(x,\boldsymbol{\xi},t) \ . \tag{2.6}$$

The corresponding Liouville equation for the conditional density $f_{x|\boldsymbol{\xi}}$ is given by

$$\frac{\partial f_{x|\boldsymbol{\xi}}}{\partial t} = -\frac{\partial}{\partial x}[h(x,\boldsymbol{\xi}=\mathbf{Y},t)f_{x|\boldsymbol{\xi}}] \ . \tag{2.7}$$

Considering positive $h(x,\boldsymbol{\xi}=\mathbf{Y},t)$, application of the MacCormack scheme with flux limiters $\psi^n_{j+\frac{1}{2}}$ and $\psi^n_{j-\frac{1}{2}}$ results in the following finite difference equation (FDE) solved on the mesh partition $\Gamma(t^{n+1},\mathbf{Y}) = \{x_1^{n+1}, x_2^{n+1}, ...\}$:

$$\begin{aligned} f_i^{n+1} = \tilde{f}_i^n - \frac{\Delta t^{n+1}}{\Delta x_i^{n+1}}\left[(h^{n+1}\tilde{f}^n)_i - (h^{n+1}\tilde{f}^n)_{i-1}\right] + \\ \frac{\Delta t^{n+1}}{2\Delta x_{i+1}^{n+1}}\left[h_{i+1}^{n+1}\left(h_i^{n+1}\frac{\Delta t^{n+1}}{\Delta x_i^{n+1}}-1\right)\tilde{f}_{i+1}^n - h_i^{n+1}\left(h_i^{n+1}\frac{\Delta t^{n+1}}{\Delta x_i^{n+1}}-1\right)\tilde{f}_i^n\right]\psi^n_{i+\frac{1}{2}} - \\ \frac{\Delta t^{n+1}}{2\Delta x_i^{n+1}}\left[h_i^{n+1}\left(h_{i-1}^{n+1}\frac{\Delta t^{n+1}}{\Delta x_i^{n+1}}-1\right)\tilde{f}_i^n - h_{i-1}^{n+1}\left(h_{i-1}^{n+1}\frac{\Delta t^{n+1}}{\Delta x_i^{n+1}}-1\right)\tilde{f}_{i-1}^n\right]\psi^n_{i-\frac{1}{2}}, \end{aligned} \tag{2.8}$$

where $\Delta x_i^{n+1} \equiv x_i^{n+1} - x_{i-1}^{n+1}$. The FDE for negative h can be obtained using symmetry considerations. The flux limiters ($\psi^n_{i+\frac{1}{2}}$ and $\psi^n_{i-\frac{1}{2}}$) are functions of the monotonicity indicator which is defined as the ratio of the slope of the profile upstream of the point i to the slope of the profile downstream of the point i. This indicator for positive and negative advection is defined as

$$\theta^n_{i+\frac{1}{2}} = \left(\frac{x_{i+1}^{n+1} - x_i^{n+1}}{x_i^{n+1} - x_{i-1}^{n+1}}\right)\frac{(h^{n+1}\tilde{f}^n)_i - (h^{n+1}\tilde{f}^n)_{i-1}}{(h^{n+1}\tilde{f}^n)_{i+1} - (h^{n+1}\tilde{f}^n)_i} \tag{2.9}$$

and

$$\theta^n_{i+\frac{1}{2}} = \left(\frac{x_{i+1}^{n+1} - x_i^{n+1}}{x_{i+2}^{n+1} - x_{i+1}^{n+1}}\right)\frac{(h^{n+1}\tilde{f}^n)_{i+2} - (h^{n+1}\tilde{f}^n)_{i+1}}{(h^{n+1}\tilde{f}^n)_{i+1} - (h^{n+1}\tilde{f}^n)_i} \ , \tag{2.10}$$

respectively. While other limiters are possible, e.g. minmod, superbee, etc., we

choose to use the MC limiter,

$$\psi(\theta) = \max[0, \min((1+\theta)/2, 2, 2\theta)] \quad , \tag{2.11}$$

as it has been shown to work well when used with the MacCormack scheme [124]. It should also be mentioned that in order to address the non-conservative nature of the applied finite difference scheme the numerical solution is re-scaled (e.g. a "normalization constant" is found) at each time-step such that the zeroth moment remains unity. Based upon the numerical experiments performed in this chapter this modification of the underlying finite difference scheme does not appear to deteriorate the basic numerical properties (order of convergence and stability) of the scheme.

2.2.3 Time-varying mesh adaptation: Adaptive mesh based upon equidistribution (AGBR)

The Liouville equation for the evolution of the conditional density of the random process is a linear, hyperbolic partial differential equation. A characteristic of hyperbolic problems is that if steep gradients exist, which move in time, the solution at a particular point in space (here $\mathbf{x}$) can change very rapidly. Hence when considering numerical solutions of such problems, it would appear desirable to employ a non-uniform mesh which adapts in time such that fine grid resolution is used in regions with large gradients and a more coarse resolution is used in smooth regions.

The equidistribution principle based mesh adaptation method implemented in this chapter was first introduced by Carey [55] to non-uniformly distribute grid points in regions of high gradients. This approach, which we refer to as the adaptive gradient based refinement (AGBR) method, improves the accuracy of a numerical solution for a given number of grid points through mesh refinement in high gradient regions. In Ref. [55] it was shown that in one-dimension with $x \in [a, b]$, defining a

mesh grading function $\eta(x)$ as:

$$\eta(x) = \frac{\int_a^x \left[f_{\mathbf{x}|\boldsymbol{\xi}}^{(k+1)}\right]^{2/[2(k+1-m)+1]} dx}{\int_a^b \left[f_{\mathbf{x}|\boldsymbol{\xi}}^{(k+1)}\right]^{2/[2(k+1-m)+1]} dx} \quad , \tag{2.12}$$

results in a mesh which is optimal with respect to the interpolation error in the H^m semi-norm. For a mesh with P points, setting $\eta(x_{i+3}^n) = \eta_i$ and $\eta_i - i/(P-1) = 0$ $(i = 1, 2, 3, ..., P-6)$ and solving for the x_i equidistributes $\left[f_{\mathbf{x}|\boldsymbol{\xi}}^{(k+1)}\right]^{2/[2(k+1-m)+1]}$. Here in this chapter, m and k are chosen to be 0 and 1 respectively which provides a theoretically optimal mesh in the L^2 norm ($m = 0$). In order to maintain adequate grid smoothness at the tails of the response, Eq. 2.12 is used to determine the interior $P-6$ points $(\eta_1, \eta_2, ..., \eta_{P-6})$ while a procedure based upon an imposed minimum value of $f_{\mathbf{x}|\boldsymbol{\xi}}$ is used to determine the boundary $S_{\Gamma(t)}$ and remaining points. See Appendix B for details.

It should be noted that determining $\Gamma(t^{n+1})$ using equidistribution alone is sufficient for the one-dimensional problems (e.g. one response variable, $M = 1$) investigated in this chapter. For problems with additional response variables the equidistribution principle alone is not enough and factors influencing mesh quality must also be considered [121].

2.2.4 Time-varying mesh adaptation: Adaptive mesh based upon truncation error (CFLB)

The second approach applied in this chapter to distribute grid points in such a way as to improve the accuracy of the numerical solution, is a CFL-based (CFLB) grid adaptation method. The local CFL number for a one-dimensional linear advection equation (e.g. Eq. 2.3 with $M = 1$) is defined as:

$$\text{CFL} = \frac{\Delta t^{n+1}}{x_i^{n+1} - x_{i-1}^{n+1}} h(x_i^{n+1}). \tag{2.13}$$

It is well known that, for explicit finite difference schemes, setting CFL = 1 provides a numerical solution which is free of error when the advection speed h is constant [17]. Unfortunately this is not true when h varies with x. For a general, spatially dependent h with the assumption of grid smoothness ($\left|x_{i+1}^{n+1} - x_i^{n+1}\right| - \left|x_i^{n+1} - x_{i-1}^{n+1}\right| = \mathcal{O}(\left(x_i^{n+1} - x_{i-1}^{n+1}\right)^2)$), expanding the terms in Eq. 2.8 in a Taylor series results in the following expression for the truncation error (TR):

$$
\begin{aligned}
TR = & \left\{ \frac{\Delta t}{2} \left(\frac{\partial}{\partial x} \left(h^{n+1} \frac{\partial F}{\partial x} \right) \right)_i - \frac{\Delta t}{4} h_i^{n+1} \psi_{i-\frac{1}{2}} \frac{\Delta x_1 + \Delta x_2}{\Delta x_1} \left(\frac{\partial^2 F}{\partial x^2} \right)_i \right. \\
& - \frac{\Delta t}{2} \psi_{i-\frac{1}{2}} \left(\left(\frac{\partial h}{\partial x} \right)^{n+1} \frac{\partial F}{\partial x} \right)_i - \frac{\Delta x_1}{2} \left(\frac{\partial^2 F}{\partial x^2} \right)_i + \frac{\Delta x_1 + \Delta x_2}{4} \left(\frac{\partial}{\partial x} \left(\left(\frac{\partial F}{\partial x} \right)_i \psi_{i-\frac{1}{2}}^n \right) \right) \\
& \left. - \frac{\Delta t}{2} h_i^{n+1} \left(\frac{\partial \psi}{\partial x} \right)_{i-\frac{1}{2}}^n \left(\frac{\Delta x_1 + \Delta x_2}{2 \Delta x_1} \right) \left(\frac{\partial F}{\partial x} \right)_i \right\} \\
& + \left\{ - \frac{\Delta t^2}{6} \left(\frac{\partial}{\partial x} \left(h^{n+1} \frac{\partial}{\partial x} \left(h^{n+1} \frac{\partial F}{\partial x} \right) \right) \right)_i + \frac{\Delta x_1^2}{6} \left(\frac{\partial^3 F}{\partial x^3} \right)_i \right. \\
& + \frac{\Delta x_1^2}{4} \left(\frac{\partial}{\partial x} \left(\left(\frac{\partial F}{\partial x} \right)_i \left(\frac{\partial \psi}{\partial x} \right)_{i-\frac{1}{2}}^n \right) \right) + \frac{\Delta t \Delta x_1}{4} \psi_{i-\frac{1}{2}}^n \left(\frac{\partial}{\partial x} \left(\frac{\partial F}{\partial x} \left(\frac{\partial h}{\partial x} \right)^{n+1} \right) \right)_i \\
& \left. - \frac{\Delta t \Delta x_1}{4} h_i^{n+1} \left(\frac{\partial}{\partial x} \left(\left(\frac{\partial F}{\partial x} \right)_i \left(\frac{\partial \psi}{\partial x} \right)_{i-\frac{1}{2}}^n \right) \right) \right\} \\
& + \mathcal{O}((\Delta x_2 + \Delta x_1 + \Delta t)^3)
\end{aligned}
\tag{2.14}
$$

where $F_i^n = (h^{n+1} \tilde{f}^n)_i$ and Δx_1 and Δx_2 denote the spatial interval to the left and right of the grid point i, respectively ($\Delta x_1 = x_i^{n+1} - x_{i-1}^{n+1}$ and $\Delta x_2 = x_{i+1}^{n+1} - x_i^{n+1}$). The result given in Eq. 2.14 demonstrates that the use of flux limiters with the MacCormack scheme reduces the formal order of accuracy from $\mathcal{O}(\Delta x^2 + \Delta t^2)$ to $\mathcal{O}(\Delta x_1 + \Delta t)$. This result is well-known [125] and is the price which is paid for reducing the spurious oscillations. It should be noted that if one assumes grid smoothness second order accuracy of the scheme is recovered in regions away from extreme points and discontinuities where $\psi = 1$ and $\partial \psi / \partial x = 0$. Thus, in most parts of the domain, the TVD scheme maintains the formal second order accuracy

of MacCormack scheme.

In the CFL = 1 case, the expression for the truncation error can be written as

$$\begin{aligned} TR &= \Delta t \times \left(\frac{1}{2} \left(\left(\frac{\partial h}{\partial x} \right)^{n+1} \frac{\partial F}{\partial x} \right)_i \left(1 - \psi^n_{i-\frac{1}{2}} \right) \right) \\ &\quad -\Delta t^2 \times \left\{ \frac{h_i^{n+1}}{2} \left(\left(\frac{\partial h}{\partial x} \right)^{n+1} \frac{\partial^2 F}{\partial x^2} \right)_i \left(1 - \frac{\psi^n_{i-\frac{1}{2}}}{2} \right) \right. \\ &\quad \left. + \left(\frac{\partial F}{\partial x} \right)^n_i \frac{h_i^{n+1}}{2} \left(\frac{1}{3} \left(\left(\frac{\partial h}{\partial x} \right)^2 \right)^{n+1}_i + h_i^{n+1} \left(\frac{\partial^2 h}{\partial x^2} \right)^{n+1}_i \left(\frac{1}{3} - \frac{\psi^n_{i-\frac{1}{2}}}{2} \right) \right) \right\} \\ &\quad +\mathcal{O}((\Delta x_2 + \Delta x_1 + \Delta t)^3) \end{aligned} \tag{2.15}$$

Comparing Eq. 2.15 with Eq. 2.14, one sees that while setting CFL = 1 does not increase the formal order of accuracy of the scheme, it does remove even-order derivatives of F from the first order terms. Also in the second order terms, the coefficient of the third order derivative of F, which represents dispersion error, becomes zero. As a result, the order of the leading terms in the expressions for the implicit numerical diffusion and dispersion errors becomes second and third order, respectively. Hence the effect of distributing the grid using the condition that the local CFL=1 results in an order of magnitude reduction in numerical dispersion and diffusion errors.

In one dimension, once the boundary (points) $S_\Gamma(t^{n+1})$ and time-step Δt^{n+1} are determined, the points x_i^{n+1} defining the mesh partition $\Gamma(t^{n+1})$ are found using the following expression:

$$x_i^{n+1} = x_{i+1}^{n+1} - |h(x_{i+1}^{n+1})| \Delta t^{n+1}. \tag{2.16}$$

As in the equidistribution-based method, the boundary $S_\Gamma(t^{n+1})$ is determined through the use of predefined (small) values of $f_{\mathbf{x}|\boldsymbol{\xi}}$. In particular as shown in Fig. 2.1, for the one-dimensional problems simulated here, the first grid points which

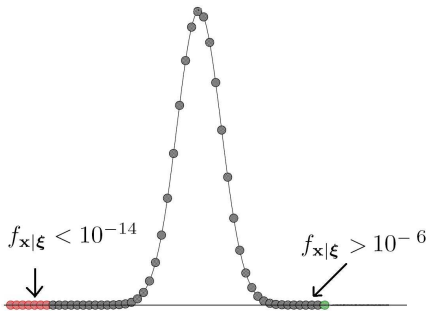

(a)

Figure 2.1: Schematic illustration of equidistribution-based grid movement in a one-dimensional space; removed and extended regions are colored in red and green, respectively

have a sufficiently large value of $f_{\mathbf{x}|\boldsymbol{\xi}}$ (here $f_{\mathbf{x}|\boldsymbol{\xi}} > 10^{-14}$) on the left and right sides of the domain are found and chosen as the new boundary points (x_P^{n+1} and x_1^{n+1}) along each ξ. If the value of $f_{\mathbf{x}|\boldsymbol{\xi}}$ for the first point interior to the right or left boundary point (e.g. x_{P-1}^n or x_2^n) has a value greater than the defined extension parameter (here $f_{\mathbf{x}|\boldsymbol{\xi}} > 10^{-6}$), a small increment proportional to the neighboring interval is added to the domain from the corresponding point and the new end point will be designated as the boundary (see Fig. 2.1). It should be noted that this procedure for determination the boundary of the computational domain is not unique, and perhaps not optimal, but it is easy to apply and has proved sufficient for the problems investigated in this chapter. Other methods such as front-tracking [126] would likely provide a more general method for determining $S_{\Gamma(t)}$ for multi-dimensional problems.

Using this approach for determining the boundary points without considering the interior grid point distribution based on the local CFL = 1 (Eq. 2.16), gives an adaptive time-varying mesh with a uniform grid spacing, which we refer to (e.g. in the text and figures in Section 2.3) as "adaptive uniform mesh". The time-varying grid adaptation in this approach is solely based on the values of the conditional density in the regions neighboring the boundary $S_\Gamma(t^n)$. In each time-step, once the boundary $S_\Gamma(t^{n+1})$ is determined as in the CFLB method, the interior grid points

are uniformly distributed within the domain.

In the CFLB grid adaptation method, once the boundary of the domain is found, the time-step Δt^{n+1} used to determine the remaining grid points via Eq. 2.16 is determined as:

$$\Delta t^{n+1} = \frac{1}{P-1} \sum_{i=1}^{P} \frac{\left| x_P^{n+1} - x_1^{n+1} \right|}{(P-1)h(x_i^n)}. \tag{2.17}$$

2.3 Results and discussion

2.3.1 Problem 1.1: Population balance

The first problem which is used to demonstrate the methodology represents a model for population growth with random growth rate [99]. The differential equation which governs the time evolution of the stochastic process x (population) is given by:

$$\frac{dx(t,\xi)}{dt} + k(\xi)x(t,\xi) = 0, \qquad x(0,\xi) = 1. \tag{2.18}$$

The growth rate k in Eq. 2.18 is assumed to be a uniformly distributed random variable with $k \in [0,1]$ and is parameterized by $\xi \in [-1,1]$ which has a marginal density, $f_\xi = \frac{1}{2}$. With $h(x) = -k(\xi)x(\xi,t)$, the resulting Liouville equation for $f_{x|\xi}$ given $\xi = Y$ is:

$$\frac{\partial f_{x|\xi}}{\partial t} - \frac{\partial}{\partial x}\left[k(\xi)x f_{x|\xi}\right] = 0, \tag{2.19}$$

where $k(\xi) = \left(\frac{1}{2} + \frac{1}{2}\xi\right)$. The conditional PDF at $t = 0$ is defined to be:

$$f_{x|\xi} = \frac{1}{\sigma\sqrt{2\pi}} \exp\left\{-\frac{(x-1)^2}{2\sigma^2}\right\}, \tag{2.20}$$

where σ is chosen to be small ($\sigma = 0.01$) in order to approximate a deterministic initial condition for x, $x(\xi,0) = 1$.

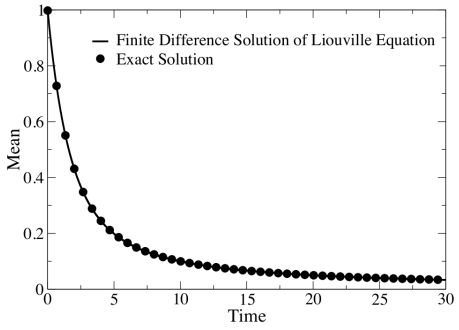

(a) The response mean

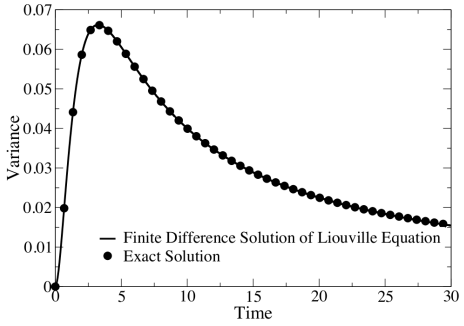

(b) The response variance

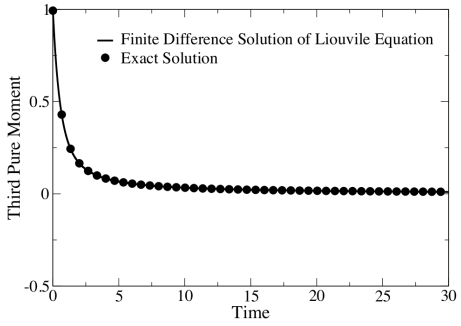

(c) The response third pure moment

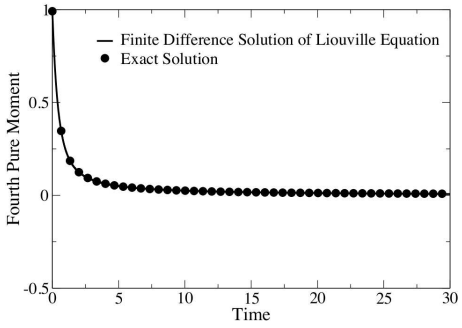

(d) The response fourth pure moment

Figure 2.2: Time evolution of response statistics for Problem 1.1. The exact solution is compared with the numerical solution obtained with CFLB mesh adaptation with $N_p = 10$ and $P = 501$.

The exact solution to Eq. 2.19 can be obtained through characteristic analysis with the result given by:

$$f_{x|\xi}(x,t) = \frac{1}{\sigma\sqrt{2\pi}} \exp\left\{-\frac{\left(x\exp\left\{k(\xi)t\right\}-1\right)^2}{2\sigma^2}\right\} \exp\left\{k(\xi)t\right\}. \tag{2.21}$$

Assuming infinitesimal standard deviation (σ) and integrating Eq. 2.21 gives the following expression for the nth moment of the (random) output variable x:

$$M_x^{(n)}(t) = \frac{1-\exp\left\{-nt\right\}}{nt}. \tag{2.22}$$

The accuracy of the method in determining the moments is demonstrated in Fig. 2.2 where the first four moments are plotted, along with the exact solution,

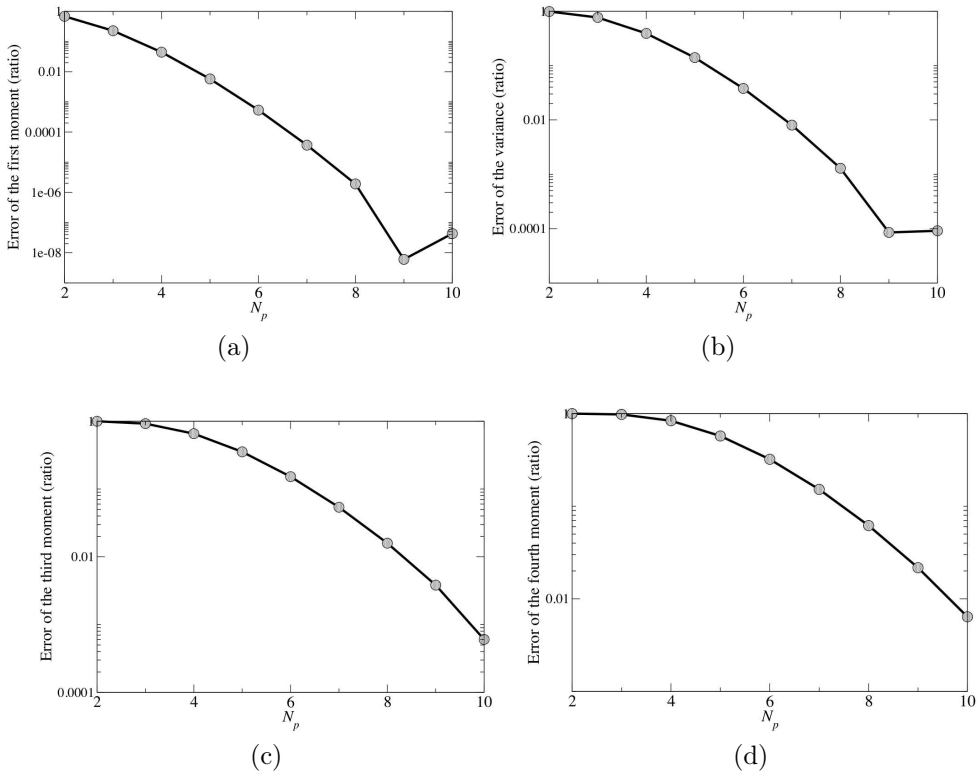

Figure 2.3: Error in the first four moments of response (at $t = 15$) versus the number of quadrature points (N_p), for Problem 1.1. The results were obtained using the CFLB mesh adaptation with $P = 501$.

for $t = 0$ to $t = 30$. The results are generated using the CFL based (CFLB) mesh adaptation with 501 grid points for x and $N_p = 10$ samples in ξ. To compare the accuracy of the method as a function of N_p, in Fig. 2.3 the error in the first four moments is plotted versus N_p for the CFLB algorithm. Figure 2.3 demonstrates that the moments are converging to the exact value; the stagnation in the value of the error for the first and second moments is due to the error inherent in approximating the deterministic initial condition with a Gaussian density.

In order to demonstrate the effect of the mesh adaptation, Figs. 2.4 and 2.5 show the error in the first four moments at $t = 3$ and $t = 5$, respectively, versus the number of grid points used in the mesh for x (with $N_p = 8$ sample points in ξ). Results are shown for the AGBR, CFLB and adaptive uniform mesh adaptation methods along with those generated using a fixed, uniform mesh. As can be seen

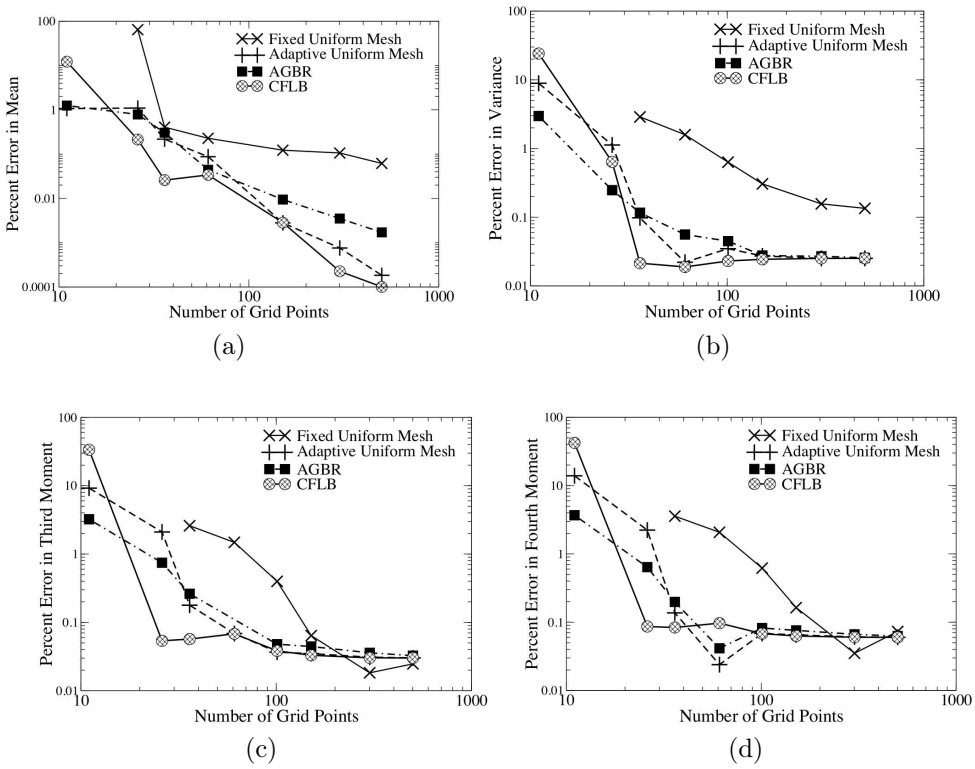

Figure 2.4: Error in the first four moments of response (in Problem 1.1, at $t = 3$) versus the number of grid points P. Results are shown for all four algorithms with fixed $N_p = 8$.

in these figures, all of the adaptive methods give comparable results and each prove to be significantly more accurate for a given number of mesh points when compared to the standard fixed mesh solution. Note that the stagnation of the error values for the statistical moments in Figs. 2.4 and 2.5 is due to both the approximate nature of the model for the deterministic initial condition along with errors in the numerical integration needed to compute the moments. That said, we believe that this minimum ("stagnated") value of the error in the moments (less than 0.1 percent) is acceptable for engineering design purposes.

As the computation of the moments requires numerical integration, which introduces some error, in order to better determine the effect of mesh adaptation on the accuracy of the computed conditional density, the L2 error of the conditional density for three different times, t =1, 3 and 5, is shown in Fig. 2.6 versus the number of

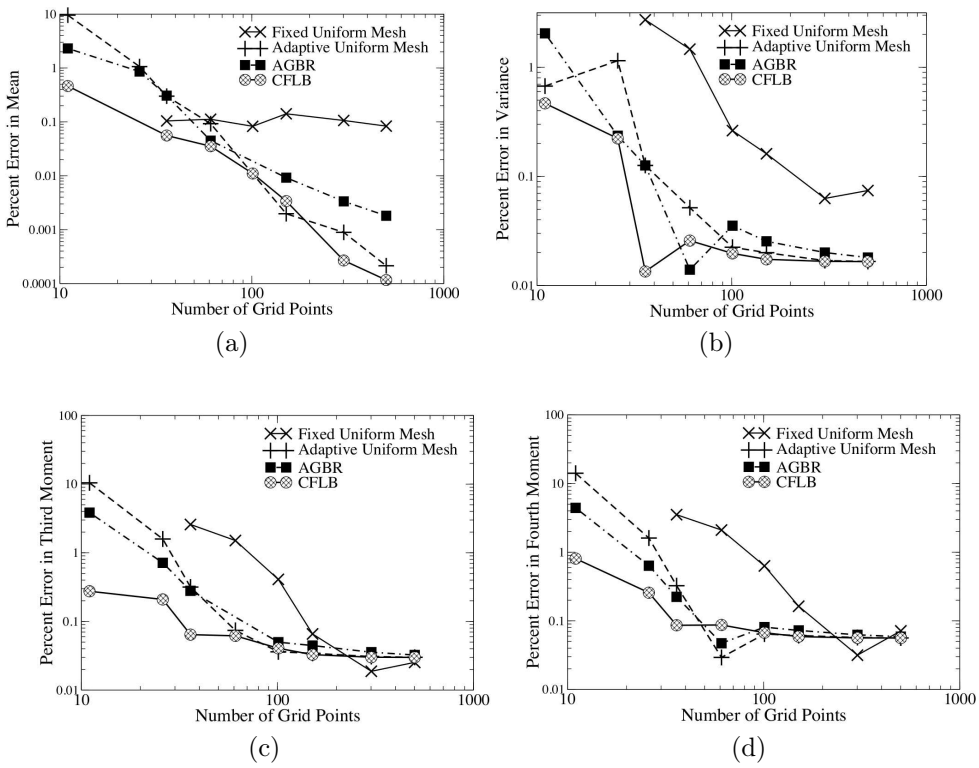

Figure 2.5: Error in the first four moments of response (in Problem 1.1, at $t = 5$) versus the number of grid points P. Results are shown for all four algorithms with fixed $N_p = 8$

grid points in x (once again $N_p = 8$). In this chapter, for P grid points in x and N_p samples in ξ, the normalized L2 error of the conditional density is obtained as:

$$\epsilon(t) = \left\{ \frac{\sum_{j=1}^{N_p} \sum_{i=1}^{P} \left(f_{\text{exact}}(x_i, Y_j, t) - f_{\text{numerical}}(x_i, Y_j, t) \right)^2}{\sum_{j=1}^{N_p} \sum_{i=1}^{P} \left(f_{\text{exact}}(x_i, Y_j, t) \right)^2} \right\}^{1/2} \tag{2.23}$$

The results shown in Fig. 2.6 further illustrate (a) the benefit of the adaptive algorithms over a fixed grid solution and (b) the general ability of the Liouville equation based method to accurately predict the time-evolution of the density. In particular, the CFLB scheme provides at least one order of magnitude improvement over the fixed grid solution and with only 100 grid points provides a solution with less than 2 percent error in the conditional density. As shown in Fig. 2.6, the expected sec-

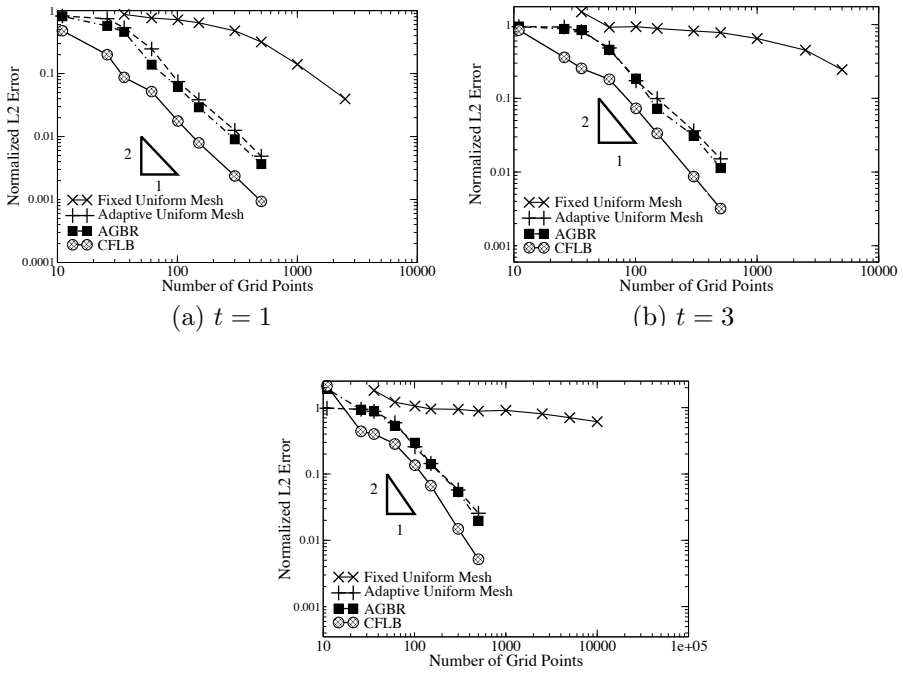

(a) $t = 1$ (b) $t = 3$

(c) $t = 5$

Figure 2.6: Error in the computed conditional density versus the number of grid points P for Problem 1.1. Results are shown for all four algorithms, with $N_p = 8$, at times $t = 1,\ 3,\ 5$.

ond order of accuracy of MacCormack scheme can be obtained much faster on the adaptive meshes, which leads to a faster convergence rate for the proposed adaptive finite difference approaches compared to the standard/fixed domain solution. This significant enhancement in computational speed is shown clearly in Fig. 2.7. For this example problem, CFLB approach gives about three orders of magnitude reduction in computational time (even compared to AGBR approach) for obtaining an equivalent accuracy.

2.3.2 Problem 1.2: One-dimensional problem with nonlinear deterministic dynamics

In order to investigate the effect of the presence of multiple attractors in the the solution on the numerical performance of the proposed adaptive approaches, the second example investigated in Chapter 2 is designed to be a problem with nonlinear

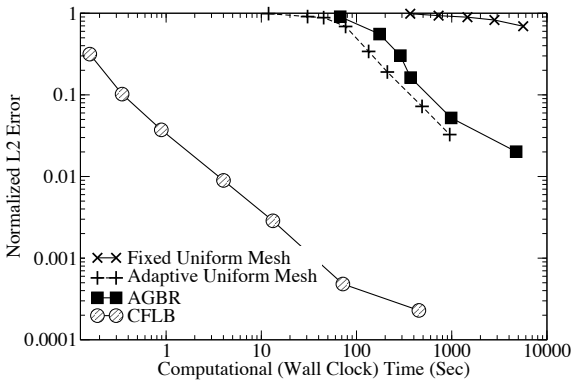

(a) $t = 5$

Figure 2.7: Error in computed conditional density for Problem 1.1 at time $t = 5$ versus the computational (wall clock) time for all 4 algorithms with $N_P = 10$.

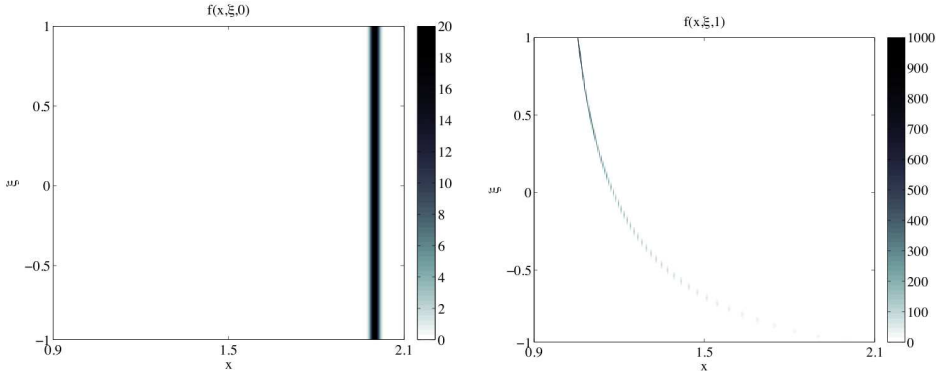

(a) Initial joint density (b) Joint density at $t = 1$

Figure 2.8: Contours of the JPDF for Problem 1.2 ($< \mu >= 2$) obtained with CFLB mesh adaptation using $N_P = 56$ and $P = 501$.

dynamics as described by the following differential equation:

$$\frac{dx(t,\xi)}{dt} + \mu(\xi)x(t,\xi)\left((x(t,\xi))^2 - 1\right) = 0, \qquad x(0,\xi) = 2.0. \tag{2.24}$$

In Eq. 2.24 μ is assumed to have the same uniform density as k in Problem 1.1 and, for the time being, the initial conditional density at $t = 0$ is defined as a Gaussian density with a mean of 2 (denoted as $< \mu >= 2$ in figure captions) and with small σ ($\sigma = 0.01$) (see Fig. 2.8a).

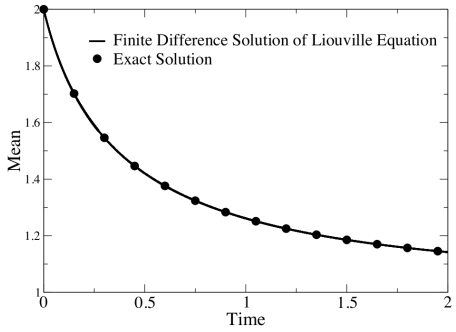

(a) Mean response

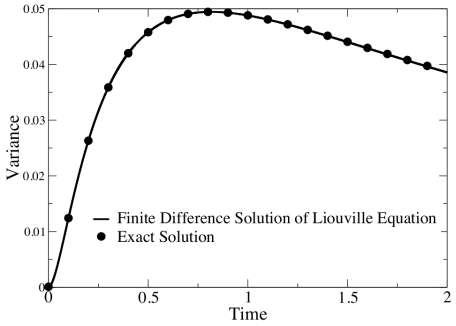

(b) Variance of response

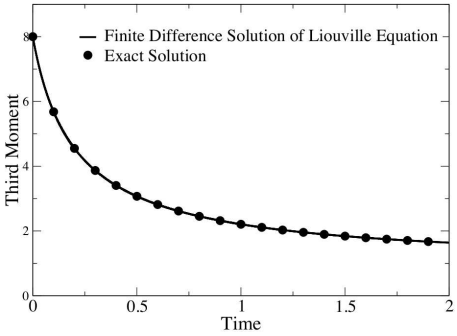

(c) Pure third moment of response

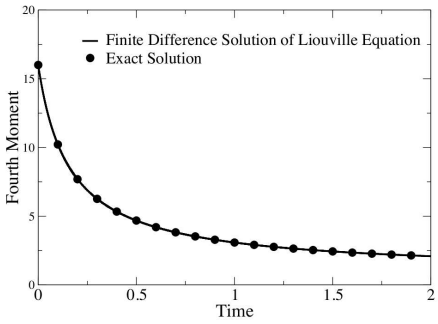

(d) Pure fourth pure moment of response

Figure 2.9: Time evolution of the response statistics for Problem 1.2 ($\langle\mu\rangle = 2$). Exact solution is compared with the numerical solution obtained with CFLB mesh adaptation using $N_p = 10$ and $P = 501$.

The Liouville equation which corresponds to the dynamics given in Eq. 2.24 is:

$$\frac{\partial f_{x|\xi}}{\partial t} - \frac{\partial}{\partial x}\left[\mu(\xi)(x^3 - x) f_{x|\xi}\right] = 0 \tag{2.25}$$

where $\mu(\xi) = \frac{1}{2} + \frac{1}{2}\xi$. As in the previous test problem, the exact solution of Eq. 2.25 can be obtained using characteristic analysis with the result:

$$\begin{aligned} f_{x|\xi} \;=\; & \frac{1}{\sigma\sqrt{2\pi}} \exp\left\{ -\frac{1}{2\sigma^2} \left(\frac{1}{\sqrt{1 - \exp\{2\mu(\xi)t\} + \frac{\exp\{2\mu(\xi)t\}}{x^2}}} - <\mu> \right)^2 \right\} \\ & \times \left| 1 - x^2 \left(1 - \exp\{-2\mu(\xi)t\}\right) \right|^{-\frac{3}{2}} \end{aligned} \tag{2.26}$$

The "exact" moments of x, which will be compared to those resulting from numerical

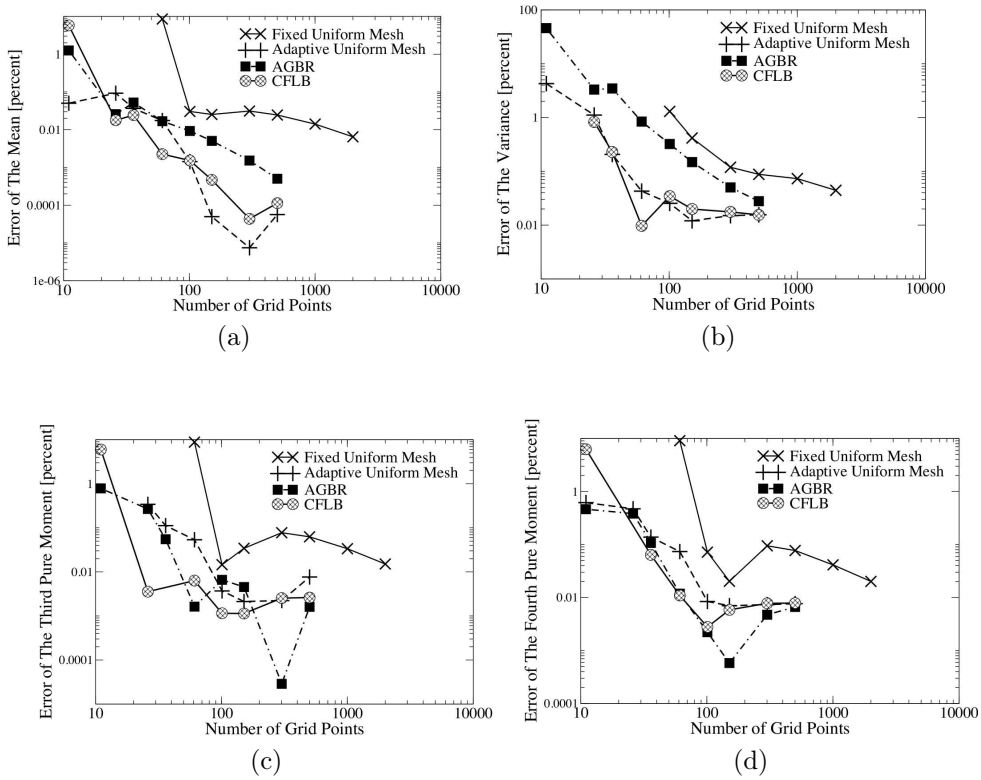

Figure 2.10: Numerical error in the first four response moments corresponding to Problem 1.2 ($< \mu >= 2$) (at time $t = 1$) versus the number of grid points P, for all four algorithms using $N_p = 8$.

solution of Eq. 2.25, are computed using numerical integration of Eq. 2.26.

Equation 2.24 has 3 fixed points: $x = -1$, 1 and 0. Both $x = -1$ and $x = 1$ are stable fixed points while $x = 0$ is an unstable fixed point. Given that the initial conditional density for x has a mean of 2 with a very small standard deviation, one would therefore expect the initial density to evolve towards $x = 1$. The contour of the joint density at $t = 1$ shown in Fig. 2.8b confirms this. Moreover, as $t \to \infty$, the density tends towards a Dirac delta distribution which is also demonstrated in Fig. 2.8.

The evolution of the first four moments of the output random variable x are shown in Fig. 2.9 for the CFLB mesh adaptation with $P = 501$ and $N_p = 10$. The numerical results obtained from the finite difference solution of the Liouville equation are in good agreement with the exact solution. Figure 2.10 compares the error in

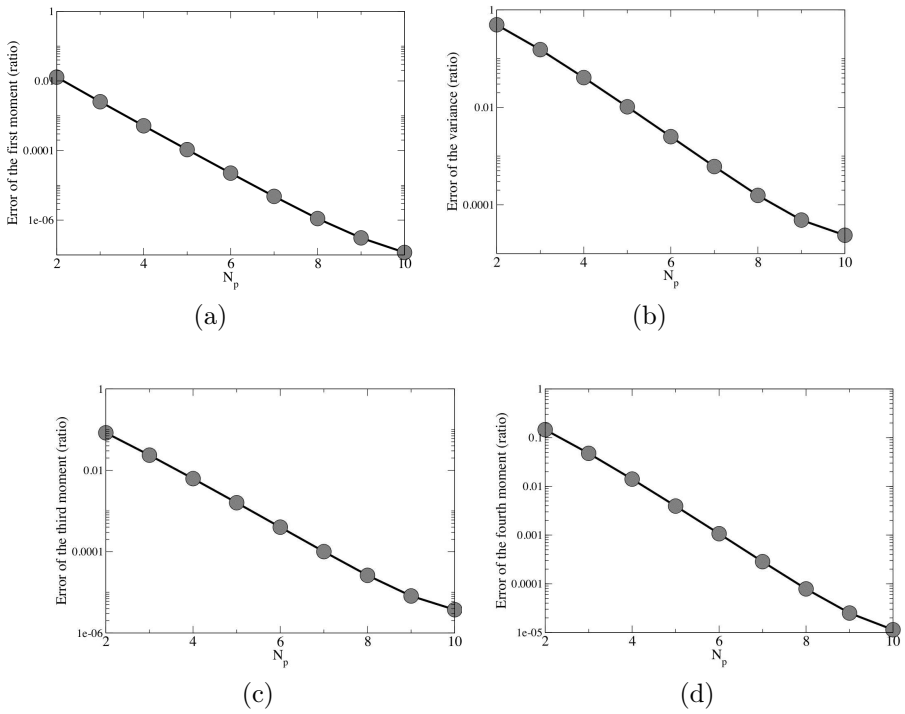

Figure 2.11: Error in the first four moments of response (in Problem 1.2, with $< \mu >= 2$) versus N_p, shown at $t = 1$. using CFLB mesh adaptation with $P = 601$.

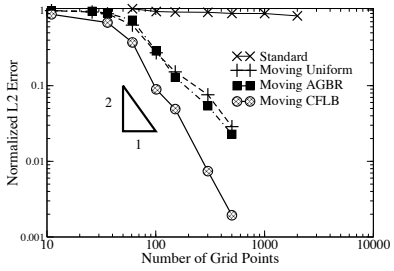

(a) $t = 1$

Figure 2.12: Error in computed conditional density for Problem 1.2 ($< \mu >= 2$) at time $t = 1$ versus the number of grid points P for all 4 algorithms with $N_P = 8$.

the first four moments versus the number of grid points for all three adaptive mesh methods and a fixed grid solution. It can be seen that, in comparison to the fixed grid solution, the adaptive methods are more accurate for a given number of grid points often demonstrating more than an order of magnitude improvement. Here the solution evolves to a deterministic state, which is represented by a Dirac delta function in the response variables space. As such, the Gauss-quadrature integration

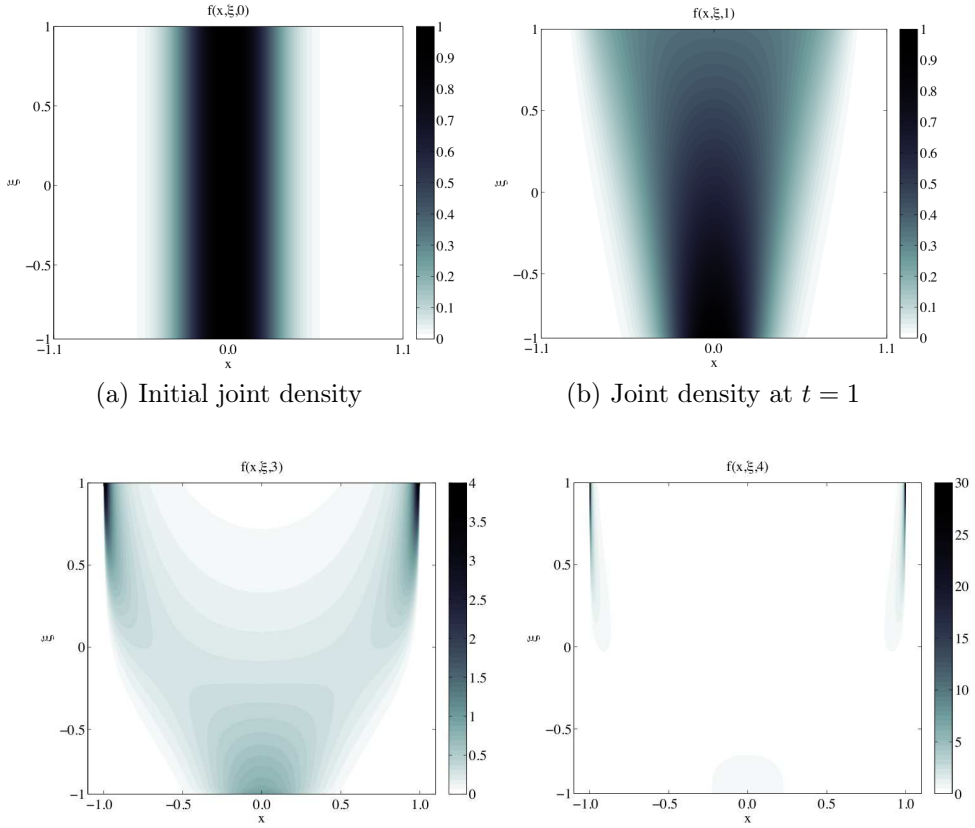

(a) Initial joint density

(b) Joint density at $t = 1$

(c) Joint density at $t = 3$

(d) Joint density at $t = 4$

Figure 2.13: Contours of the JPDF for Problem 1.2 ($< \mu >= 0$) obtained with CFLB mesh adaptation using $N_P = 56$ and $P = 451$.

approach based upon its applied polynomial approximation is unable to fully resolve this discontinuity. Furthermore, high order derivatives does not exist anymore in the response variable space as a result. So the expected order of accuracy can not be obtained and computed values for all moments converge to a value with negligible error. Using the CFLB algorithm with 601 grid points in x, the accuracy of the first four moments versus the number of quadrature points in ξ (N_p) is shown in Fig. 2.11. Similar to the results obtained for the Problem 1.1, the moments accuracy increases as N_p increases.

In Fig. 2.12 the normalized L2 error of the conditional density at $t = 1$ versus the number of grid points in x is shown for each of the adaptive mesh methods and the fixed grid solution. We find that the finite difference solutions on adaptive meshes

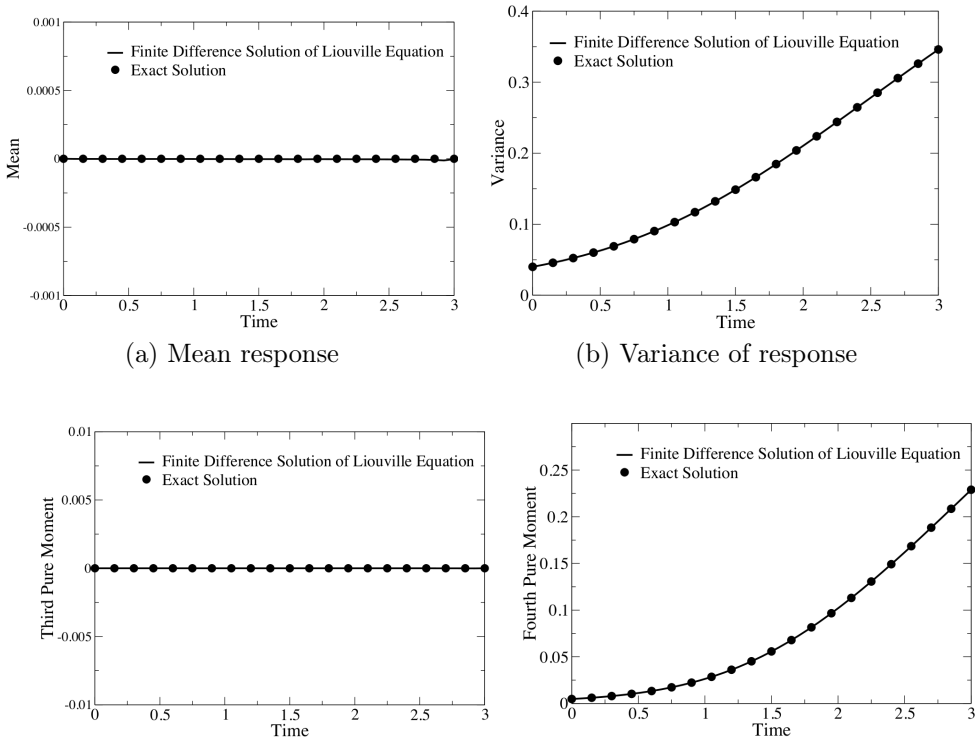

(a) Mean response (b) Variance of response

(c) Pure third moment of response (d) Pure fourth moment of response

Figure 2.14: Time evolution of the response statistics for Problem 1.2 ($< \mu >= 0$). The exact solution is compared with the numerical solution obtained with the AGBR mesh adaptation using $N_p = 10$ and $P = 451$.

not only capture the expected second order accuracy, but also have a lower computational cost (in comparison to the fixed domain based methods). The advantage of adapting the mesh is evident as a solution with less than 10 percent error in the conditional density is found for each of the adaptive methods using 300 points or less. In particular, the results from the CFLB scheme are quite good with an error less than 10 percent with only 100 grid points.

Considering the same uniform density for μ, it is expected that a bimodal density will develop if the initial conditional density is given a mean of 0 (denoted as $< \mu >= 0$ in figure captions). To investigate this case, the Gaussian density for the initial conditional density of μ is assumed to be standard normal($N(0, 0.04)$). Contours of the joint density evolution from $t = 0$ to $t = 4$ are illustrated in Figure 2.13. Figure 2.13c shows the resulting joint density for $t = 3$ where it can be seen that

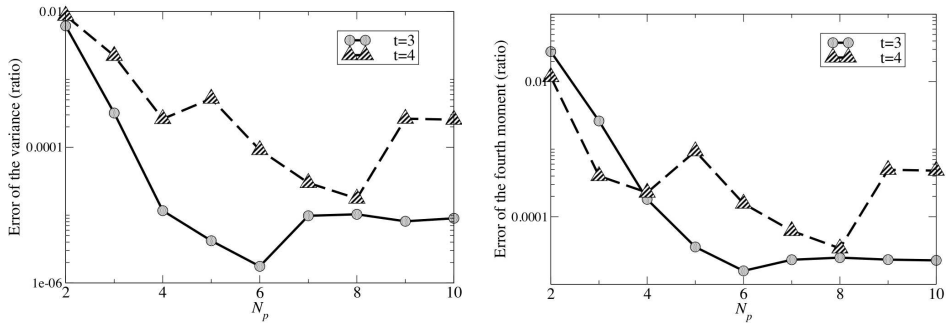

Figure 2.15: Error in computed response variance and fourth moment for Problem 1.2 ($< \mu >= 0$) at times $t = 3$ and $t = 4$ versus the number of quadrature points N_p. Results have been obtained using the AGBR mesh adaptation with $P = 601$.

the density becomes bimodal when ξ is "large positive" while it is unimodal when ξ is near -1. This characteristic becomes more evident as the joint density evolves in time(see Fig. 2.13d).

In Fig. 2.14 the first four moments of the random variable x are shown as a function of time. The computational results obtained using the AGBR method with 451 grid points along x and 8 quadrature points along ξ are in close agreement with the moments computed numerically from the exact solution. In Fig. 2.15 the error in the variance and fourth moment of x versus the number of samples in ξ (N_p) are shown for the AGBR scheme with 601 grid points in x at $t = 3$ and $t = 4$. As can be noted in Fig. 2.15, when compared to the other two cases examined in this chapter, at small times fewer samples of the conditional variable are required for convergence of the moments. This characteristic is likely due to the smoother variation of the JPDF with ξ when compared to the other two problems. At larger times (see the results for $t = 4$ in Fig. 2.15), more samples are required for the convergence as this variation becomes increasingly less smooth with time (compare the probability distribution in Figs. 2.13c and 2.13d). Here the stagnation of the error in the moments (to a small value) is due to the use of a grid in x (601 points) which does not fully resolve the response.

The L2 error in the conditional density at $t = 1, 3$ and 4 is shown in Fig. 2.16 versus the number of grid points in x. Results are shown for each of the adaptive mesh solutions along with the fixed, uniform mesh solution. First it should be noted that this figure demonstrates further that the numerical solution of the Liouville equation is able to give a very accurate approximation ($< 1\%$ error) to the conditional density for each of the methods presented . In particular, the adaptive schemes are able to produce results with this accuracy with less than 500 grid points for each of the times shown. At early times, unlike the previous problems, the adaptive methods do not show as dramatic an improvement over the fixed grid solution. However, the improvement in the accuracy, over the fixed mesh solution, through the use of the adaptive methods increases with time as the JPDF develops sharper gradients. It should be noted that for t=4, none of results exhibit the expected second order accuracy. This is due to the development of two regions of discontinuity in the response space. Moreover, due to accumulation of a large number of grid points at these discontinuities, the solution on the AGBR mesh becomes super convergent at some points in time (see Fig. 2.16b).

One issue which arises when applying the CFLB method to this particular problem is due to the presence of three fixed points within the domain of the numerical solution. At a fixed point $h = 0$ and according to Eq. 2.16 the mesh spacing should go to zero. This problem was not encountered in the previous examples due to the fixed points being located on the boundary of the domain. As zero mesh spacing is obviously not possible, a modification to the base scheme must be developed in order to be able to apply the CFLB method. The modification proposed here involves two steps. First, in regions near the fixed points, the grid is distributed such that, while the grid spacing is still small, the CFL=1 condition is not imposed. The result of this choice is a sharp change in the CFL values as one approaches the fixed points which, in turn, causes instability in the finite difference solution. To over-

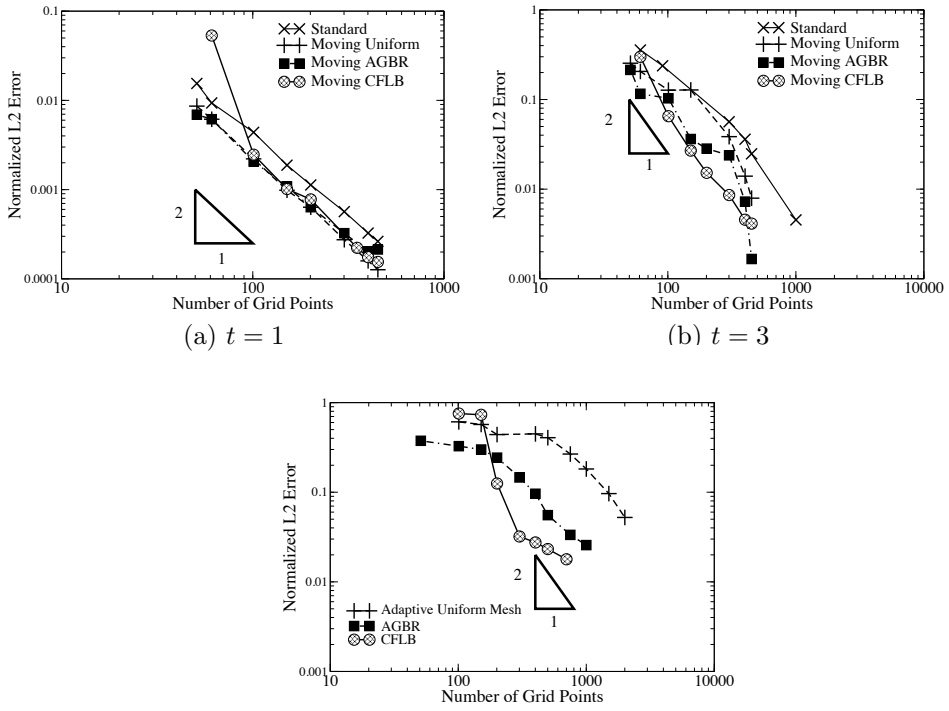

(a) $t = 1$ (b) $t = 3$

(c) $t = 4$

Figure 2.16: Error in computed conditional density for Problem 1.2 ($< \mu >= 0$), at various points in time, versus the number of grid points P (with fixed $N_P = 8$), for all four algorithms.

come this, the numerical solution at the points where CFL$\neq$ 1 (and two neighboring points) is not computed using the finite difference scheme but instead is interpolated (with order equivalent to the finite difference scheme) from the computed data at adjacent nodes. As Fig. 2.16 demonstrates, this modification appears to adequately resolve the problem. However, as stated above, the amount of improvement in the CFLB numerical solution over the fixed mesh solution, which increases with time (see Fig. 2.16c), is not as large for this problem when compared to the other test examples. This outcome may be a result of larger dispersion and diffusion errors due to the local CFL=1 condition not being imposed everywhere. Additional methods for addressing this issue will be investigated in the next chapter.

2.4 Summary

In this chapter, three different adaptive finite difference methods were considered in the context of computational uncertainty quantification (CUQ), in order to achieve improvements in accuracy and efficiency of numerical solution of the underlying hyperbolic PDEs. In particular, the CUQ problem is formulated in terms of the Liouville equation, a linear hyperbolic PDE, that governs the temporal evolution of the joint probability density function of random response (and parameter) variables and the proposed adaptive grid based methods are used to solve it. This application in CUQ is significant from the point of view that finite difference methods are simple to implement for the solution of a hyperbolic PDE like the Liouville equation. The adaptive schemes, which distribute grid points in the response space based upon the problem solution and were demonstrated with two test problems, allow for accurate solution of nonlinear, time varying problems in computational uncertainty quantification. The grid adaptive method, presented in this chapter along with the Gauss-quadrature sampling in the excitation space can be considered as an accurate and efficient alternative to the Monte Carlo simulation for the systems with a limited number of random variables. Furthermore, based on their excellent accuracy at large times for time dependent problems, the methods appear to be good alternatives to conventional intrusive methods like PCE, which have difficulties when applied to such problems.

CHAPTER 3

Grid Adaptation and Non-iterative Defect Correction for Numerical Solution of PDEs

In order to further improve the CFLB method proposed in Chapter 2, we present in this chapter two computational approaches that can improve the order of accuracy of a given finite difference method for solution of linear and nonlinear hyperbolic partial differential equations in one-dimension (besides time). Both methodologies consist of analysis of leading order terms in the discretization error of any given finite difference method, leading to a modified version of the original partial differential equation. Singular perturbations of this modified equation are regularized using an adaptive grid distribution and a non-iterative defect correction method is used to eliminate the leading order, regular perturbation terms in the modified equation. We find that implementation of any of these two approaches on a low order finite difference solution not only increases the order of accuracy but also leads to improvement in numerical stability due to regularization of singular perturbations.

These two methodologies are different only with regard to the grid adaptation technique. In the first approach, the grid adaptation is designed such that the spatial grid and time-step are chosen based on a constrained minimization problem, where the objective function is a chosen global error measure that represents the influence of the leading order singular perturbation term in the truncation error, subject to constraints of numerical stability and geometric bounds. On the other hand, in the second proposed approach a particular choice of an adaptive, non-uniform grid where the local Courant-Friedrich-Levy (CFL) number is unity is used with a remap

procedure whereby a monotonicity preserving interpolant is further used to map the dependent variables from the non-uniform to uniform grids and vice versa.

The proposed approaches are applied to three different canonical problems including the numerical solution of (1) the inviscid Burgers (2) nonlinear reaction-advection and (3) Liouville equations. When compared to exact solutions, the numerical results demonstrate the ability of this method in both boosting the accuracy of finite difference schemes by one order and also providing a fully stable numerical solution. When the proposed method is applied to the first order upwind scheme, the results indicate an improvement in the order of accuracy. In this context, the proposed methods also appears to lack the severe numerical diffusion errors generally found in first order upwind scheme.

3.1 The first approach: Grid adaptation based upon constrained minimization

3.1.1 Theoretical foundation

In this chapter, we consider a first order hyperbolic PDE in the following general form:

$$\frac{\partial f}{\partial t} + \frac{\partial \left(D(f,x,t) f \right)}{\partial x} = S(f,x,t), \tag{3.1}$$

where D and S denote drift and reaction functions, respectively. Equation 3.1 is a nonlinear non-homogeneous PDE which can be solved through approximation of the temporal and spatial derivatives with p-th order accurate finite difference formulas: Eq. 3.2.

$$\sum_{m=n-m_1}^{n+m_2} \beta_m f_i^{(m)} + \sum_{l=i-l_1}^{i+l_2} \alpha_l D_l^{(n)} f_l^{(n)} - S\left(f_i^{(n)} \right) = 0, \tag{3.2}$$

where β_m and α_l are coefficients that depend on the type of finite difference formula

used to approximate the derivatives in Eq. 3.1. It is well known that the solution of of the finite difference equation given in Eq. 3.2, which approximately solves Eq. 3.1, is the exact solution of a different, infinite order partial differential equation often called the modified differential equation [60]. Using Taylor series, the modified equation corresponding to Eq. 3.2 can be derived and its subtraction from the original PDE gives the truncation error expression at grid point x_i and time-step n:

$$\mathrm{TE} = C_P^t \left(\frac{\partial^{p+1} f}{\partial t^{p+1}} \right)_i^n (\Delta t)^p + C_P^x \left(\frac{\partial^{p+1} (Df)}{\partial x^{p+1}} \right)_i^n (\Delta x)^p + \mathcal{O}(\Delta t + \Delta x)^{p+1}, \quad (3.3)$$

where TE denotes the truncation error of the p-th order accurate finite difference approximation and C_P^t and C_P^x are functions of β_m and α_l, respectively. For a first order difference scheme, after elimination of all time-derivatives higher than order one in Eq. 3.3, the truncation error can be written as

$$\begin{aligned} \mathrm{TE} \;=\; & \left(C_P^t D_i^n \Delta t + C_p^x \Delta x\right) \left(\frac{\partial^2 (Df)}{\partial x^2} \right)_i^n + C_P^t \Delta t \Bigg\{ \left(\frac{\partial S}{\partial t} \right)_i^n - \quad (3.4) \\ & \left(\frac{\partial}{\partial x} (DS) \right)_i^n + \left(\frac{\partial D}{\partial x} \frac{\partial (Df)}{\partial x} \right)_i^n - \left(\frac{\partial}{\partial x} \left(f \frac{\partial D}{\partial t} \right) \right)_i^n \Bigg\} + \mathcal{O}(\Delta t + \Delta x)^2. \end{aligned}$$

This truncation error analysis can be easily extended to higher order schemes. The leading order terms in the truncation error expressions can be classified into singular and regular perturbations of the original partial differential equation [33]. A simple means of improving the order of accuracy of finite difference schemes, using information from the truncation error expression, is to subtract the complete leading order expression from the original discretized equation. If the derivative terms in the leading order error expression are then approximated with finite difference formulas of equal or higher order than those used to derive the original finite difference equation, the resulting scheme order will be increased by one. Unfortunately it has been found that inclusion of the singular perturbation terms, in the subtracted expres-

sion, typically results in a unstable numerical solution [30]. An iterative approach using an underlying implicit scheme has been suggested to resolve this issue [30, 32].

The singular perturbative terms in the truncation error expression for a p-th order finite difference scheme can be identified as having the form

$$\Gamma\left(\Delta x, \Delta t\right) = C_P^x \left(\Delta x\right)^p + C_P^t G(D) \left(\Delta t\right)^p, \tag{3.5}$$

where G is a function of drift (D) in Eq. 3.1. If G is constant, the OTS-NIDC approach can be used. This first involves choosing a time-step which makes Eq. 3.5 identically zero thereby resulting in the elimination of the leading order singular perturbative expression. The remaining leading order terms in the truncation error are then subtracted from the original finite difference equation such that the regular perturbative expression is resolved. The final result of the OTS-NIDC approach is a stable numerical solution which has an order of accuracy which is increased by one when compared to the original finite difference equation. Unfortunately if $G(D)$ in Eq. 3.5 is spatially dependent, the OTS-NIDC approach can not be easily applied as the time-steps which result from the procedure are spatially dependent. An alternate way of dealing with this problem is to minimize the singular perturbation terms through proper selection of both temporal and local spatial increments. This is the approach which we use in our constrained minimization method for enhancing the formal order of accuracy of FD schemes.

3.1.2 Underlying finite difference scheme

Here, in order to demonstrate the constrained minimization approach, first order (in space and time) upwinding is chosen as the underlying finite difference scheme whose order of accuracy will be improved through the combined grid adaptation and defect correction approach. Application of the upwinding scheme to Eq. 3.1 results

in the finite difference equation:

$$\begin{aligned} f_i^{n+1} &= f_i^n + (\Delta t/\Delta x)\left(D_{i-1}^n f_{i-1}^n - D_i^n f_i^n\right) + S_i \quad \text{, if } D_i \geq 0, \\ f_i^{n+1} &= f_i^n + (\Delta t/\Delta x)\left(D_i^n f_i^n - D_{i+1}^n f_{i+1}^n\right) + S_i \quad \text{, if } D_i < 0. \end{aligned} \tag{3.6}$$

From Eq. 3.6 C_P^t and C_P^x in Eq. 3.5 can be identified, for $D_i \geq 0$, as -0.5 and 0.5, respectively and as $C_P^t = C_P^x = 0.5$ for $D_i < 0$. Also accordingly $G(D)$ in Eq. 3.5 can be identified as being equal to D. Based upon the heuristic stability analysis approach proposed by Warming and Hyett [60], if the coefficient of the lowest even-order derivative in the truncation error expression is positive, the finite difference scheme is numerically stable. Thus, this scheme is stable if the Courant-Friedrichs-Lewy number ($CFL = D_i^n \Delta t/\Delta x$) is less than or equal to one.

3.1.3 Adaptive grid generation through minimization of an objective function

Over the past several decades a number of different methodologies have been developed for grid adaptation in the context of solving partial differential equations [27, 20, 127, 128]. Typically, these grid adaptation techniques are either based upon the equidistribution principle [55] or minimization of truncation error [51]. In this chapter, the redistribution strategy which is proposed is aimed at eliminating the leading order singular perturbation terms, e.g. Γ in Eq. 3.5, of the modified partial differential equation [129]. The ideal case where the leading order terms are identically zero may not always be attainable, except in a selected classes of PDEs (e.g. one-dimensional wave equation, with a constant wave speed). Hence, minimization of a global error measure is sought, where the error measure is driven to a small quantity (e.g. less than a tolerance value at least smaller than a high-order error term following the leading order error term). In general this can be accomplished

through the solution of a nonlinear, constrained minimization problem for the time-step Δt^n and spatial increments Δx_i^n. Given the set of P_i grid points at time t^n, $\{x_1^n, x_2^n, ..., x_{P_i}^n\}$, along with the values of f on this grid, $\mathbf{F}^n = \{f_1^n, f_2^n, ..., f_{P_i}^n\}$, this minimization problem can be defined as

$$\begin{cases} \min \parallel \mathbf{\Gamma} \parallel_2^2 \\ \sum_{i=1}^{P_i-1} \Delta x_i^n = x_{P_i}^n - x_1^n, \\ x_{P_i}^n = x_{P_i}^{n-1}, \\ x_1^n = x_1^{n-1}, \\ 0 < \Delta t^n < \delta_t, \\ 0 < \Delta x_i^n < x_{P_i}^n - x_1^n \quad i = 1, 2, 3, ..., P_i - 1, \end{cases} \tag{3.7}$$

where

$$\Delta x_i^n = x_{i+1}^n - x_i^n \tag{3.8}$$

$$\Gamma_i \equiv \Gamma_i(\Delta x_i^n, D^n, \Delta t^n) \equiv \Delta x_i^n - |D_{i+1}^n| \Delta t^n \quad , i = 1, 2, 3, ..., P_i - 1 \tag{3.9}$$

In Eq. 3.7, the symbol δ_t denotes the upper bound for Δt^n which is set here to a value of 0.5. Equation 3.7 is solved for the P_i unknowns $\{\Delta x_1^n, \Delta x_2^n, ..., \Delta x_{P_i-1}^n, \Delta t^n\}$ using a standard trust region algorithm designed to solve problems with linear bound constraints [130]. For the particular PDE and finite difference method (based on first order upwinding of Eq. 3.1) used to demonstrate the constrained minimization approach presented in this chapter, the minimum of the objective function, $\parallel \Delta x_i^n - |D_{i+1}^n| \Delta t^n \parallel_2^2$, is always found to be less than a tolerance value of 10^{-13}. Thus, the contribution of the singular perturbations to the leading order terms in the discretization error are neglected (or eliminated). In other words, the original singularly perturbed modified differential equation can be regularized (numerically; with reference to a small tolerance value) via the time adaptive spatial grid obtained

from the constrained minimization approach described above.

If the domain of x, Ω, is infinite, the problem is simplified to the determination of the grid points x_i^n and time-step Δt^n as

$$x_i^n = x_{i+1}^n - \left|D_{i+1}^n\right| \Delta t^n \tag{3.10}$$

$$\Delta t^n = \frac{1}{P_i} \sum_{i=1}^{P_i} \frac{\left|x_{P_i}^n - x_1^n\right|}{(P_i - 1)\, D_i^n} \tag{3.11}$$

The mesh generated with the general approach given in Eq. 3.9, or the simplified approach given in Eqs. 3.10 and 3.11, automatically satisfies the numerical stability condition (e.g. CFL ≤ 1) and eliminates the leading order singular perturbative terms in the modified PDE. It should be noted, however, that a solution of Eq. 3.7 is only possible if $G(D)$ does not contain a fixed point in Ω.

3.1.4 Non-iterative defect correction

In our proposed approaches, similar to the OTS-NIDC approach [33], non-iterative defect correction is used to resolve regular perturbations in the modified differential equation. As the leading order singular perturbation terms are eliminated through the grid redistribution procedure outlined in Section 3.1.3, or alternatively Section 3.2.1, they need not be included in the defect correction which in turn significantly improves the numerical stability of the method. Singularities of the modified equation contribute significantly in the numerical stability of the proposed defect correction approach. Once the singular perturbations are (numerically) regularized through the grid redistribution, the remaining leading order terms in the truncation error expression are eliminated through subtraction from the original low-order discretized equation.

As mentioned, the defect correction involves subtraction of the leading order regular perturbative terms from the original finite difference equation. These terms

then need to be approximated using finite difference approximations. As the purpose of applying the defect correction technique is to improve the accuracy of the scheme, these finite difference approximations must be of the same, or higher order, accuracy as those used to derive the original finite difference equation. When a first order upwinding (see Eq. 3.6) scheme is used, the first oder spatial derivatives contained in the defect correction expression are approximated, on a nonuniform mesh, as:

$$\left(\frac{\partial f}{\partial x}\right)_i = \frac{-\alpha^2 f_{i-1} + f_i\left(\alpha^2 - 1\right) + f_{i+1}}{\Delta x_{i-1}\alpha\left(1+\alpha\right)} + \mathcal{O}(\Delta x_{i-1}^2), \tag{3.12}$$

where $\alpha = \frac{x_{i+1}-x_i}{\Delta x_{i-1}}$. Specific forms of defect corrected finite difference equations will be given in the results section for the various test problems investigated. The combination of the grid redistribution procedure and defect correction eliminates the entire leading order truncation error, resulting in a (at least) one order of magnitude improvement in both the spatial and temporal accuracy.

3.2 The second approach: Remapping with monotonicity preserving interpolation

3.2.1 General approach

The method of modified equation [60] is a tool to study the accuracy, consistency and stability of finite difference schemes. Some authors refer to the modified differential equation as the true PDE that a difference scheme actually solves [60, 16]. Warming and Hyett developed a procedure to remove temporal and mixed derivatives from the first form of the modified equation obtained by Taylor series expansion [60]. Following Hirt stability theory [131], they have introduced a heuristic stability criterion that complies with Von Neumann stability analysis for linear PDEs. Irregular perturbations can be found from the modified equation using this criterion.

Consider a one-dimensional hyperbolic conservation law in its general form:

$$\frac{\partial f}{\partial t} + \frac{\partial F(f,x)}{\partial x} = 0, \quad x \in [a,b] \tag{3.13}$$

where a and b are the domain bounds. Applying the Warming and Hyett approach, the corresponding modified equation for the difference scheme, which approximates the solution of Eq. 3.13 and is mth and nth order accurate in time and space respectively, can be written as

$$\frac{\partial f}{\partial t} + \frac{\partial F(f,x)}{\partial x} + \sum_{i=m}^{\infty}\sum_{j=n}^{\infty}\left(\Delta t^i Q_i(f,x,\Delta x) + \Delta x^j R_j(f,x,\Delta t)\right) = 0, \tag{3.14}$$

where Q_i and R_j are the spatial differential operators corresponding to the terms Δt^i and Δx^j, respectively. For the sake of simplicity, this expression has been written for an equally spaced grid point stencil. Otherwise, the unequal spacing should be taken into account in this expression. According to the heuristic stability theory [131], when a finite difference scheme is numerically stable, the coefficient of the lowest order even derivative among the leading terms in the truncation error expression must be positive. Such a term is classified as an irregular perturbation to the modified equation. Thus, Eq. 3.14 can be rewritten in the following form:

$$\begin{aligned}\frac{\partial f}{\partial t} \quad + \quad & \frac{\partial F(f,x)}{\partial x} + \sum_{i=m}^{\infty}\sum_{j=n}^{\infty}\Delta t^i Q_i'(f,x,\Delta x) + \Delta x^j R_j'(f,x,\Delta t) + \\ & \Gamma(f,x,\Delta t,\Delta x)\mu(f,x) = 0,\end{aligned} \tag{3.15}$$

where the irregular perturbation is assumed to be separable in Δt and Δx and is written as $\Gamma(f,x,\Delta t,\Delta x)\mu(f,x)$. Q_i' and R_j' are Q_i and R_j modified by the removal of the irregular perturbation. As discussed in Section 3.1, a general approach for regularization of these perturbations is to use a grid adaptation based upon the

grading function obtained from setting Γ equal to zero. The remaining terms in the expression for truncation error up to the desired order of accuracy, which correspond to regular perturbations, can simply be discretized and subtracted from the original lower order discretized equation in a non-iterative procedure. It should be noted that the order of finite difference approximation of these terms must be at least equal to or higher than the desired order of accuracy. Accuracy of the solution can be enhanced via numerical solution of the resultant equation using an adaptive mesh.

Unfortunately the approach outlined in Section 3.1.3 is not necessarily monotonicity preserving which can cause Gibbs-like phenomena and spurious oscillations around local extrema or discontinuities. Furthermore considering problems on finite sized spatial domains as well as numerical stability constraints for the original finite difference scheme, it is impractical to redistribute grid points using this strategy over a fixed domain and keep the number of grid points fixed. This problem is difficult to resolve using the constrained minimization approach discussed in Section 3.1.3. However the remapping procedure with monotonicity preserving interpolation proposed here not only resolves the problem but is also more easily extendable to multiple dimensions. In order to enable the grid distribution relation, $\Gamma = 0$, to be satisfied for a fixed domain we allow the number of grid points to be variable and determined based upon both the domain length and the grid distribution equation ($\Gamma = 0$). In this approach, the temporal increment in each time-step is determined by considering a rough estimate derived from the grid distribution equation. Here, $F(x,t)$ in Eq. 3.13 is the product of a drift function ($D(x,t)$) and independent variable f and the distribution equation for the test problems studied in this dissertation reads:

$$\Gamma_i = D_i \Delta t - \Delta x_{i-\frac{1}{2}}, \tag{3.16}$$

where $\Delta x_{i-\frac{1}{2}} \equiv x_i - x_{i-1}$. As such, the temporal increment at the nth time-step can

be found as

$$\Delta t^n = \frac{2\Delta x}{\min\left(D\right)_{a\leq x\leq b} + \max\left(D\right)_{a\leq x\leq b}}, \tag{3.17}$$

Thus, the number of grid points on the adaptive grid ($\mathcal{T}_A$) which depends on the desired number of grid points on the uniform grid ($\mathcal{T}_F$) with a spatial increment of Δx, domain length (L_i), temporal increment (Δt^n) and the grading function can be determined as

$$M_i = 1 + \sum_{j=2} \frac{L_i}{D(x_i,t)\Delta t^n} \boldsymbol{G}\left(L_i - a - \sum_{k=2}^{j} D(x_k,t)\Delta t^n\right). \tag{3.18}$$

where M_i denotes the number of grid points, for the ith dimension (here, $i = 1$), on the adaptive mesh ($\mathcal{T}_A$) and $\boldsymbol{G}(x)$ is an indicator function defined as:

$$\boldsymbol{G}(x) = \begin{cases} 1 & x \geq 0, \\ 0 & x < 0. \end{cases} \tag{3.19}$$

Here, the Dirichlet boundary conditions are imposed through an interpolation.

Prior to performing finite difference computations on the resultant adaptive grid, the response must be known on the newly generated mesh at the previous time step. For this purpose, a monotonicity preserving piecewise cubic Hermite interpolation is applied [123]. Finally, after solving the defect corrected difference equations on the adaptive grid for the current time-step, the solution is interpolated back to the uniform grid. The process is repeated for each time-step as in general Γ varies with time. These steps are outlined in Algorithm 1.

The interpolant, which is used to map the data between $\mathcal{T}_F$ and $\mathcal{T}_A$, is a cubic polynomial with coefficients c_1 to c_4:

$$\tilde{f}(x) = c_1 + c_2(x - x_i) + c_3(x - x_i)^2 + c_4(x - x_i)^3, \tag{3.20}$$

Algorithm 1 Enhancement of the order of accuracy of finite difference schemes by a combination of adaptive grid, non-iterative defect correction and monotonicity preserving interpolation in one dimension

1: set the number of grid points on the uniform mesh
2: set T equal to the desired time
3: set $t = 0$ and $n = 1$
4: set Δt^n using Eq. 3.17
5: find the appropriate number of grid points which covers the entire domain using Eq. 3.18
6: generate the adaptive grid using the grading function derived from $\Gamma = 0$
7: perform the piecewise monotonicity preserving interpolation to find the data on the newly generated grid
8: solve the defect corrected discretized equation on the adaptive grid
9: perform the piecewise monotonicity preserving interpolation to find the solution on the original uniform grid
10: while $t < T$: set $t + \Delta t^n$; set $n = n + 1$; go to step 4

where $x_i \leq x \leq x_{i+1}$. These coefficients are functions of f and the first order spatial derivative, $\dot{f}_i$. They can be evaluated as:

$$\begin{aligned} c_1 &= f(x_i) = f_i, \\ c_2 &= \dot{f}_i, \\ c_3 &= \frac{3S_{i+\frac{1}{2}} - \dot{f}_{i+1} - 2\dot{f}_i}{\Delta x_{i+\frac{1}{2}}}, \\ c_4 &= -\frac{2S_{i+\frac{1}{2}} - \dot{f}_{i+1} - \dot{f}_i}{\Delta x^2_{i+\frac{1}{2}}}, \end{aligned} \tag{3.21}$$

where

$$S_{i+\frac{1}{2}} = \frac{f_{i+1} - f_i}{x_{i+1} - x_i}, \tag{3.22}$$

and $\Delta x_{i+\frac{1}{2}} = x_{i+1} - x_i$. As the accuracy of this cubic interpolant is tied to the accuracy of $\dot{f}_i$, for second order accuracy a parabolic approximation is used:

$$\dot{f}_i = \frac{\Delta x_{i-\frac{1}{2}} S_{i+\frac{1}{2}} + \Delta x_{i+\frac{1}{2}} S_{i-\frac{1}{2}}}{x_{i+1} - x_{i-1}}. \tag{3.23}$$

However, when higher order accuracy is desired, a fourth order finite difference

approximation is applied:

$$\dot{f}_i = \frac{-f_{i+2} + 8f_{i+1} - 8f_{i-1} + f_{i-2}}{-x_{i+2} + 8x_{i+1} - 8x_{i-1} + x_{i-2}}. \tag{3.24}$$

It should be noted that in order to preserve the monotonicity of the function f, Hyman filters limit the values of $\dot{f}_i$ to be restricted to the de Boor-Schwartz piecewise monotonicity range [132, 123, 133]. Thus, the resulting data from this interpolation procedure retain piecewise monotonicity. Even when the initial data are not monotone, by setting $\dot{f}_i = 0$ the interpolant enforces inter-interval monotonicity on the data [123].

3.2.2 Application to first order upwind scheme

In order to better illustrate the proposed approach, we consider a one-dimensional Liouville equation:

$$\frac{\partial f}{\partial t} + \frac{\partial \left(D(x) f\right)}{\partial x} = 0. \tag{3.25}$$

Applying a first order upwind scheme to approximate the solution of Eq. 3.25 and assuming $D(x) \geq 0$, one can write:

$$f_i^{n+1} = f_i^n - \Delta t \frac{D_i f_i^n - D_{i-1} f_{i-1}^n}{\Delta x_{i-\frac{1}{2}}}, \tag{3.26}$$

and when $D(x) < 0$, it reads

$$f_i^{n+1} = f_i^n - \Delta t \frac{D_{i+1} f_{i+1}^n - D_i f_i^n}{\Delta x_{i+\frac{1}{2}}}, \tag{3.27}$$

where $D_i = D(x_i)$ and $\Delta x_{i-\frac{1}{2}} = x_i - x_{i-1}$. Using the Warming and Hyett technique [60], the corresponding modified equation for Eq. 3.26 is obtained as follows:

$$\frac{\partial f}{\partial t} + \frac{\partial D(x) f}{\partial x} + \frac{1}{2}\left(D_i \Delta t - \Delta x_{i-\frac{1}{2}}\right)\left(\frac{\partial^2 (Df)}{\partial x^2}\right)_i^n - \frac{\Delta t}{2}\left(\frac{dD}{dx}\frac{\partial (Df)}{\partial x}\right)_i^n + \mathcal{O}(\Delta x_{i-\frac{1}{2}}^2 + \Delta t^2) = 0. \tag{3.28}$$

Based on the heuristic stability analysis theory [131], Γ is the coefficient of lowest even order derivative in Eq. 3.28:

$$\Gamma_i = D_i \Delta t - \Delta x_{i-\frac{1}{2}}. \tag{3.29}$$

Equation 3.29 is the characteristic equation for this discretization and can be used as the grading function for generating the adaptive grid and consequently automatic regularization of the singularity in the modified equation. The remaining terms can be used to improve the order of accuracy up to the desired level. For instance, based on Eq. 3.28, the following discretized equation is derived to obtain second order accuracy in both space and time:

$$\tilde{f}_i^{n+1} = \tilde{f}_i^n + \left(\Delta t^n / \Delta x_{i-\frac{1}{2}}^n\right)\left(D_{i-1}^n \tilde{f}_{i-1}^n - D_i^n \tilde{f}_i^n\right) + \frac{(\Delta t^n)^2}{2}\left(\tilde{f}_i^n \left((D_x)_i^n\right)^2 + D_i^n \frac{-\alpha^2 \tilde{f}_{i-1}^n + \tilde{f}_i^n (\alpha^2 - 1) + \tilde{f}_{i+1}^n}{\Delta x_{i-\frac{1}{2}}^n \alpha (1+\alpha)} (D_x)_i^n\right). \tag{3.30}$$

Similarly when $D_i < 0$, the resultant second order discretization is obtained as:

$$\tilde{f}_i^{n+1} = \tilde{f}_i^n + \left(\Delta t^n / \Delta x_{i+\frac{1}{2}}^n\right)\left(D_i^n \tilde{f}_i^n - D_{i+1}^n \tilde{f}_{i+1}^n\right) + \frac{(\Delta t^n)^2}{2}\left(\tilde{f}_i^n \left((D_x)_i^n\right)^2 + D_i^n \frac{-\alpha^2 \tilde{f}_{i-1}^n + \tilde{f}_i^n (\alpha^2 - 1) + \tilde{f}_{i+1}^n}{\Delta x_{i-\frac{1}{2}}^n \alpha (1+\alpha)} (D_x)_i^n\right), \tag{3.31}$$

where $\tilde{f}_i^n$ is the interpolated value of the function at the ith grid point of the adaptive grid generated at nth time-step using Eq. 3.29 and $\alpha = \Delta x_{i+\frac{1}{2}}/\Delta x_{i-\frac{1}{2}}$. Also, the subscript $_x$ denotes differentiation with respect to x.

As mentioned earlier, this procedure can be used to improve the accuracy of any base scheme up to any desired accuracy. For example, performing truncation error analysis for the first order upwind scheme (Eq. 3.27) while considering $\Delta x_{i-\frac{1}{2}}$ to be spatially dependent ($\Delta x_{i-\frac{1}{2}} = D_i \Delta t$), the following expression is derived for non-iterative defect correction to obtain third order of accuracy both in space and time:

$$\begin{aligned} \text{TE} \;=\; & -\frac{\Delta t}{2}\left(\frac{dD}{dx}\frac{\partial (Df)}{\partial x}\right) + \frac{\Delta t^2}{6}\left(f\left(\frac{dD}{dx}\right)^3 + 4f\left(D\frac{dD}{dx}\frac{d^2D}{dx^2}\right) + \right. \\ & \left. 7D\left(\frac{dD}{dx}\right)^2\frac{\partial f}{\partial x} + D^2\frac{d^2D}{dx^2}\frac{\partial f}{\partial x} + 3D^2\frac{dD}{dx}\frac{\partial^2 f}{\partial x^2}\right) + \\ & \mathcal{O}(\Delta x_{i-\frac{1}{2}}^3 + \Delta t^3), \end{aligned} \tag{3.32}$$

Finite difference approximation of higher order derivatives in this expression up to a desired accuracy can be evaluated on a uniform grid using a simple transformation to a computational coordinate system. Here in order to obtain third order accuracy, fourth order finite difference approximations on a uniform stencil are used and then through a computational mapping the derivatives are computed on the adaptive mesh. the discretized form of Eq. 3.32 is subtracted from the original discretization (Eq. 3.27) resulting in the defect corrected scheme to be solved on the adaptive grid.

A question that could be raised is the possibility of using non-iterative defect correction alone to remove singular perturbations and obtain a numerically stable solution. As mentioned by Kress [30], it can be shown with a simple example that such a possibility does not exist. For this purpose, assume D in Eq. 3.31 to be a constant ($D(x) = c > 0$). It is well-known that choosing an optimal time-step $\Delta t = \Delta x_{i-\frac{1}{2}}/c$ eliminates all of the truncated error terms resulting in

an exact numerical results [17]. However, if one desires to use non-iterative defect correction instead to achieve second order accuracy, the resultant difference scheme on a uniform grid becomes:

$$f_i^{n+1} = f_i^n + (\Delta t \times c/\Delta x)\left(f_{i-1}^n - f_i^n\right) + \frac{c\Delta t}{2}(c\Delta t - \Delta x)\frac{f_{i+1}^n - 2f_i^n + f_{i-1}^n}{\Delta x^2}. \quad (3.33)$$

Equation 3.33 can be rewritten as

$$f_i^{n+1} = f_i^n + \frac{\sigma}{2}(\sigma - 1)\delta f_{i+\frac{1}{2}}^n - \frac{\sigma}{2}(\sigma + 1)\delta f_{i-\frac{1}{2}}^n, \quad (3.34)$$

where $\sigma = c\Delta t/\Delta x$ and $\delta f_{i+\frac{1}{2}}^n = f_{i+1}^n - f_i^n$. Based on the monotonicity criteria put forth by Harten [38], this scheme is not monotonicity preserving and produces spurious oscillations near local extrema or discontinuity as

$$C_{i+\frac{1}{2}}^{-(1)} = \frac{c}{2}(\sigma - 1) < 0, \quad (3.35)$$

for the numerically stable region in which $|\sigma| \leq 1$. Here, C is a constant derived from the incremental discretization (Eq. 3.34), which is used for the monotonicity test. This constant must be positive for the scheme to be TVD [38]. This result can be confirmed just by examining the propagation of a simple Gaussian distribution with a small standard deviation (see Fig. 3.1). Such an unfavorable outcome signifies the importance of employing grid adaptation as a general solution to eliminate singular perturbations without producing numerical instability or spurious oscillations.

3.2.3 Application to second order MacCormack scheme

It is also interesting to study the application of this methodology to higher order schemes. The MacCormack scheme gives the following discretized equation when it

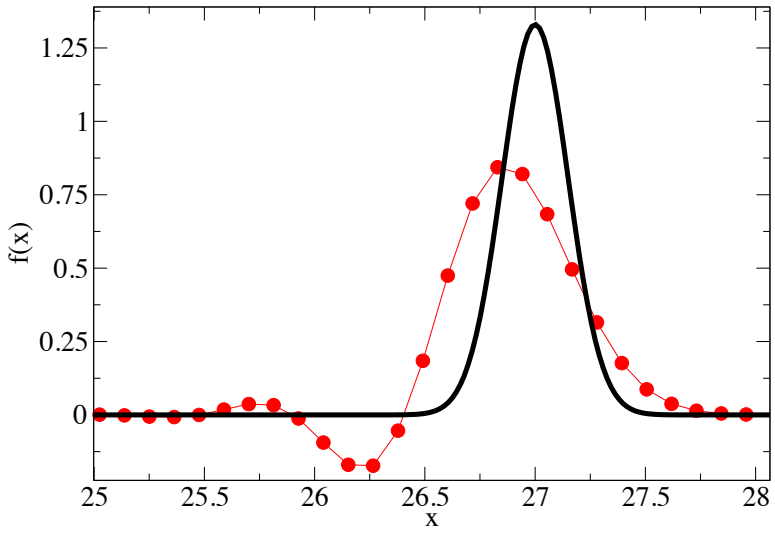

Figure 3.1: Gibbs-like phenomena near a local extrema for a discretization modified by non-iterative defect correction (Eq. 3.34); Comparison includes the exact solution (solid line) and the solution with non-iterative defect correction (circles)

is applied to Eq. 3.25:

$$\begin{aligned} f_i^{n+1} &= f_i^n - \frac{\Delta t}{\Delta x_{i-\frac{1}{2}}}\left(D_i f_i^n - D_{i-1} f_{i-1}^n\right) + \\ &\quad \frac{\Delta t}{2\Delta x_{i+\frac{1}{2}}}\left(D_i \frac{\Delta t}{\Delta x_{i-\frac{1}{2}}} - 1\right)\left(D_{i+1} f_{i+1}^n - D_i f_i^n\right) - \\ &\quad \frac{\Delta t}{2\Delta x_{i-\frac{1}{2}}}\left(D_{i-1} \frac{\Delta t}{\Delta x_{i-\frac{1}{2}}} - 1\right)\left(D_i f_i^n - D_{i-1} f_{i-1}^n\right). \end{aligned} \tag{3.36}$$

Similar to the results obtained for the first order upwind scheme, truncation error analysis gives Eq. 3.29 as the characteristic equation ($\Gamma = 0$) of the MacCormack method. Assuming that D_i and D_{i+1} are negative and setting $x_{i-\frac{1}{2}} = -D_i \Delta t$ and $x_{i+\frac{1}{2}} = -D_{i+1}\Delta t$, an expression for the second order defect correction can be obtained in a similar manner as Eq. 3.32 (see the Appendix C). The resultant expression includes some first order error terms which are produced only due to the non-uniformity of the adaptive grid. Applying this defect correction (Eq. C.1) to the MacCormack scheme (Eq. 3.36) and performing the finite difference computations on the adaptive grid results in third order accuracy for both space and time. Such an

approach can be used to enhance the order of accuracy of the MacCormack scheme to any desired order of accuracy.

3.3 Results and discussion

3.3.1 Problem 3.1: Inviscid Burgers equation

In this section the numerical solution of Burgers equation, a well-known model equation in fluid dynamics [16], will be investigated using both minimization and remap methods for grid adaptation. In its inviscid form, this equation is a nonlinear homogeneous hyperbolic PDE and can be written as:

$$f_t + \left(\frac{f^2}{2}\right)_x = 0. \tag{3.37}$$

Applying the first order upwind method, the original low-order discretized equation is given by:

$$\begin{cases} f_i^{n+1} = f_i^n + \left(\frac{\Delta t^n}{2\Delta x_{i-1}^n}\right)\left(\left(f_{i-1}^n\right)^2 - \left(f_i^n\right)^2\right), & \text{if } f_i^n \geq 0, \\ f_i^{n+1} = f_i^n + \left(\frac{\Delta t^n}{2\Delta x_i^n}\right)\left(\left(f_i^n\right)^2 - \left(f_{i+1}^n\right)^2\right), & \text{if } f_i^n < 0 \end{cases} \tag{3.38}$$

where we recognize that D and S from Eq. 3.6 are $\frac{f^2}{2}$ and $S = 0$ respectively. Thus, the truncation error expression can be derived from Eq. 3.5 as:

$$\text{TE} = \frac{f_i^n}{2}\left(f_{xx}\right)_i^n\left(\Delta x_{i-1}^n - f_i^n \Delta t^n\right) + \left(\frac{\Delta x_{i-1}^n}{2} - f_i^n \Delta t^n\right)\left(\left(f_x\right)_i^n\right)^2 + \mathcal{O}(\Delta t^n + \Delta x_{i-1}^n)^2. \tag{3.39}$$

and

$$\text{TE} = -\frac{f_i^n}{2}\left(f_{xx}\right)_i^n\left(\Delta x_i^n + f_i^n \Delta t^n\right) - \left(\frac{\Delta x_i^n}{2} + f_i^n \Delta t^n\right)\left(\left(f_x\right)_i^n\right)^2 + \mathcal{O}(\Delta t^n + \Delta x_i^n)^2. \tag{3.40}$$

for $f_i^n \geq 0$ and $f_i^n < 0$, respectively. The terms used to redistribute the grid are $\Gamma_i = (\Delta x_{i-1} - f_i^n \Delta t^n)$ and $\Gamma_i = (\Delta x_i + f_i^n \Delta t^n$ for $f_i^n \geq 0$ and $f_i^n < 0$, respectively. Subtraction of the remaining (regular perturbative) leading order truncation terms from Eq. 3.38 gives

$$\begin{aligned} f_i^{n+1} &= \tilde{f}_i^n + \left(\frac{\Delta t^n}{2\Delta x_{i-1}^n}\right)\left(\left(\tilde{f}_{i-1}^n\right)^2 - \left(\tilde{f}_i^n\right)^2\right) - \\ &\Delta t^n \left(\frac{-\alpha^2 \tilde{f}_{i-1}^n + \tilde{f}_i^n\left(\alpha^2 - 1\right) + \tilde{f}_{i+1}^n}{\Delta x_{i-1}^n \alpha\left(1+\alpha\right)}\right)^2 \left(\frac{\Delta x_{i-1}^n}{2} - \tilde{f}_i^n \Delta t^n\right), \quad \text{if } \tilde{f}_i^n \geq 0, \end{aligned} \tag{3.41}$$

$$\begin{aligned} f_i^{n+1} &= \tilde{f}_i^n + \left(\frac{\Delta t^n}{2\Delta x^n}\right)\left(\left(\tilde{f}_i^n\right)^2 - \left(\tilde{f}_{i+1}^n\right)^2\right) + \\ &\Delta t^n \left(\frac{-\alpha^2 \tilde{f}_{i-1}^n + \tilde{f}_i^n\left(\alpha^2 - 1\right) + \tilde{f}_{i+1}^n}{\Delta x_{i-1}^n \alpha\left(1+\alpha\right)}\right)^2 \left(\frac{\Delta x^n}{2} + \tilde{f}_i^n \Delta t^n\right), \quad \text{if } \tilde{f}_i^n < 0, \end{aligned} \tag{3.42}$$

For this test problem, the initial velocity profile at $t = 0$ is defined to be:

$$f(x, 0) = 3 - \cos(x), \tag{3.43}$$

in the domain of computation which is bounded within $x = 0$ and $x = 8$ and the boundary conditions for f are given as

$$f(0, t) = f(8, t) = 2. \tag{3.44}$$

The exact solution to Eqs. 3.37, with boundary conditions given by Eq. 3.44, is

$$f(x, t) = 3 - \cos(x - f(x, t)t). \tag{3.45}$$

Setting the solution of the (nonlinear) Eq. 3.45, obtained with the Newton-Raphson method, as the reference solution, the L2 error is computed. In this dis-

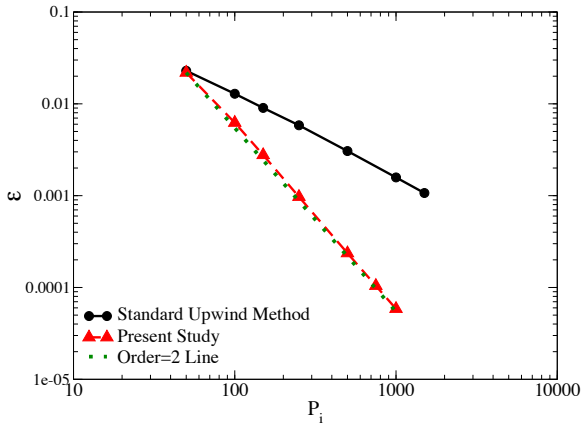

Figure 3.2: Error in the numerical solution for Problem 3.1 at t =0.8 versus the number of grid points, P_i. Numerical solutions obtained from the standard first order upwind finite difference method are compared with those obtained using grid adaptation and non-iterative defect correction (with constrained minimization). In the computation of error, the analytical solution is considered as the reference solution.

sertation, for P_i grid points in x, the normalized L2 error is obtained as:

$$\varepsilon(t) = \left\{ \frac{\sum_{i=1}^{M} \left(f_{\mathrm{e}}(x_i,t) - \tilde{f}(x_i,t) \right)^2}{\sum_{i=1}^{M} \left(f_{\mathrm{e}}(x_i,t) \right)^2} \right\}^{1/2}, \tag{3.46}$$

where f_{e} is the fully resolved (or exact when known) solution. The L2 error for the original and modified scheme, at $t = 0.8$, are shown in Fig. 3.2. Comparison of the the convergence rate in the results clearly indicates one order of accuracy enhancement when the proposed methodology is used. Here, since the domain of computation is bounded, the grid at each time-step is generated based upon the nonlinear constrained minimization problem defined in Eq. 3.7. Using the set of grid point locations from the previous time-step as the initial guess for the trust-region algorithm, the number of iterations necessary to reach convergence is less than 10. In this algorithm, the iterations are converged if any of the following values are smaller than predefined tolerances $(\varepsilon_1, \varepsilon_2, ..., \varepsilon_6)$: the trust region area Δ, L2 norm of the functional values $||f||_2$, L2 norm of the Jacobian matrix $||J||_2$, the trial step size of the iterations λ or the expression $||f||_2 - ||f - J \times S||_2$. Here, the tolerance

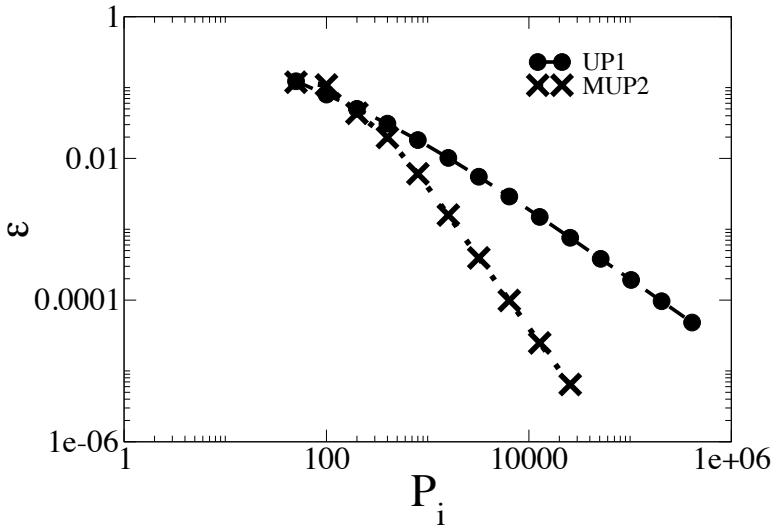

Figure 3.3: L2 Error in the computed solution for Problem 3.1 with a Gaussian initial distribution at t =30 versus the number of (uniform) grid points, P_i. Numerical solutions obtained from the standard first order upwind (UP1) finite difference method are compared with those obtained using grid adaptation and non-iterative defect correction (second order modified upwind method, MUP2, modified using remap with monotonicity preserving interpolation). In the computation of the error, the analytical solution is considered as the reference solution.

ε_1 is set to 10^{-10} and the remaining convergence criteria (or tolerances) are fixed at a value smaller than machine precision.

The major drawback with the constrained minimization approach is the grid adaptation issue with the regions in which very small values of drift function (which is $\frac{f}{2}$ here) exist. In such cases the constrained minimization problem (Eq. 3.9) becomes impossible to solve as the coefficient of Δt^n in the objective function Γ_i becomes very small. Such an issue can be solved using the remap methodology by keeping a uniform grid spacing in the regions where $|f_i^n \Delta t^n| < \gamma\,(x_i - x_{i-1})$. For instance, if the function f initially is given as:

$$f(x,0) = \frac{1}{\sqrt{2\pi}\sigma} \exp\left\{ -\frac{(x-\mu)^2}{2\sigma^2} \right\}, \tag{3.47}$$

where $\sigma = 2$, $\mu = 12.0$ and $x \in [0, 30]$. Application of the approach based upon remapping and monotonicity preserving interpolation, for the case $\gamma = 0.1$, results

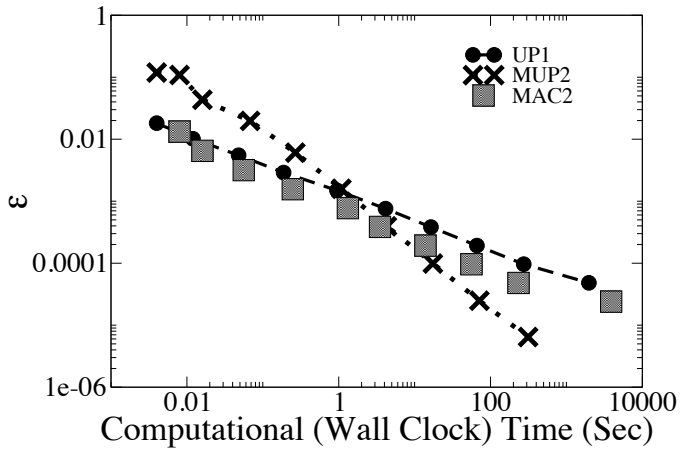

Figure 3.4: L2 Error in the computed solution for Problem 3.1 with a Gaussian initial distribution at t =30 versus computational (wall clock) time. Numerical solutions obtained from the standard first order upwind (UP1) and the second order MacCormack (MAC2) methods are compared with those obtained using grid adaptation and non-iterative defect correction (second order modified upwind method, MUP2, modified using remap approach). In the computation of the error, the analytical solution is considered as the reference solution.

in improving the formal order of accuracy from one to two for the underlying scheme (first order upwind scheme). Such an enhancement is illustrated in Fig. 3.3. Also as shown in Fig. 3.4, comparison with respect to the computational (wall clock) time very well demonstrate the computational efficiency of this approach which is even higher than that of the MacCormack scheme. Here, unlike the MacCormack scheme results, the solution obtained from our proposed technique gives second order accuracy at a time very close to the occurrence of a discontinuity (shock) in the response.

3.3.2 Problem 3.2: Nonlinear reaction-advection equation

The next test problem in this chapter consists of the numerical solution of a nonlinear non-homogeneous hyperbolic PDE which represents logistic population growth coupled with an advective process. Here, only results from constrained minimization based grid adaptation will be presented.

The differential equation which governs the time evolution of the scaled, strictly

positive, population density ρ, which contains both reaction and drift functions, is given by [134]:

$$\rho_t - \left(\rho^2/2\right)_x = \rho\left(1-\rho\right) \tag{3.48}$$

with an initial distribution for ρ given as:

$$\rho(x,0) = \frac{1}{2}\left[2 + \mathrm{e}^x + \mathrm{e}^{\frac{x}{2}}\sqrt{4+\mathrm{e}^x}\right]. \tag{3.49}$$

Eq. 3.48 is solved on a fixed domain of computation $x \in [0,1]$, where the time-dependent boundary conditions are given as:

$$\rho(0,t) = \frac{\mathrm{e}^{-t}}{2}\left[2\mathrm{e}^t + 1 + \sqrt{4\mathrm{e}^t+1}\right]. \tag{3.50}$$

$$\rho(1,t) = \frac{\mathrm{e}^{-t}}{2}\left[2\mathrm{e}^t + \mathrm{e} + \mathrm{e}^{\frac{1}{2}}\sqrt{4\mathrm{e}^t+\mathrm{e}}\right]. \tag{3.51}$$

After considerable algebra, the exact solution of Eq. 3.48, with the corresponding initial and boundary conditions, is obtained as

$$\rho(x,t) = \frac{\mathrm{e}^{-t}}{2}\left[2\mathrm{e}^t + \mathrm{e}^x + \mathrm{e}^{\frac{x}{2}}\sqrt{4\mathrm{e}^t+\mathrm{e}^x}\right]. \tag{3.52}$$

As in the previous problems, the first order upwind scheme is applied to approximate the solution of Eq. 3.48 and the expression for the truncation error is given by:

$$\begin{aligned} \mathrm{TE} \;=\; & \left(\frac{1}{2}\right)\left(\Delta x_i^n - \rho_i^n \Delta t^n\right)\rho_i^n\left(\rho_{xx}\right)_i^n + \left(\frac{\Delta x_i^n}{2} - \rho_i^n \Delta t^n\right)\left(\left(\rho_x\right)_i^n\right)^2 + \\ & \frac{\Delta t^n}{2}\left\{\rho_i^n\left(\rho_x\right)_i^n\left(3-5\rho_i^n\right) - 3\left(\rho_i^n\right)^2 + 2\left(\rho_i^n\right)^3 + \rho_i^n\right\} + \mathcal{O}(\Delta t^n + \Delta x_i^n)^2. \end{aligned} \tag{3.53}$$

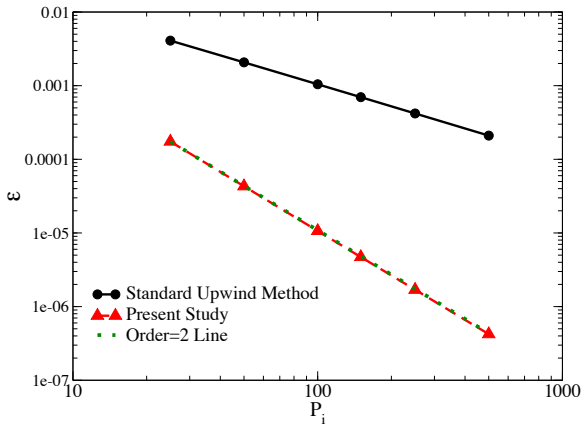

Figure 3.5: Error in the computed solution for Problem 3.2 at t =1 versus the number of grid points, P_i. Numerical solutions obtained from the standard first order upwind finite difference method are compared with those obtained using grid adaptation and non-iterative defect correction (with constrained minimization). In the computation of error, the analytical solution is considered as the reference solution.

From Eq. 3.54 we identify the term used to redistribute the grid as:

$$\Gamma_i = \Delta x_i^n - \rho_i^n \Delta t^n. \tag{3.54}$$

Based upon the modified equation approach proposed by Warming and Hyett [60], which gives the necessary condition for numerical stability, it is found that the numerical solution is stable only if Γ_i is positive, e.g. the local CFL number must be less than one. After subtraction of the leading order regular perturbative expression from the original low-order finite difference equation we arrive at the finite difference

equation used to solve for ρ_i and time-step $n+1$:

$$\begin{aligned}\rho_i^{n+1} &= \tilde{\rho}_i^n + \left(\frac{\Delta t^n}{2\Delta x_i^n}\right)\left(\left(\tilde{\rho}_{i-1}^n\right)^2 - \left(\tilde{\rho}_i^n\right)^2\right) + \\ &\Delta t^n \tilde{\rho}_i^n\left(1-\tilde{\rho}_i^n\right) - \Delta t^n\left(\frac{-\alpha^2\tilde{\rho}_{i-1}^n + \tilde{\rho}_i^n\left(\alpha^2-1\right) + \tilde{\rho}_{i+1}^n}{\Delta x_{i-1}^n \alpha\left(1+\alpha\right)}\right)^2\left(\frac{\Delta x_i^n}{2} - \tilde{\rho}_i^n \Delta t^n\right) + \\ &\left(\frac{\left(\Delta t^n\right)^2}{2}\right)\left(\tilde{\rho}_i^n \frac{-\alpha^2\tilde{\rho}_{i-1}^n + \tilde{\rho}_i^n\left(\alpha^2-1\right) + \tilde{\rho}_{i+1}^n}{\Delta x_{i-1}^n \alpha\left(1+\alpha\right)} \times\right. \\ &\left.\left(3-5\tilde{\rho}_i^n\right) + \tilde{\rho}_{i+1}^n + 2\left(\tilde{\rho}_{i+1}^n\right)^3 - 3\left(\tilde{\rho}_{i+1}^n\right)^2\right), \quad \tilde{\rho}_i^n \geq 0.\end{aligned} \tag{3.55}$$

In Eq. 3.56, we have approximated the first derivative terms contained in the regular perturbative expressions using Eq. 3.12. If the finite difference computations are performed on an adaptive grid defined through Eq. 3.7, with Γ_i defined in Eq. 3.54, the finite difference equation given in Eq. 3.56 is second order accurate and numerically stable. This is confirmed by the results given in Figs. 3.5 and 3.6, where it can be seen that the numerical results obtained with the proposed method are second order accurate in both space and time (in contrast to the base first order upwind method). Here, as the temporal increment is variable in time an averaged value ($\Delta t_{\text{average}}$) is considered in Fig 3.6 when verifying the temporal order of accuracy. Also, similar to the previous test problems, in order to compute the L2 error the exact solution is considered as the reference value.

3.3.3 Problem 3.3: One-dimensional Liouville equation

The last test problem which is used to demonstrate both proposed methodologies, involves the numerical solution of the Liouville equation [135, 136, 137]:

$$f_t + \left(D(x)f\right)_x = 0. \tag{3.56}$$

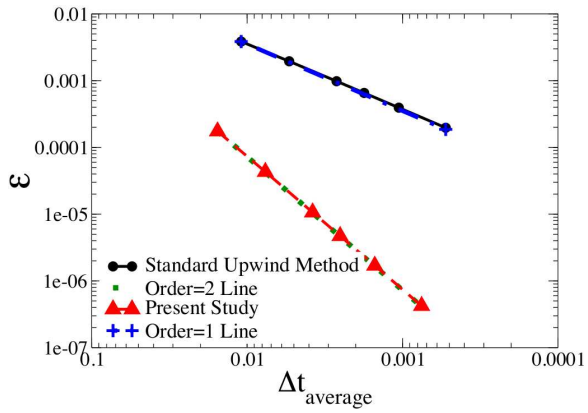

Figure 3.6: Error in the computed solution for Problem 3.2 at t =1 versus the averaged time-step, $\Delta t_{\text{average}}$. Numerical solutions obtained from the standard first order upwind finite difference method are compared with those obtained using grid adaptation and non-iterative defect correction (with constrained minimization). In the computation of error, the analytical solution is considered as the reference solution.

In the Liouville equation the drift function, $D \equiv D(x)$, is only a function of the spatial component x, and there is no source term. After application of the first order upwind scheme to approximate the solution of Eq. 3.56, the leading order truncation error can be written as

$$\text{TE} = -\frac{1}{2}\left(D_i^n \Delta t \mp \Delta x_i\right)\left((Df)_{xx}\right)_i^n - \frac{\Delta t}{2}\left(D_x\left(Df\right)_x\right)_i^n + \mathcal{O}(\Delta t + \Delta x_i)^2, \quad (3.57)$$

for $D \geq 0$ and $D < 0$, respectively, and $\Gamma_i = D_i^n \Delta t \mp \Delta x_i$. Next, applying the defect correction step on the original discretized equation gives Eqs. 3.30 and 3.31.

In this test problem framework, two different cases with linear ($D(x) = -x$) and nonlinear ($D(x) = x - x^3$) drift functions are investigated with the both proposed approaches. First, we consider the case for $D(x) = -x$, where the domain of x is given by $x \in [0.1, 45]$. A standard benchmark test problems used to demonstrate the ability of finite difference schemes to accurately capture discontinuities is the square wave propagation problem. Here, the initial condition for the function f is

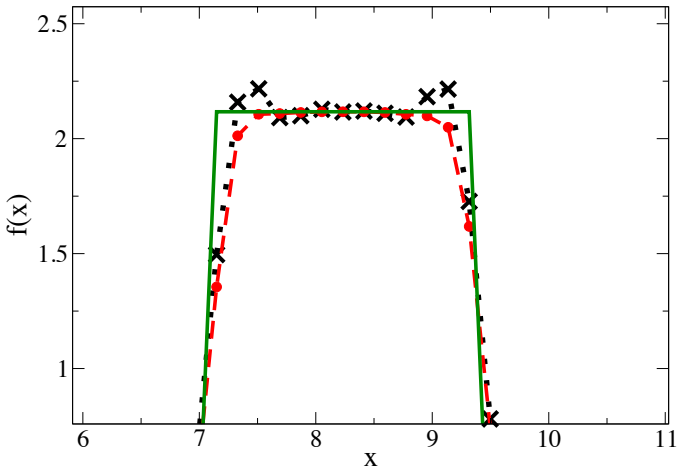

Figure 3.7: Square wave propagation under Liouville equation using remap method at $t = 0.75$; Comparison includes the exact solution (solid line), the solution with cubic spline interpolation (crosses) and the solution with monotonicity preserving interpolation (dotted line)

given as

$$f(x,0) = \begin{cases} 1 & \text{if } 15 \leq x \leq 20, \\ \\ 0 & \text{otherwise.} \end{cases} \tag{3.58}$$

The exact solution for this equation and initial condition reads

$$f(x,t) = \begin{cases} e^t & \text{if } 15 \leq xe^t \leq 20, \\ \\ 0 & \text{otherwise.} \end{cases} \tag{3.59}$$

Equation 3.25 is solved with different approaches such as the third order ENO/second order Runge-Kutta scheme and the results at $t = 0.75$ are illustrated in Figs. 3.7 and 3.8 in which P_i is the number of grid points on the original uniform grid in the ith dimension (here, $i = 1$). The importance of using a monotonicity preserving interpolation scheme is highlighted in Fig. 3.7, where the modified scheme (Eq. 3.31) based on standard cubic spline interpolation (i.e. without the monotonicity preserving feature) performs worse (in the context of capturing discontinuities without

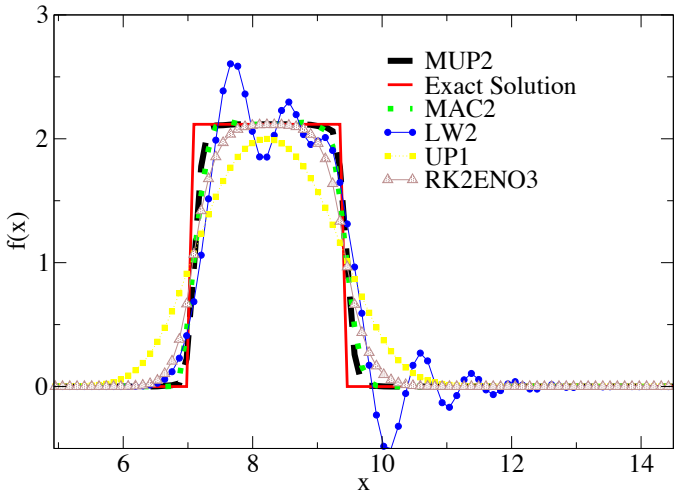

Figure 3.8: Numerical solution for square wave propagation under Liouville equation at $t = 0.75$; comparison between different standard schemes includes the exact solution, second order MacCormack scheme (MAC2), second order Lax-Wendroff (LW2), first order upwind (UP1), second order Runge-Kutta third order ENO (RK2ENO3) and the second order upwind method modified by the remap method (MUP2)

spurious oscillations) on adaptive grids than the remap method with a monotonicity preserving cubic spline interpolation. A more detailed comparison of this proposed method with other methods is shown in Fig. 3.8, where we note that while other linear finite difference approaches such as the second order Lax-Wendroff fail to provide an oscillation-free solution, the scheme modified by this new technique is successful in capturing the discontinuities in the solution. This feature can be attributed to the monotonicity preserving nature of the interpolation scheme being used in our approach.

The accuracy of our scheme degrades to first order near a discontinuity. To further study the impact of this approach on the order of accuracy, a smoother initial condition without any discontinuity is considered. Here, the initial condition for f is

$$f(x,0) = \frac{1}{\sqrt{2\pi}\sigma} \exp\left(-\frac{(x-\mu)^2}{2\sigma^2}\right), \tag{3.60}$$

and the value of the function f at the domain boundaries is zero. In Eq. 3.60, μ and σ are the mean and standard deviation of the initial Gaussian distribution function,

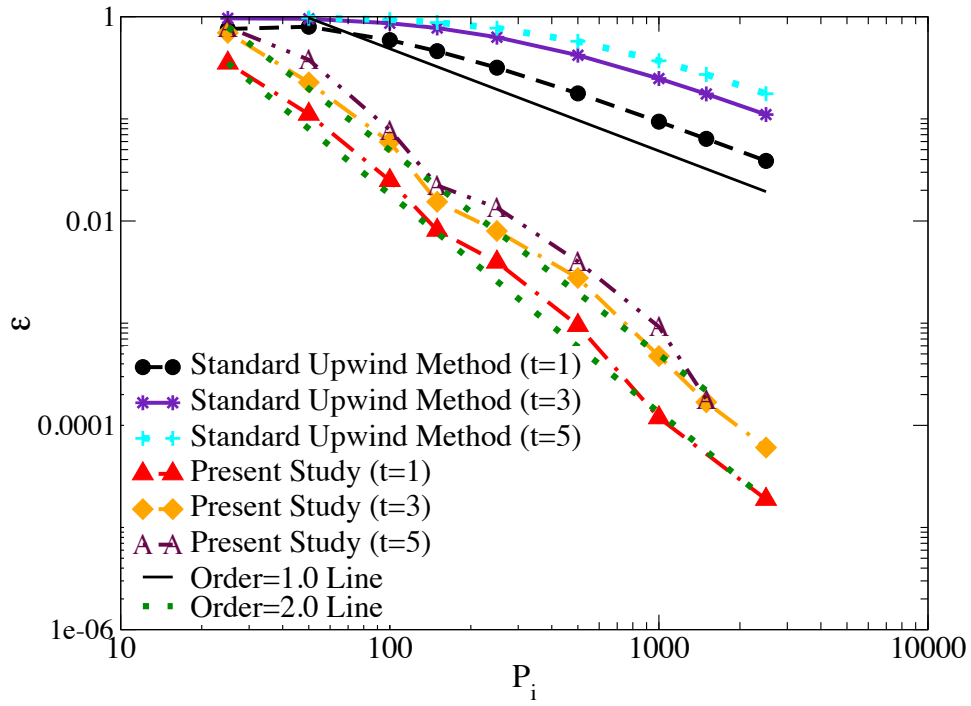

Figure 3.9: Error in the numerical solution for Problem 3.3; case with the linear drift function ($D(x) = -x$) at times t =1, 3 and 5 versus the number of grid points, P_i. Numerical solutions obtained from the standard first order upwind finite difference method are compared with those obtained using grid adaptation and non-iterative defect correction (with constrained minimization). In the computation of error, the analytical solution is considered as the reference solution.

respectively. Here, $\mu = 1$ and $\sigma = 0.1$. Applying characteristic analysis to solve Eq. 3.25 with this initial condition, the exact solution is derived:

$$f(x,t) = \frac{e^t}{2\sqrt{2\pi}\sigma_x} \exp\left(-\frac{(e^t x - \mu_x)^2}{2\sigma_x^2}\right). \tag{3.61}$$

As the domain for the continuous problem is infinite, at each time-step the grid is found using Eqs. 3.10 and 3.11 and the time-dependent boundary $S_\Omega(t)$ is determined based upon the tails of the response [115, 135]. For comparison purposes, numerical solutions are also generated with the standard upwinding scheme on a uniform grid within $S_\Omega(t)$. In order to determine the impact of application of this approach on the accuracy of the numerical solution, the L2 error of the response (with linear drift) for three different times, t =1, 3 and 5, is shown in Fig. 3.9 versus the number

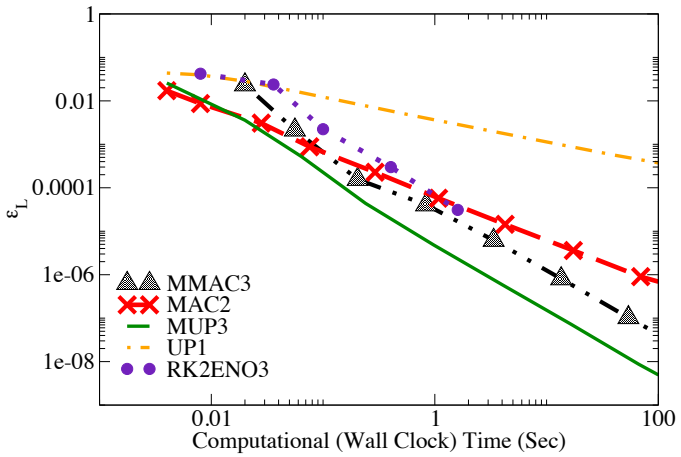

Figure 3.10: Local Error, ϵ_L, in the computed solution for Problem 3.3 at t =0.75 and $x = 12$ versus computational (wall clock) time. Numerical solutions obtained from the standard first order upwind (UP1), the second order MacCormack (MAC2) and ENO (RK2ENO3) finite difference methods are compared with those obtained using grid adaptation and non-iterative defect correction (modified schemes using the remap approach) including the third order modified MacCormack (MMAC3) and third order modified upwind methods (MUP3). In the computation of the error, the analytical solution is considered as the reference solution.

of grid points in x.

In order to demonstrate the remap approach, we assume σ_x and μ_x to be 2 and 30 in Eq. 3.60, respectively. This time we solve Eq. 3.56 on a fixed domain where $x \in [0.1, 45.0]$. With Eq. 3.60 as the initial condition, the Liouville equation (Eq. 3.56) is solved using different approaches and the local error, ϵ_L, defined as the difference in numerical and exact solution at $x = 12$ and $t = 0.75$, was evaluated. The results illustrated in Fig. 3.10 clearly show the computational advantage of the schemes modified with the remap method over standard difference schemes with respect to computational (wall clock) time. It should be noted that the errors in all of the results presented in this chapter for the remap methodology are estimated on a uniform grid for each of the schemes for which results are shown. Here, a global error estimate ϵ is used to study the impact of applying the proposed methodology on the overall accuracy of difference schemes.

As shown in Figs. 3.10- 3.12, depending on the level of defect correction, second

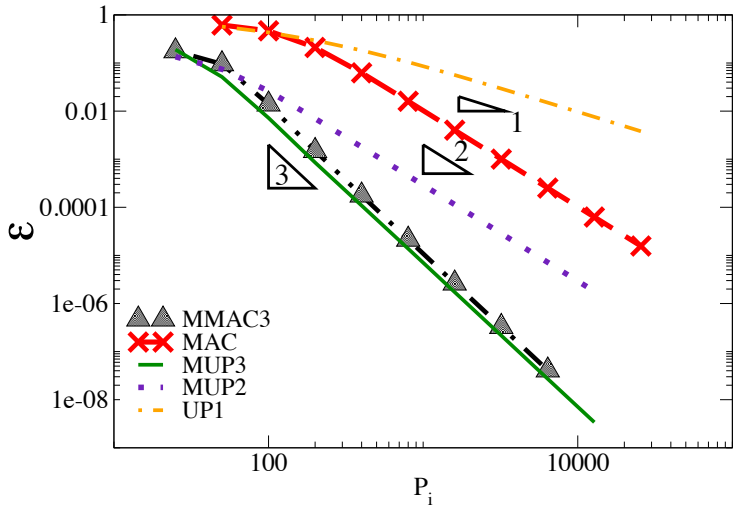

Figure 3.11: L2 Error in the computed solution for Problem 3.3 at t =0.75 versus the number of (uniform) grid points, P_i. Numerical solutions obtained from the standard first order upwind (UP1), the second order MacCormack (MAC2) and ENO (RK2ENO3) finite difference methods are compared with those obtained using grid adaptation and non-iterative defect correction (modified schemes using the remap approach) including the third order modified MacCormack (MMAC3), second and third order modified upwind methods (MUP2, MUP3). In the computation of the error, the analytical solution is considered as the reference solution.

and third order of accuracy in both space and time can be obtained. Also, the accuracy of $\dot{f}$ in the interpolation must be set in accordance to the desired accuracy. The results show a corresponding increase in the order of accuracy of upwind scheme from one to two and two to three. Such improvement is possible up to any desired order of accuracy.

Moreover, grid adaptation corresponding to Eq. 3.29, which regularizes the irregularities in the solution, requires the local CFL (Courant-Friedrichs-Lewy) number to be equal to one all over the domain. Such a requirement results in the average time-step and spatial increment being proportional throughout the course of computations and as a result the orders of accuracy in time and space become coupled. Therefore, as shown in Fig. 3.12, an increase in the spatial order of accuracy results in an increase in the temporal order of accuracy. When compared with standard schemes of the same (high) order, the proposed method gives similar error with less

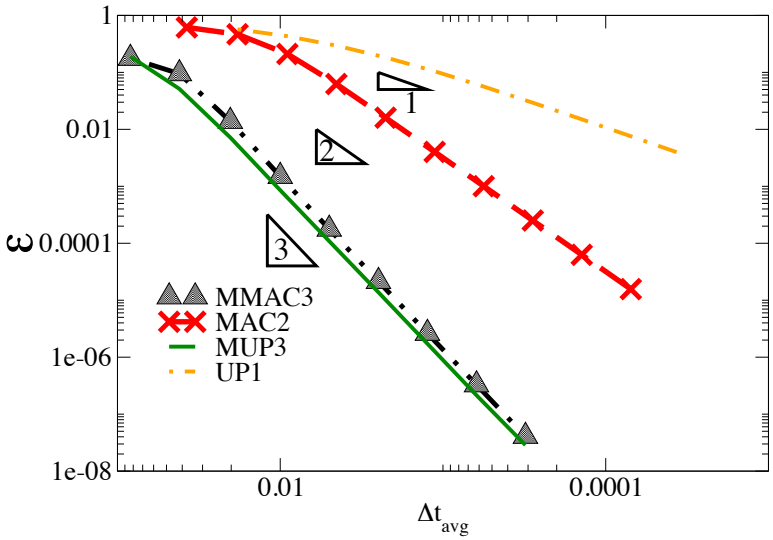

Figure 3.12: L2 Error in the computed solution for Problem 3.3 at t =0.75 versus average time-step, $\Delta t_{\text{average}}$. Numerical solutions obtained from the standard first order upwind (UP1) and the second order MacCormack (MAC2) finite difference methods are compared with those obtained using grid adaptation and non-iterative defect correction (modified schemes using the remap approach) including the third order modified MacCormack (MMAC3) and third order modified upwind methods (MUP3). In the computation of the error, the analytical solution is considered as the reference solution.

computational effort.

When $D(x) = x - x^3$ and f initially is given as Eq. 3.60 with $\mu = 2$ and $\sigma = 0.1$, the exact solution can be obtained through characteristic analysis with the result given by

$$f(x,t) = \frac{1}{\sigma\sqrt{2\pi}} \exp\left(-\frac{1}{2\sigma^2}\left(\frac{\exp(-t)}{\sqrt{\exp(-2t) - 1 + x^{-2}}} - \mu\right)^2\right) \times \left|1 - x^2\left(1 - \exp(-2t)\right)\right|^{-3/2}. \quad (3.62)$$

For this case in Fig. 3.13, the numerical results are shown for only one time-step. Comparison between the results illustrated in Figs. 3.9- 3.13 clearly indicates that the application of the both proposed methods results in an improvement in the numerical solution by one order of accuracy. Unlike the standard upwinding

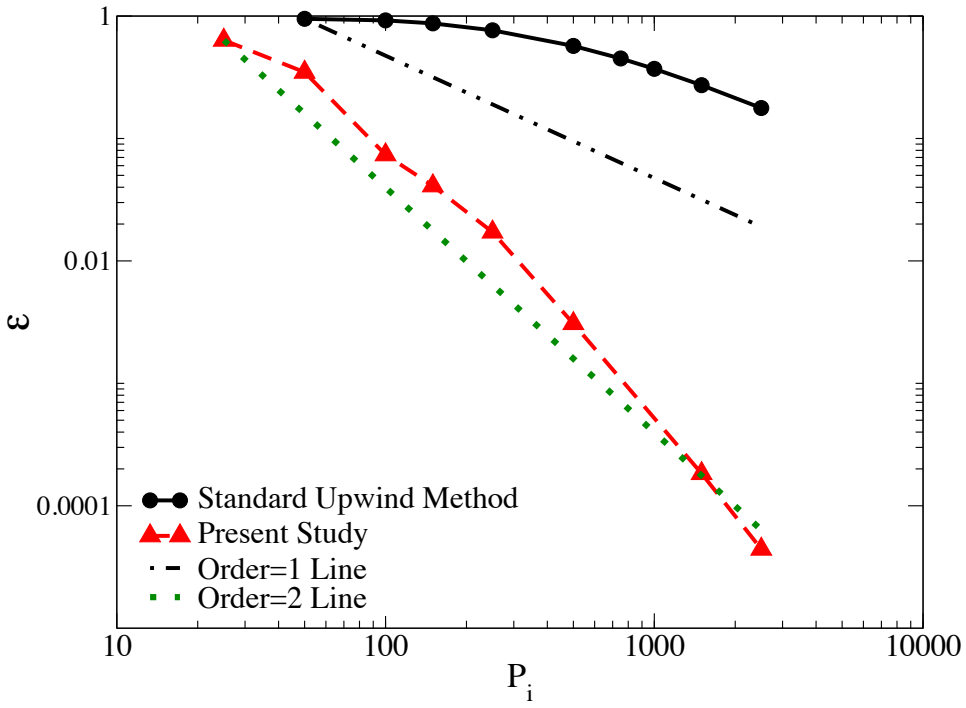

Figure 3.13: Error in the numerical solution for Problem 3.3; case with the nonlinear drift function ($D(x) = x - x^3$) at t =1 versus the number of grid points, P_i. Numerical solutions obtained from the standard first order upwind finite difference method are compared with those obtained using grid adaptation and non-iterative defect correction (with constrained minimization). In the computation of error, the analytical solution is considered as the reference solution.

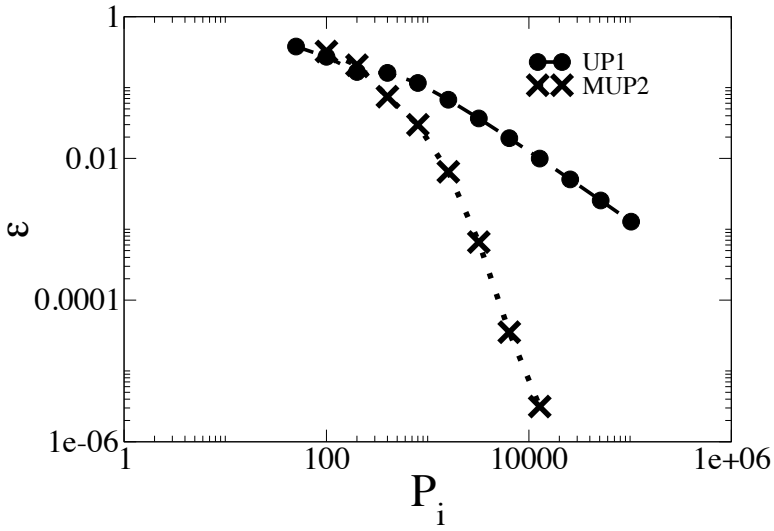

Figure 3.14: L2 Error in the computed solution for Problem 3.3 (case with the nonlinear drift function ($D(x) = x - x^3$) with $\mu = 2$) at t =3.5 versus the number of (uniform) grid points, P_i. Numerical solutions obtained from the standard first order upwind (UP1) finite difference method are compared with those obtained using grid adaptation and non-iterative defect correction (second order modified upwind method, MUP2, modified using the remap approach). In the computation of the error, the analytical solution is considered as the reference solution.

solution, which approaches its formal first order accuracy gradually as the number of grid points increase, the solutions obtained from these methods exhibit formal second order accuracy even with a few grid points, which further indicates that the modified difference scheme is significantly less diffusive.

If μ is initially set to be zero in Eq. 3.60, similar to the first test problem, the constrained minimization methodology is unable to deal with regions near the three fixed points of $x = -1, 0$ and 1 in which $D(x)$ becomes zero and fails. Setting γ equal to 0.01 for the regions with equal grid point spacing in which $|D_i^n \Delta t^n| < \gamma\,(x_i - x_{i-1})$, and applying the remap method, this issue can be dealt with perfectly. As shown in Fig. 3.14, due to the resultant higher resolution of grid points on the adaptive mesh near the stable fixed point where the response is attracting to, the modified scheme becomes super-convergent. Interestingly, such a significant enhancement in the accuracy of the underlying scheme, which is first order upwind

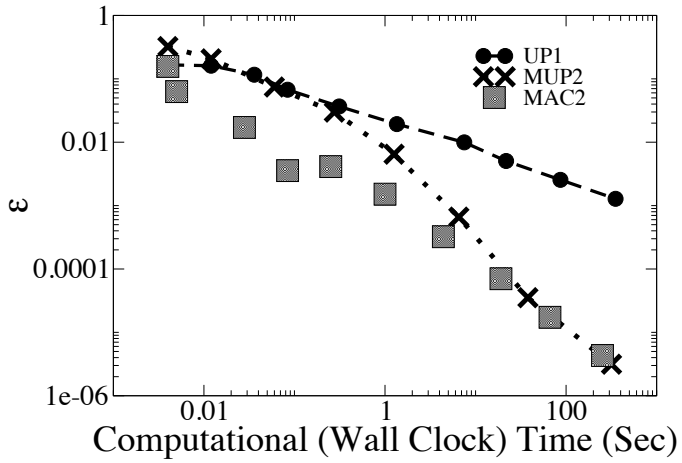

Figure 3.15: L2 Error in the computed solution for Problem 3.3 (case with the nonlinear drift function ($D(x) = x - x^3$) with $\mu = 2$) at t =3.5 versus computational (wall clock) time. Numerical solutions obtained from the standard first order upwind (UP1) and the second order MacCormack (MAC2) methods are compared with those obtained using grid adaptation and non-iterative defect correction (second order modified upwind method, MUP2, modified using the remap approach). In the computation of the error, the analytical solution is considered as the reference solution.

method, comes at a reasonable computational cost when its required computational (wall clock) time is compared with that of second order MacCormack method for a given accuracy (see Fig. 3.15).

While standard linear upwinding finite difference schemes of order higher than one are known to be numerically unstable for solution of the advection equation [124, 16], it strongly appears that the outcome of the approaches presented in this chapter is a numerically stable and monotonicity preserving solution method. While second order methods which employ nonlinear finite difference schemes, such as essentially non-oscillatory (ENO) [42] and TVD MacCormack [124] schemes, also result in stable and monotonicity preserving numerical approximations, both proposed approaches are simpler to implement and do not require the use of flux or slope limiters to avoid spurious oscillations in the response. It should also be noted that, as shown by Yamaleev [54], gradient (equidistribution) based refinement schemes can not be used to improve the order of accuracy for the first order finite difference schemes.

3.4 Summary

In this chapter, two novel approaches are introduced to improve the formal order of accuracy of finite difference solutions of linear and nonlinear hyperbolic partial differential equations (PDEs), by one order or higher. These approaches represent improvements over those presented in Chapter 2, as the enhancement in order of accuracy was shown to be less than one order in Chapter 2 for the problems selected therein. Both approaches presented in this chapter, using adaptive grids, are based on truncation error analysis of an underlying low-order finite difference scheme. Within the framework of both methods, depending on the type of error terms characterized as either regular or irregular perturbations, specific strategies are chosen for the elimination of truncation error terms up to a desired order of accuracy. While non-iterative defect correction is used in both approaches for removing regular perturbation, singular perturbations are eliminated by either (i) solving a constrained minimization problem to determine the grid distribution or (ii) a remap procedure whereby interpolation of dependent variables from adaptive non-uniform grids to uniform grids and vice versa is accomplished using a monotonicity preserving interpolant. The latter approach is also important in the context of Godunov's barrier theorem, as the approach addresses the possibility of having a second or higher order linear monotonicity preserving schemes under certain conditions (e.g. when CFL is set to unity). The outcome of these modifications is a scheme which has the desired order of accuracy. Moreover when the remap approach was used, a better computational performance was obtained when compared to standard high order finite difference solutions.

CHAPTER 4

Numerical Solution of Multidimensional PDEs Based on Grid Adaptation

While the focus of Chapters 2 and 3 is on adaptive grid based finite difference solutions for selected hyperbolic PDEs in one-dimension, the focus of Chapters 4 and 5 is on extensions of some of the methods proposed in Chapters 2 and 3 to multiple dimensions. This Chapter (Chapter 4) is entirely devoted to time-varying uniform computational domain/mesh adaptation in multidimensional spaces and its application in computational uncertainty quantification (CUQ). In the context of CUQ, as discussed in Chapter 2, our proposed numerical solution of the Liouville equation features (a) sampling at Gauss-quadrature nodes of random variables corresponding to uncertain parameters and (b) evolution of the associated conditional probability density functions using a finite difference method with time-adaptive computational domains. Using these two features, along with dimensional splitting of operators in the state space, computational performance of the numerical solution of the Liouville equation for uncertainty quantification is improved significantly.

The proposed approach is designed to accurately predict long-time statistics of random variables corresponding to system states, including moments and probability density function, for dynamical systems of moderate dimension. In order to demonstrate the capabilities of the proposed intrusive approach, it is applied to four different dynamical systems, including (i) single spring-mass system, (ii) Van der Pol oscillator, (iii) double spring-mass system and (iv) a typical section nonlinear aeroelastic model. When compared to a conventional finite difference based nu-

merical solution on a fixed grid, the solution obtained from the proposed adaptive grid based approach involves a considerable reduction in the required number of grid points for equivalent accuracy. For the single spring-mass system, for which an analytical solution is found, comparison with Monte Carlo simulation results indicates that the proposed adaptive numerical solution approach is generally one to two orders of magnitude more computationally efficient for a given level of accuracy.

4.1 Numerical method

4.1.1 Finite difference solution

In the present chapter the second order MacCormack finite difference method, with flux limiting [124], is used in alternate directions to numerically solve Eq. 2.3. Using the explicit alternate direction (EAD) technique [124], one can apply one dimensional schemes to solve multidimensional hyperbolic partial differential equations. In this context, the numerical solution of the Liouville equation is obtained through a second order accurate splitting procedure [124], where unidimensional numerical solutions are combined as

$$f_j^{n+1} = \left(L_{\frac{\Delta t}{2}}^{(x_{1,j})} L_{\frac{\Delta t}{2}}^{(x_{2,j})} \dots L_{\frac{\Delta t}{2}}^{(x_{M-1,j})} L_{\Delta t}^{(x_{M,j})} L_{\frac{\Delta t}{2}}^{(x_{M-1,j})} \dots L_{\frac{\Delta t}{2}}^{(x_{2,j})} L_{\frac{\Delta t}{2}}^{(x_{1,j})} \right) \tilde{f}_j^n \quad . \tag{4.1}$$

Here, for simplicity of notation, the conditional density obtained after employing the rezoning approach at time-step n is denoted by $\tilde{f}^n$ and subscript j represents the position index of the grid point in the domain of computation. Also, $L_{\Delta t}^{(x_{i,j})}$ denotes the numerical scheme which solves the Liouville equation in the x_i direction over time-step Δt. When $h_{i,j}^n > 0$ (see Eq. 2.3), using the total variation diminishing MacCormack scheme, $L_{\Delta t}^{(x_{i,j})}$ can be written as

$$L_{\Delta t}^{(x_{i,j})}\tilde{f}_j^n = \tilde{f}_j^n - \Delta t^n \frac{\delta_-\left(h_i^n \tilde{f}^n\right)_j}{\delta_-(x_{i,j}^n)} + \tag{4.2}$$
$$\frac{\Delta t^n}{2}\frac{\delta\left(h_i^n \tilde{f}^n\right)_j}{\delta(x_{i,j}^n)} \times \left(h_{i,j}^n \frac{\Delta t^n}{\delta_-(x_{i,j}^n)} - 1\right)\psi_{i,j+\frac{1}{2}}^n -$$
$$\frac{\Delta t^n}{2}\frac{\delta_-\left(h_i^n \tilde{f}^n\right)_j}{\delta_-(x_{i,j}^n)} \times \left(h_{i,j-}^n \frac{\Delta t^n}{\delta_-(x_{i,j}^n)} - 1\right)\psi_{i,j-\frac{1}{2}}^n,$$

where δ and δ_- denote the forward and backward difference operators (along direction i) respectively and $h_{i,j-}^n = h_{i,j}^n - \delta_- h_{i,j}^n$. For negative $h_{i,j}^n$, $L_{\Delta t}^{(x_{i,j})}$ can be obtained using symmetry considerations. The flux limiters ($\psi_{i,j+\frac{1}{2}}^n$ and $\psi_{i,j-\frac{1}{2}}^n$) are functions of the monotony indicator which is defined as the ratio of the slope of the profile upstream of the point j to the slope of the profile downstream of the point j. Also, it should be noted that no finite difference operation is performed for the boundary grid points and the conditional probability density function (f) at the boundaries is assumed to be zero.

In this chapter, Δt^n in Eq. 4.2 is determined by defining the maximum local Courant-Friedrichs-Lewy (CFL) number to be equal to a fixed value (which is 0.9 for the first three test problems). The temporal increment (Δt^n) is then evaluated as a function of this maximum local CFL number as

$$\Delta t^n = \min\left(\mathrm{CFL}_i \times \left(\frac{\delta_-(x_{i,j}^n)}{h_{i,j}^n}\right)\right)_{i=1,2..,M;j=1,2,..,\prod_{i=1}^M P_i}, \tag{4.3}$$

where CFL_i is the maximum local CFL number and P_i is the maximum number of grid points for the ith state (random response variable). As discussed in the next section, in the proposed method the spatial increments ($\delta_-(x_{i,j}^n)$, $\delta(x_{i,j}^n)$) vary with time and Δt^n is determined at every time-step.

4.1.2 Multidimensional time-varying computational domain/mesh adaptation

The Liouville equation for the evolution of the conditional density of the random process is a linear, hyperbolic partial differential equation and, as such, has a solution which convects in the spatial domain. Thus it is more computationally efficient to carry out the numerical solution on a time-varying (or moving) mesh which is determined in order to best capture this convective behavior. Unlike in the one-dimensional case, grid adaptation in multidimensional space is a significant challenge, especially in the presence of excessive deformation of grid cells (which may be unavoidable in order to capture high gradient regions with sufficient accuracy while keeping the total number of grid points fixed).

While most adaptive mesh methods which have been applied for the numerical solution of hyperbolic PDEs are based on non-uniform, time-dependent grid distributions within a fixed domain [50, 51, 52, 53, 54], a uniform grid within a time-dependent domain (hyper-rectangle) is used in this chapter. This approach features simplicity of implementation and both uniformity and smoothness of grids. Moreover, it is well-suited with both the hyperbolic nature of the Liouville equation and application for a moderate dimensional space of state variables. In each time-step the computational domain boundary, $S_\Gamma(t)$, is determined by comparing the values of the conditional density in the neighborhood of the boundaries at the previous time-step to predefined criteria including contraction and growth indices (ε_c and ε_g, respectively; $\varepsilon_g > \varepsilon_c$). Considering $x_{i,u}(t^n)$ and $x_{i,l}(t^n)$ $(i = 1, 2, ..., M)$ as the upper and lower bounds of the hyper-rectangular domain in the x_i direction at time-step n, respectively, the computational domain boundaries are determined as follows:

$$x_{i,u}\left(t^{n+1}\right) = \tilde{x}_{i,u} + \boldsymbol{G}\left(f^n\left(x^-_{i,u}\left(t^n\right)\right) - \varepsilon_g\right) \times \frac{\left|x_{i,u}\left(t^n\right) - x_{i,l}\left(t^n\right)\right|}{P_i - 1} \quad , \tag{4.4}$$

$$x_{i,l}\left(t^{n+1}\right) = \tilde{x}_{i,l} - \boldsymbol{G}\left(f^n\left(x^+_{i,l}\left(t^n\right)\right) - \varepsilon_g\right) \times \frac{\left|x_{i,u}\left(t^n\right) - x_{i,l}\left(t^n\right)\right|}{P_i - 1} \quad , \tag{4.5}$$

where $\boldsymbol{G}(x)$ is an indicator function defined as Eq. 3.19 and $\tilde{x}_{i,u}$ and $\tilde{x}_{i,l}$ are defined as

$$\tilde{x}_{i,u} = \inf\left\{z : \ z \in Z, \ f^n(\mathbf{x}) < \varepsilon_c \ \ , \ \forall \ \ x_i^+ > z\right\}, \tag{4.6}$$

$$\tilde{x}_{i,l} = \sup\left\{z : \ z \in Z, \ f^n(\mathbf{x}) < \varepsilon_c \ \ , \ \forall \ \ x_i^- < z\right\}. \tag{4.7}$$

Here the conditional density, f, is considered to be zero outside the computational domain ($x_i \leq x_{i,l}\left(t^n\right)$ and $x_i \geq x_{i,u}\left(t^n\right)$) and Z is a set of discrete grid point locations and can be written as follows

$$Z = \left\{z : \ z = k\Delta z| \ k \in \mathbb{Z}\right\}. \tag{4.8}$$

It should be noted that superscript $^{+/-}$ denotes the adjacent grid point on the right/left of the discrete grid point of location x_i, respectively. Also in the problems solved in this chapter, ε_g and ε_c are considered to be 10^{-6} and 10^{-14}, respectively. The effect of these parameters on the accuracy of the computed moments is investigated in section 4.1. Also, if the response splits (either initially or in the course of its evolution) into two (or more) compactly supported functions, the domain is split into multiple adaptive hype-rectangular domains in which the boundaries are determined using Eqs. 4.4 and 4.5. These domains are moved and resized separately unless they merge into each others. Thus, the resultant numerical solution lends itself nicely to parallelization in an MPI environment. In order to detect a potential domain coalescence, the boundaries of these split domains must be checked in each time-step. The domain coalescence occurs if a corner of a smaller hyper rectangular domain enters into a larger one.

The process of determining the boundaries is schematically illustrated in Fig. 4.1

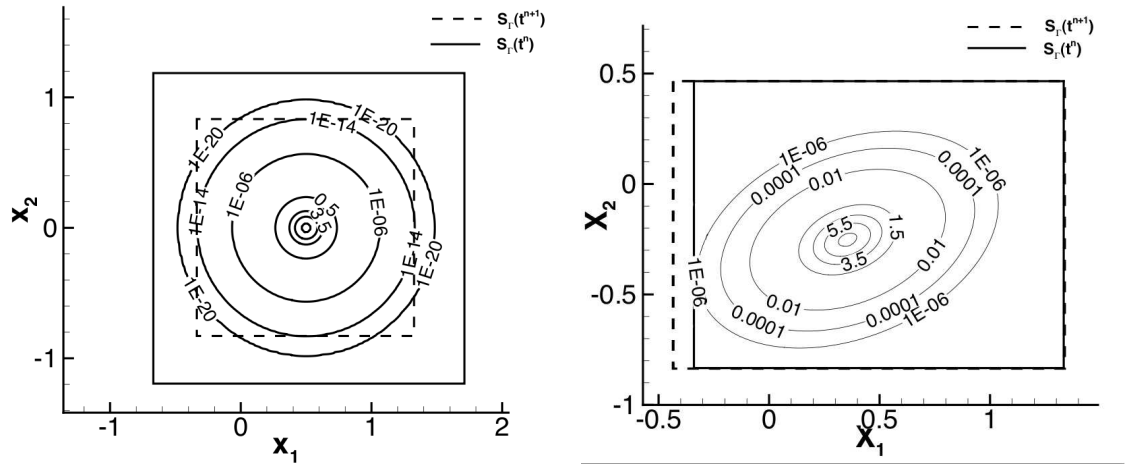

(a) (b)

Figure 4.1: Schematic illustrating (a) cutting and (b) growth mechanisms with $\varepsilon_c = 10^{-6}$ and $\varepsilon_g = 10^{-14}$, respectively, in the proposed adaptive grid movement technique. Dashed lines in this figure represent the newly determined boundaries of the computational domain after applying the boundary adaptation procedure (Eqs. 4.4 and 4.5).

for a two-dimensional space. Once the location of the computational domain boundary is determined, the interior grid points are generated uniformly in each dimension of the hyper-rectangle and the values of the conditional density at the newly determined interior grid locations are obtained through the use of a piecewise polynomial interpolant. In the problems solved in this chapter at each time-step the boundaries are relocated based on Eqs. 4.4 and 4.5. As illustrated in Fig. 4.1, in this process ε_g and ε_c are the controlling parameters that govern the domain growth and contraction mechanisms. Here, as $\varepsilon_c < \Delta x_i^2$ always holds, the error incurred by such boundary determination procedure is very small and does not affect the numerical solution formal order of accuracy. It should also be noted that as the boundary condition, all values of conditional density at the domain boundary are set to zero.

In order to account for the small loss of probability content of the conditional density as a result of the movement and resizing of the computational domain, the numerical solution is re-scaled at each time-step such that the computed zeroth

moments remain unity. The re-scaling formula used in this chapter is given by:

$$\tilde{f}^* = \left(\frac{1}{I_1}\right) \tilde{f}^n, \tag{4.9}$$

where $\tilde{f}^*$ is the scaled value of the conditional density and I_1 is the computed zeroth moment at time-step n:

$$I_1 = \int_{\Re^M} f_{\mathbf{x}|\mathbf{Y}}(\mathbf{x}, \mathbf{Y}, t) d\mathbf{x}. \tag{4.10}$$

This integral is computed using a numerical quadrature with the same global order of accuracy as that of the finite difference solution and as such the re-scaling should preserve the formal order of accuracy of the underlying finite difference scheme. The proof presented in the Appendix D, along with numerical experiments (for example, the slope of 2 in the logarithmic error graph presented in Section 4.2; see Fig. 4.5), both confirm this statement.

4.2 Results and discussion

4.2.1 Problem 4.1: Single spring-mass system

The first test problem addresses the uncertainty quantification of a linear multi-state dynamical system with an exact solution available for its corresponding Liouville equation. This system is a single linear spring-mass oscillator. The stiffness of the spring, k, is assumed to be a uniformly distributed random parameter with $k \in [0.4, 0.6]$ and is parameterized by $\xi \in [-1, 1]$ which has a marginal density, $f_\xi = 1/2$. The equations governing the time-evolution of the states x_1 and x_2 can

be written as a set of first order differential equations:

$$\begin{aligned} \dot{x}_1 &= x_2, \\ \dot{x}_2 &= -k(\xi)x_1. \end{aligned} \tag{4.11}$$

The initial conditions for both mass displacement (x_1) and velocity (x_2) are considered to be random and have Gaussian distributions ($N(0.5, 0.01)$ and $N(0.0, 0.01)$ for the point mass displacement and velocity, respectively).

The initial distributions for x_1, x_2 and ξ are assumed to be independent and a multivariate Gaussian distribution is used to model the initial condition for the conditional density:

$$f(x_1, x_2, \xi, 0) = \frac{1}{4\pi\sigma_1\sigma_2} \exp\left\{ -\frac{(x_1 - \mu_1)^2}{2\sigma_1^2} - \frac{(x_2 - \mu_2)^2}{2\sigma_2^2} \right\}, \tag{4.12}$$

where $\mu_1 = 0.5$, $\mu_2 = 0.0$ and $\sigma_1 = \sigma_2 = 0.1$.

The exact solution of the resulting Liouville equation, with an initial condition defined in Eq. 4.12, can be found using the method of characteristics:

$$\begin{aligned} f(x_1, x_2, \xi, t) &= \frac{1}{4\pi\sigma_1\sigma_2} \exp\left\{ -\frac{1}{2\sigma_1^2} \left(\frac{\sqrt{k}x_1 \cos\left[\sqrt{k}t\right] - x_2 \sin\left[\sqrt{k}t\right]}{\sqrt{k}} - \mu_1 \right)^2 \right\} \times \\ &\quad \exp\left\{ -\frac{1}{2\sigma_2^2} \left(\sqrt{k}x_1 \sin\left[\sqrt{k}t\right] + x_2 \cos\left[\sqrt{k}t\right] - \mu_2 \right)^2 \right\}. \end{aligned} \tag{4.13}$$

The numerical scheme introduced in Eq. 4.1 (explicit alternate direction method with TVD MacCormack scheme) is used on a uniformly distributed fixed and moving rectangular grid to solve the Liouville equation. Here, in order to solve the Liouville equation on a fixed grid, MPI parallelization of the computations through full decomposition of the space of random variables (input parameter and states) is used. Conversely, when the grid adaptation technique is used, parallelization is

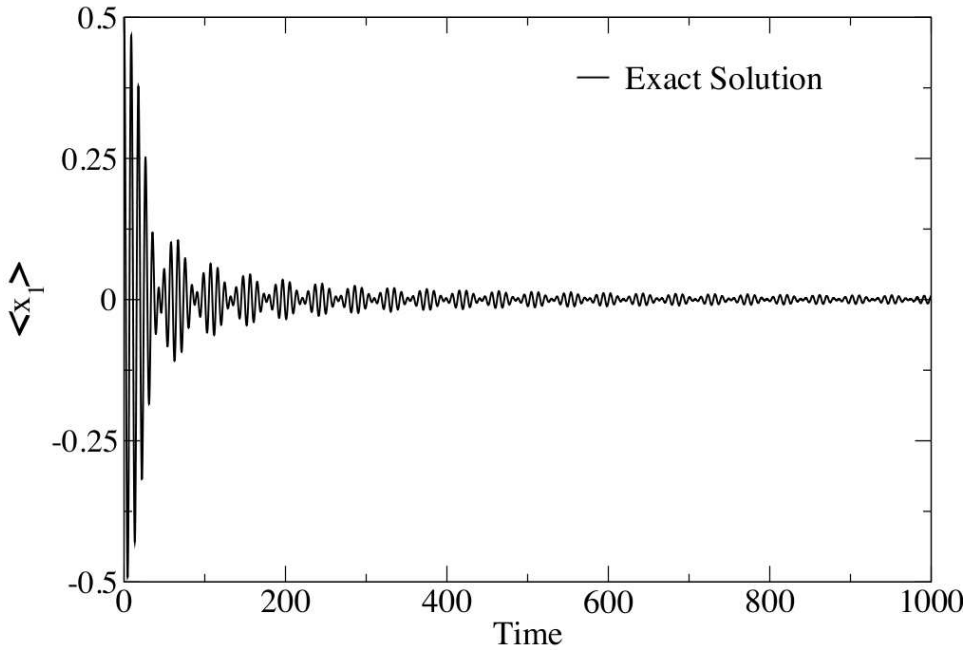

Figure 4.2: Exact solution for the evolution of the mean displacement $\langle x_1 \rangle$ of the mass in the linear spring-mass oscillator (in Problem 4.1 with a unimodal initial condition).

implemented just in the space of random variables corresponding to model parameters, which is a "perfectly" parallel decomposition. What is meant by perfectly parallel in this context, is that each single Liouville equation for the probability density conditioned on an abscissa in the space of random variables (corresponding to model parameters) is solved individually on a separate computational node. These separate computational nodes only communicate when the calculation of the moments is necessary.

In Fig. 4.2, the evolution of the mean of the point mass displacement is shown. As can be seen from this figure, the exact solution for the mean for this problem evolves to a stationary state. As shown in Fig. 4.3, such an outcome occurs as a result of unimodal PDF decaying oscillations about $x = 0$ due to the increasing phase difference in time which leads to the cancellation of terms in the Eq. 4.11 solution time series [138]. In Fig. 4.4, and all other figures which show moment errors at a given time, in order to better interpret the numerical results especially

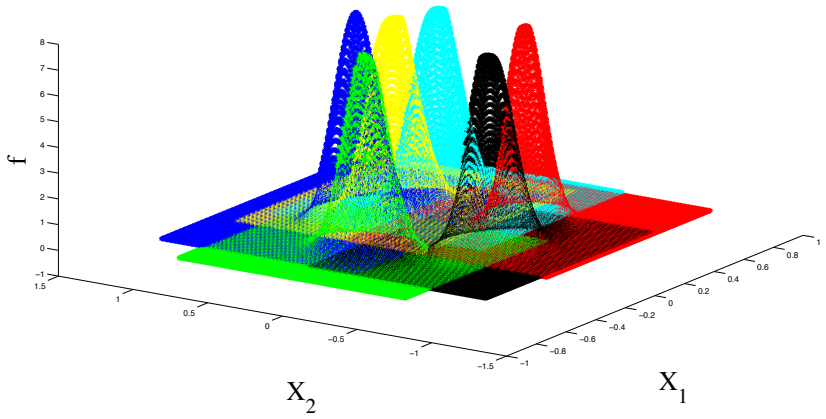

Figure 4.3: Joint PDF evolution for the linear spring-mass oscillator (in Problem 4.1 with the unimodal initial condition) for the parameter $\xi = 0.974$ at different time-steps: $t = 0$ (blue); $t = 5$ (red); $t = 10$ (green); $t = 15$ (cyan); $t = 20$ (black); $t = 40$ (yellow). Results are obtained using an adaptive moving uniform grid with $P_i = 150$.

when the reference values are very small, the error is actually computed over the interval $I_\delta = [t - \delta, t + \delta]$ as

$$\varepsilon_M^{(n)}(t) = \left\{ \frac{\sum_{t_j \in I_\delta} \left(M^{(n)}(t_j) - m^{(n)}(t_j) \right)^2}{\sum_{t_j \in I_\delta} \left(m^{(n)}(t_j) \right)^2} \right\}^{1/2}, \tag{4.14}$$

where $M^{(n)}(t_j)$ and $m^{(n)}(t_j)$ denote the computed and reference values of the nth moment at time-step t_j ($t_j \in I_\delta$), respectively. For the problems which are solved in this chapter the value of δ is set to 2. The results illustrated in Fig. 4.4, which show L2 errors in the first four moments of x_1 at three different times, demonstrate the ability of the adaptive grid methodology to give improved accuracy for a given number of grid points in comparison to the fixed grid solution. As shown in this figure, in order to obtain an acceptable level of accuracy for the moments (less than 10 percent error or $\varepsilon_M^{(n)}(t) < 0.1$), one needs to use many fewer grid points when the proposed grid adaptation technique is used (e.g. 700 times fewer grid points to

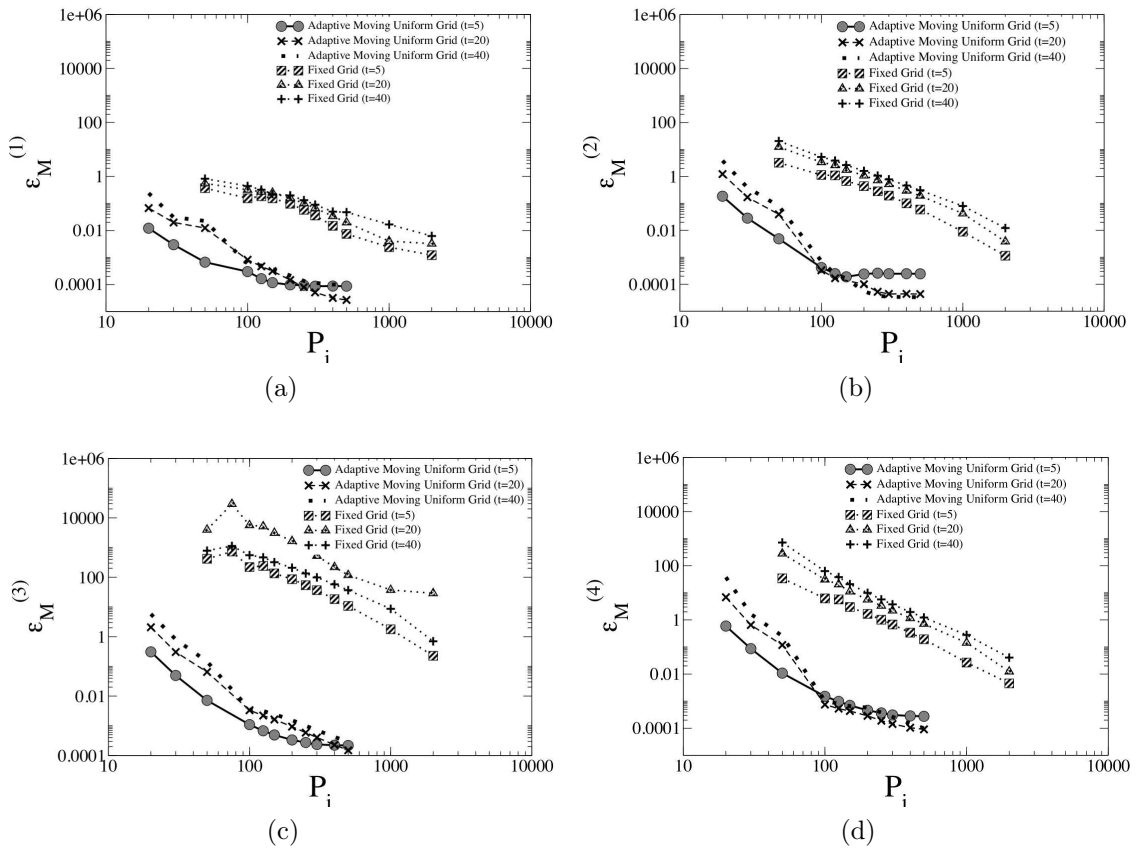

Figure 4.4: Error in the first four moments of mass displacement (x_1), shown at $t = 5,\ 20$ and 40. Comparison is made between finite difference solutions on fixed and adaptive grids for Problem 4.1 with a unimodal initial distribution and $N_P = 10$. In the computation of error, the analytical solution is considered to be the reference solution.

obtain the same level accuracy for the fourth moment). It should also be noted that the finite difference solutions were computed using N_p=10 Gauss quadrature points (conditioning samples) in ξ.

The accuracy of the computed moments is a function of both the truncation error of the finite difference scheme and the numerical integration method. Therefore in order to more directly determine the effect of the mesh adaptation, on the accuracy of the computed conditional density, the L2 error of the conditional density for three different times, t =5, 20 and 40, is shown in Fig. 4.5 versus the number of grid points in each dimension (with $N_p = 10$). For multiple states, with P_i grid points for each state and N_p samples in ξ, the normalized L2 error of the conditional density is

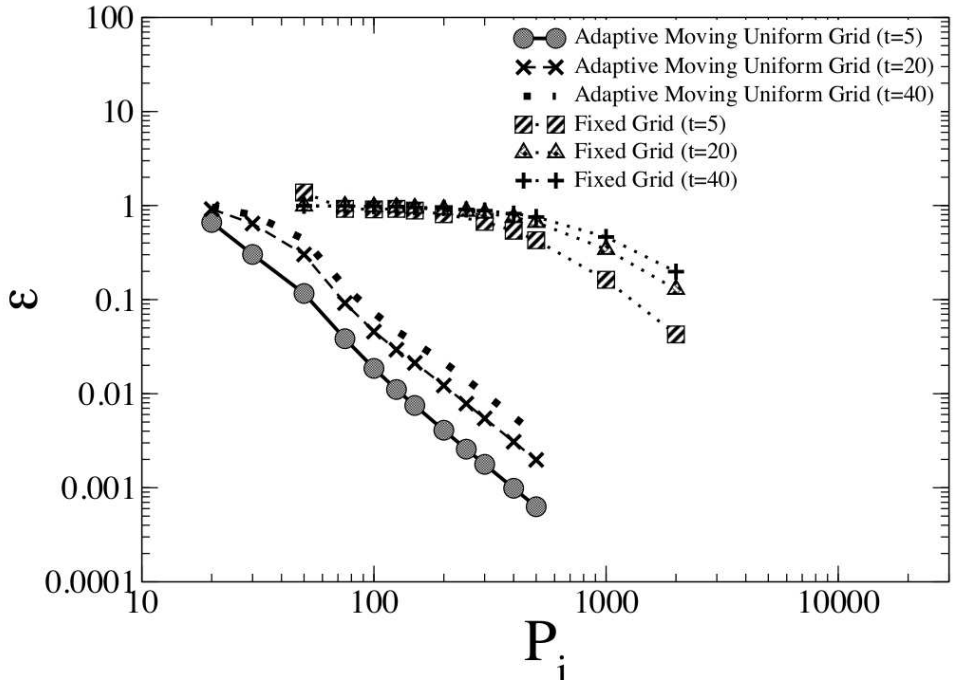

Figure 4.5: Error in the computed conditional density for Problem 4.1 with the unimodal initial distribution at times $t = 5$, 20 and 40 versus the number of grid points in each direction, P_i. Comparison is made between finite difference solutions on fixed and adaptive grids and $N_p = 10$. In the computation of error, the analytical solution is considered to be the reference solution.

obtained as:

$$\varepsilon(t) = \left\{ \frac{\sum_{k=1}^{N_p} \sum_{i=1}^{M} \sum_{j=1}^{P_i} \left(f_{\text{exact}}(x_{i,j}, Y_k, t) - f_{\text{numerical}}(x_{i,j}, Y_k, t) \right)^2}{\sum_{k=1}^{N_p} \sum_{i=1}^{M} \sum_{j=1}^{P_i} \left(f_{\text{exact}}(x_{i,j}, Y_k, t) \right)^2} \right\}^{1/2}. \quad (4.15)$$

As can be seen in Fig. 4.5, for a fixed value of P_i the solution computed on the adaptive mesh is anywhere from one to three orders of magnitude more accurate, depending on the value of P_i. Such enhanced accuracy is obtained due to the high resolution of the grid points in the regions of the domain where PDF contents exist.

While here in the problems which are solved in this chapter the boundary contraction (ε_c) and growth (ε_g) parameters are chosen to be 10^{-14} and $10^8 \times \varepsilon_c$ respectively, it is reasonable to expect a dependence between the accuracy of our adaptive grid

based numerical solution and the choice of the boundary contraction and growth parameters. In order to further investigate this behavior, we consider a constant ratio of $\varepsilon_g/\varepsilon_c = 1.1$ and show, in Fig. 4.6, the dependence of the error in the numerical solution versus the contraction parameter ε_c for different grid resolutions. In this figure, we see that for a given number of grid points (except for $P_i = 50$), there appears to be an optimal value of the boundary contraction parameter at $\varepsilon_c = \varepsilon_{c_{opt}}$, where the error is a minimum. For cases $\varepsilon_c > \varepsilon_{c_{opt}}$ where the boundary contraction parameter is greater than the minimizer (for a given number of grid points), the error is found to increase (as expected) due to insufficient representation of the tails of the PDF (where the truncation becomes effective for larger values of the PDF). Similarly, for cases $\varepsilon_c < \varepsilon_{c_{opt}}$ where the boundary contraction parameter is less than the minimizer (for a given number of grid points), the error is found to increase due to sparsity of grid points in regions of interest (resulting from an increased domain size for a given number of grid points), where the gradients of the PDF could be considerable. We also note from Fig. 4.6 that both the minimizer and the minimum value of error decrease with an increase in the number of grid points (as expected).

It is also important to note that the values of the optimum and the minimizer are case-dependent and are strongly dependent upon the behavior of the joint conditional probability density function, number of states, number of grid points and the ratio of the boundary contraction to growth parameter. Thus, finding the optimum values for these parameters requires an extensive investigation of the numerical results obtained using different values of ε_c and ε_g for each UQ problem. As such an approach is barely feasible for moderate dimensional UQ problems, and for the sake of consistency in the chapter, conservative values are assigned to both parameters in the four canonical problems solved in Chapter 4.

In Fig. 4.7 the wall clock times to obtain various levels of accuracy (percent error in $\langle x_1^n \rangle$, denoted as $\varepsilon_{\langle x_1^n \rangle}$) in Monte Carlo simulation, and the finite difference

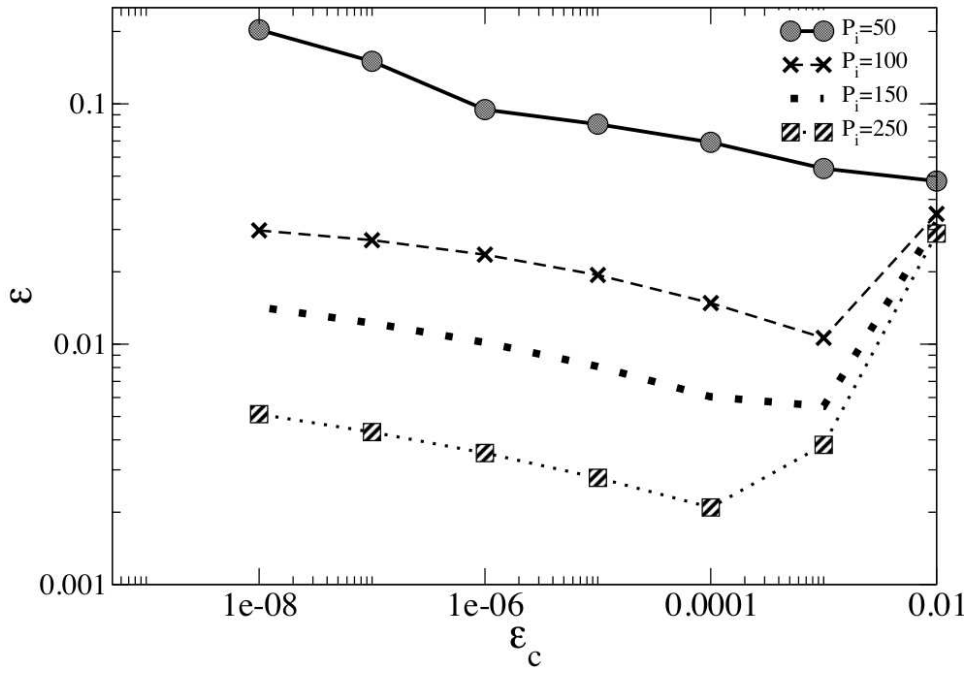

Figure 4.6: Impact of contraction parameter (ε_c) on the error in the computed conditional density for Problem 4.1 with a unimodal initial distribution at $t = 15$ for various number of grid points ($\varepsilon_g = 1.1\varepsilon_c$).

solution of the Liouville equation on fixed and adaptive moving uniform meshes, are shown. For a given level of accuracy, the comparison for different moments obtained from Monte Carlo simulation and the adaptive and fixed grid finite difference solutions demonstrates the improved computational efficiency of the adaptive finite difference approach. While the Monte Carlo simulations are run on a single processor, the data reported in Fig. 4.7 are found by taking the actual wall clock time and dividing through by the number of processors used in the adaptive grid finite difference solutions (10). In each test case, including this one, a fourth order Runge-Kutta scheme is used for the time integration of each realization in the Monte Carlo simulation.

Also in order to demonstrate the proposed adaptive approach capability in dealing with PDFs split into multiple compactly supported functions, another form of initial condition for the Liouville equation, which is a bimodal initial Gaussian dis-

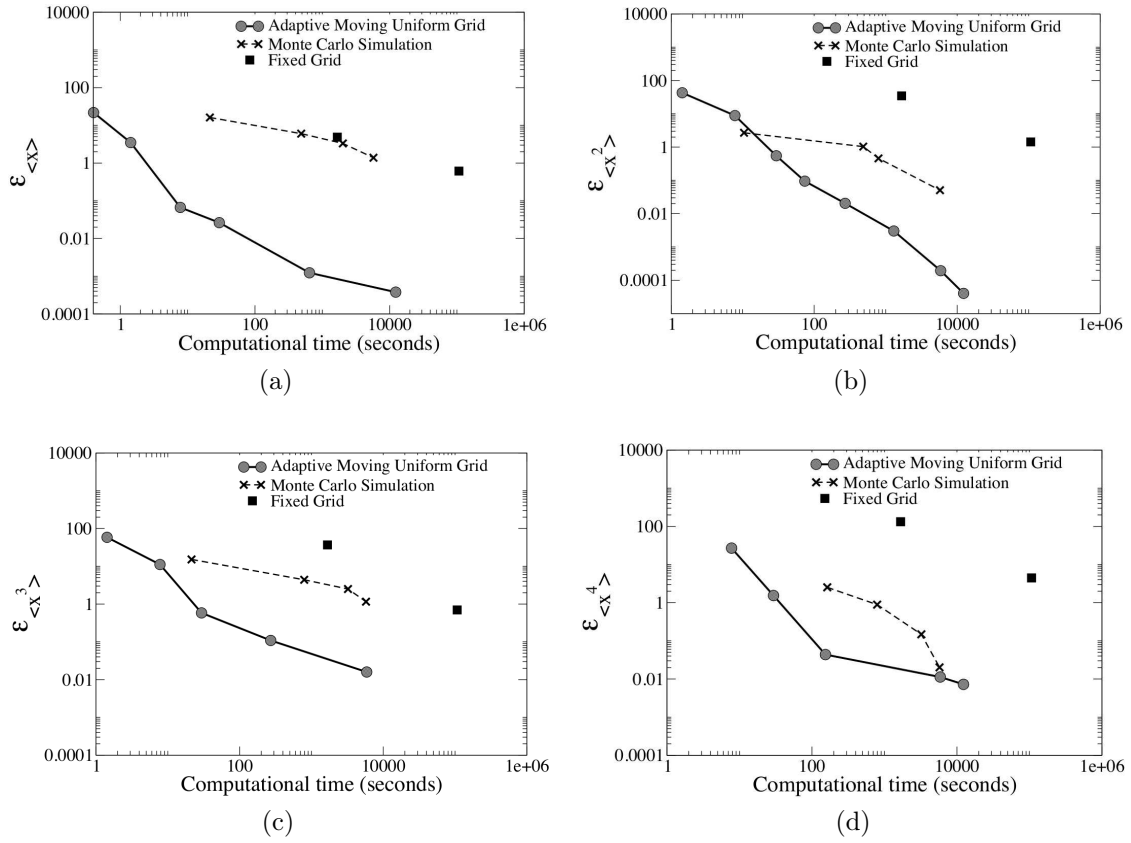

Figure 4.7: Percent error ($\varepsilon_{\langle x_1^n \rangle}$), for $t = 40$, in the first four moments of mass displacement (x_1) versus the computational time for Problem 4.1, with a unimodal initial distribution. Comparison is made between Monte Carlo simulation results and finite difference solutions on fixed and adaptive grids with $N_P = 10$. In the computation of errors, the analytical solution is considered to be the reference solution.

tribution, is considered:

$$f(x_1, x_2, \xi, 0) = \frac{3}{16\pi\sigma_1\sigma_2} \exp\left\{ -\frac{(x_1-\mu_1)^2}{2\sigma_1^2} - \frac{(x_2-\mu_2)^2}{2\sigma_2^2} \right\} + \frac{1}{16\pi\sigma_1\sigma_2} \exp\left\{ -\frac{(x_1-\mu_1-3)^2}{2\sigma_1^2} - \frac{(x_2-\mu_2-3)^2}{2\sigma_2^2} \right\}, \quad (4.16)$$

where $\mu_1 = \mu_2 = 1.5$ and $\sigma_1 = \sigma_2 = 0.1$. Using the adaptive strategy for the response, the domain is split into two separated adaptive meshes. The convergence of the proposed adaptive approach compared to the standard/fixed finite difference solution is shown in Fig. 4.8. The comparison indicates at least one order magnitude

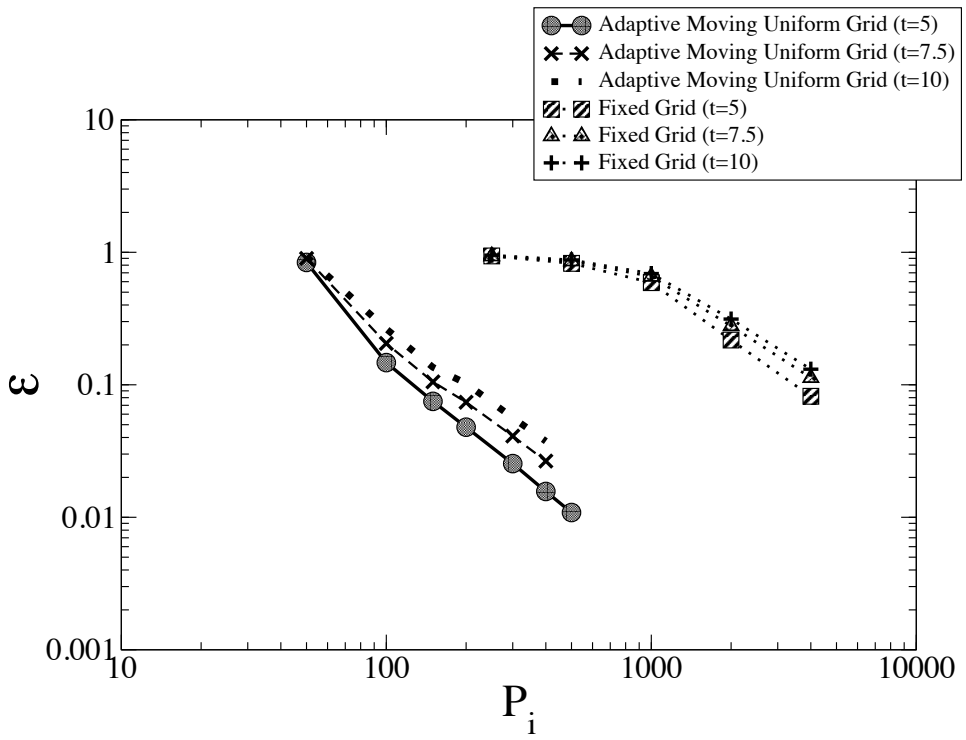

Figure 4.8: Error in the computed conditional density for Problem 4.1, with a bimodal initial distribution, at times $t = 5$, 7.5 and 10 versus the number of grid points in each direction, P_i. Comparisons are made between finite difference solutions on fixed and adaptive grids and $N_p = 8$. In the computation of error, the analytical solution is considered to be the reference solution.

enhancement in the accuracy of the finite difference solution when split adaptive grids, shown in Fig. 4.9, are used. Here, in order to obtain the results 8 Gauss quadrature points are sampled from the excitation space ($N_p = 8$). The joint PDF evolution for $\xi = 0.960289856$ is also shown in Fig. 4.9. As it can be seen in this figure, both PDF modes are oscillating back and forth with a constant amplitude in a circle of $1.5\sqrt{2}$ radius, which is the absolute value of their distance from each other. Such behavior is due to the simple harmonic nature of the solution of Eq. 4.11.

4.2.2 Problem 4.2: Van der Pol oscillator

In order to demonstrate the capability of the proposed approach for uncertainty quantification of a multi-state nonlinear dynamical system, a Van der Pol oscillator

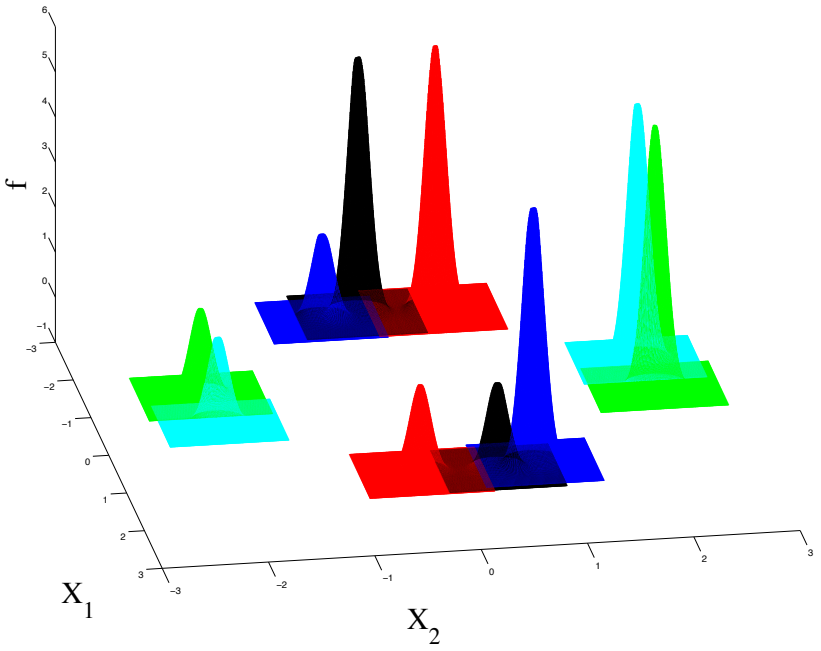

Figure 4.9: Joint PDF evolution for the linear spring-mass oscillator (in Problem 4. 1 with a bimodal initial condition) for the parameter $\xi = 0.960$ at different time-steps: $t = 1$ (red); $t = 2.5$ (green); $t = 7$ (black); $t = 8.5$ (cyan); $t = 10$ (blue). Results are obtained using an adaptive moving uniform grid with $P_i = 150$.

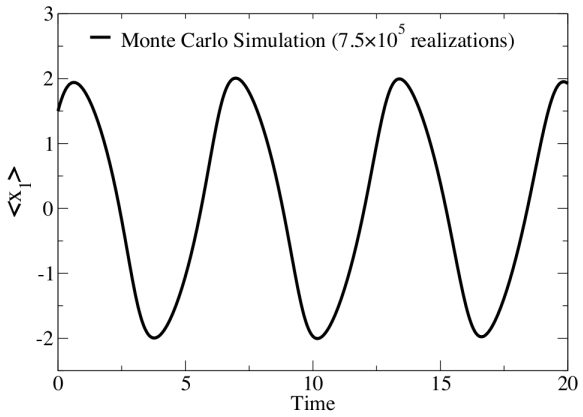

Figure 4.10: Evolution of the mean displacement $\langle x_1 \rangle$ in a Van der pol oscillator (Problem 4.2) computed using a Monte Carlo simulation with 7.5×10^5 realizations.

with a random damping coefficient is considered in this UQ problem. Similar to the previous test problem, a uniform distribution is assumed for the damping coefficient, C ($C \in [0, 1]$). The evolution of random response variables corresponding to system states for this test problem can be described by the following differential equations:

$$\dot{x}_1 = x_2, \tag{4.17}$$

$$\dot{x}_2 = C(\xi) x_2 \left(1 - x_1^2\right) - x_1. \tag{4.18}$$

where x_1 and x_2 denote the oscillator displacement and velocity, respectively and $C(\xi) = \frac{1}{2} + \frac{1}{2}\xi$. Here, the random initial conditions at $t = 0$ are defined as Gaussian densities of $N(1.5, 0.01)$ for both x_1 and x_2. The time evolution of the mean of x_1 for this problem, computed using Monte Carlo simulation, is shown in Fig. 4.10. The proposed adaptive finite difference solution shown in Fig. 4.11 confirms the occurrence of periodic fluctuations in the response mean. Considering the converged Monte Carlo simulation with 7.5×10^5 realizations as the reference solution, the error in the moments ($\varepsilon_M^{(n)}(t)$) at three different times are computed for both fixed and adaptive grid numerical solution of the Liouville equation with the results shown in Fig. 4.12. Here, the Liouville equation is solved using 5 Gauss

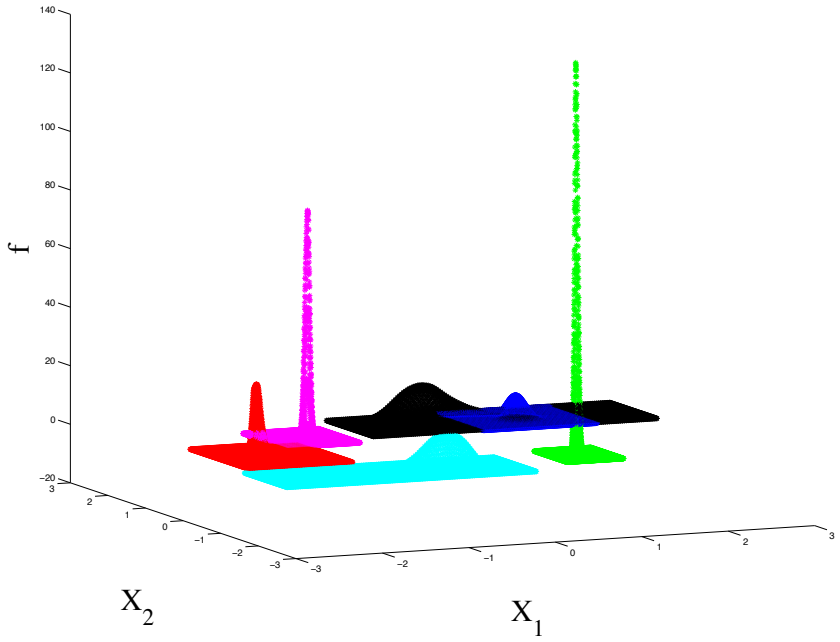

Figure 4.11: Joint PDF evolution for a Van der pol oscillator (Problem 4.2) for the parameter $\xi = 0.906$ at different time-steps: $t = 0$ (blue); $t = 2.5$ (red); $t = 5$ (green); $t = 10$ (green); $t = 15$ (magenta); $t = 20$ (black). Results are obtained using an adaptive moving uniform grid with $P_i = 150$.

quadrature points ($N_p = 5$). Figure 4.12 demonstrates the good agreement between the numerical results and the statistical data obtained from Monte Carlo simulation. Again, the comparison indicates that considerable improvement in accuracy can be achieved using the proposed adaptive mesh method. As can be seen in these figures, for a given number of grid points, generally there is some slight degradation in the accuracy of the moments as time increases. While the amount of degradation does not vary significantly with number of grid points for the fixed grid solution, in the adaptive grid solution an increase in the number of grid points improves this result.

4.2.3 Problem 4.3: Double spring-mass system

A system comprised of two linear springs and two point masses, illustrated in Fig. 4.13, is studied using the proposed approach. This problem can be represented

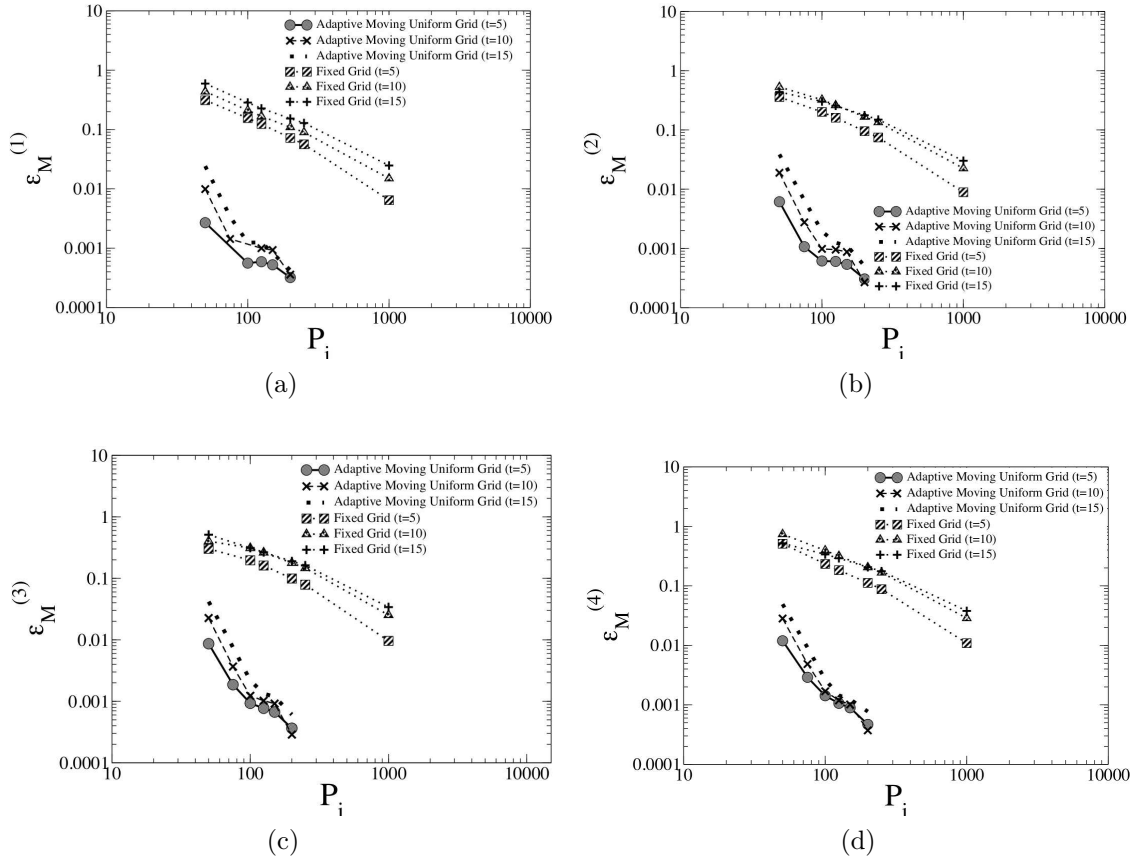

Figure 4.12: Error in the first four moments of the Van der pol oscillator displacement (x_1), for $t = 5,\ 10$ and 15 for Problem 4.2. Comparison is made between the finite difference solutions on fixed and adaptive grids (with $N_P = 5$). In the computation of the error, a Monte Carlo solution with 7.5×10^5 realizations is considered to be the reference solution.

by the following system of equations.

$$\dot{x}_1 = x_2, \tag{4.19}$$

$$\dot{x}_2 = -\frac{k_1}{m_1}x_1 + \frac{k_2(\xi)}{m_1}(x_3 - x_1), \tag{4.20}$$

$$\dot{x}_3 = x_4, \tag{4.21}$$

$$\dot{x}_4 = -\frac{k_2(\xi)}{m_2}(x_3 - x_1), \tag{4.22}$$

where k_1, m_1 and m_2 denote the first spring stiffness, first and second point mass, respectively. Here k_2 is assumed to be a uniformly distributed random parameter in

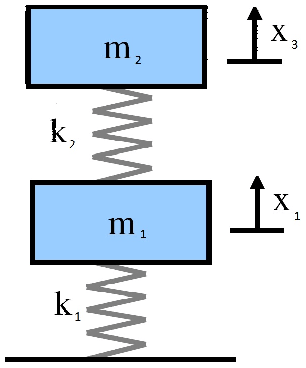

Figure 4.13: Double spring-mass system; Problem 4.3

the domain $k_2 \in [0.25, 0.75]$, $k_1 = 1$ and $m_1 = m_2 = 1$. Setting the initial conditions for x_1, x_2, x_3 and x_4 to be normally distributed, results in the following expression for the initial conditional density:

$$f(x_1, x_2, x_3, x_4, \xi, 0) = \frac{1}{4\pi^2 \sigma_1 \sigma_2 \sigma_3 \sigma_4} \exp\left\{ -\sum_{k=1}^{4} \frac{(x_k - \mu_k)^2}{2\sigma_k^2} \right\}, \tag{4.23}$$

where $\sigma_1 = \sigma_2 = \sigma_3 = \sigma_4 = 0.5$, $\mu_1 = 0.5$ and $\mu_2 = \mu_3 = \mu_4 = 0.0$. $N_p = 5$ conditioning samples are used in ξ. In Fig. 4.14 the result from Monte Carlo simulation for the evolution of the first point mass (m_1) displacement (x_1) mean is shown. As expected, similar to the first test problem the response mean exhibits an oscillatory behavior, which after a large time reaches a stationary state. Considering the results obtained from Monte Carlo simulation with 1.25×10^6 realizations as the reference solution, the errors in the moments of x_1 for two different times are computed and shown in Fig. 4.15. As illustrated in Fig. 4.15, the comparison once again indicates significant improvement, over the fixed grid solution, in the computational performance of the adaptive grid finite difference solution. For instance, on a fixed mesh 43 times the number of grid points used in the adaptive mesh solution are needed to obtain a similar level of accuracy for the fourth moment at $t = 5$.

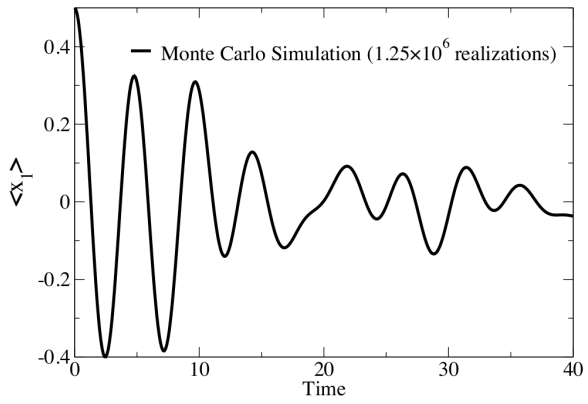

Figure 4.14: Evolution of the mean displacement $\langle x_1 \rangle$ of m_1 in the double spring oscillator (Problem 4.3) as obtained from a Monte Carlo simulation with 1.25×10^6 realizations.

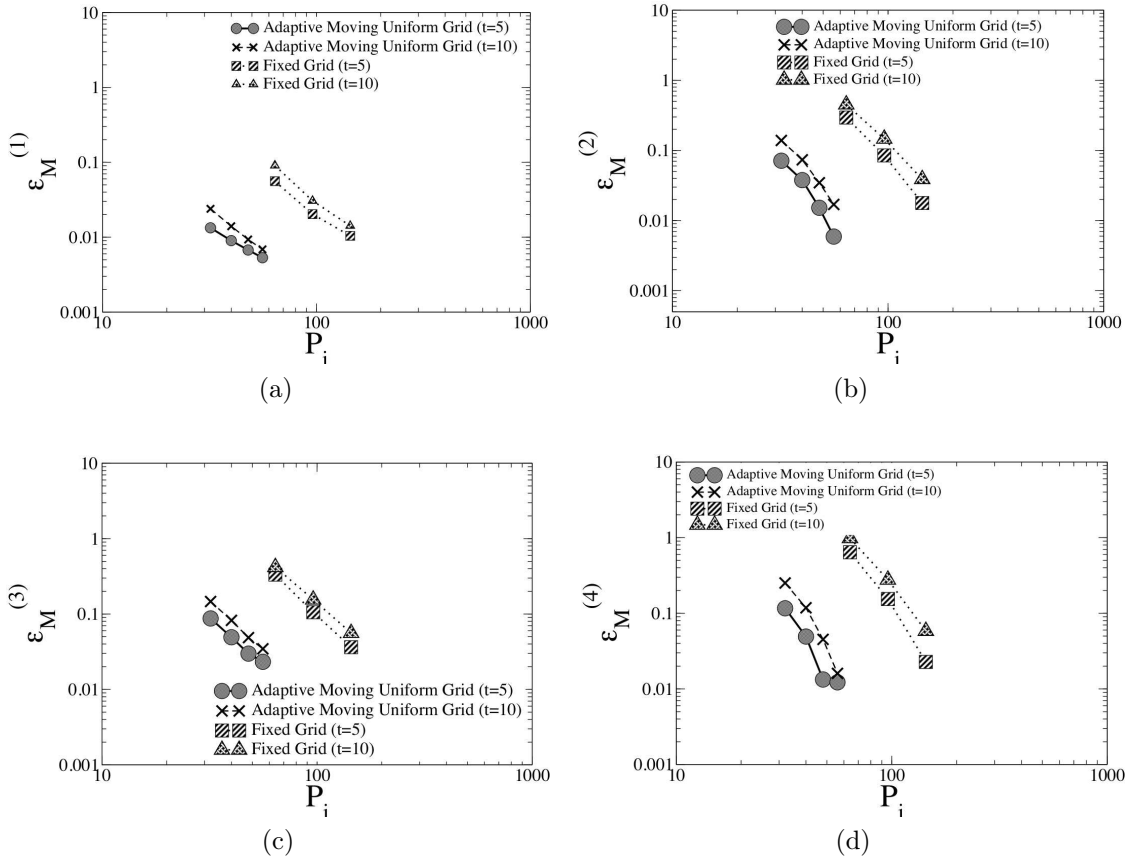

Figure 4.15: Error in the first four moments of the displacement (x_1) of mass m_1, shown at $t = 5$ and 10, for Problem 4.3. Comparison is made between the finite difference solutions on fixed and adaptive grids ($N_P = 5$). In the computation of error, a Monte Carlo solution with 1.25×10^6 realizations is considered to be the reference solution.

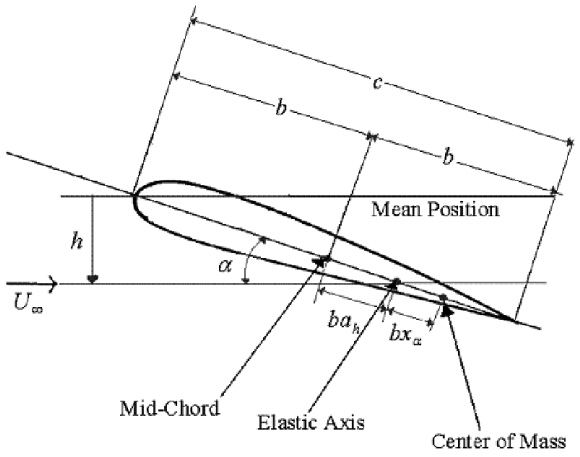

Figure 4.16: Schematic of a typical section airfoil with pitch (α) and plunge (h) degrees of freedom (Problem 4.4).

4.2.4 Problem 4.4: Nonlinear aeroelastic system

The fourth canonical problem is studied here in this chapter as a benchmark problem to demonstrate the capability of the proposed approach in dealing with nonlinear dynamical systems containing parametric uncertainties. As shown in Fig. 4.16, in this test problem a two degree-of-freedom typical section airfoil oscillating in pitch (α) and plunge (h) is considered. The airfoil is subjected to an incompressible air flow with free stream velocity U_∞. Ignoring thickness and camber effects, a quasi-steady aerodynamic model [139] is applied for this problem. The elastic axis of the airfoil is located at a distance $a_h b$ from its mid-chord and the distance between its center of mass and elastic axis is $x_\alpha b$. The system contains a hardening cubic nonlinearity in pitch resulting in the occurrence of supercritical limit cycle oscillations (LCO) at flow velocities above the linear flutter speed [140]. The coefficient of the cubic restoring force is assumed to be a random parameter with a lognormal distribution, $\beta_\alpha \sim \ln N(0,1)$.

The differential equations which govern the time evolution of the random variables x_1, x_2, x_3 and x_4 corresponding to the aeroelastic system states, which represent non-dimensional pitch displacement, pitch velocity, plunge displacement and

velocity, respectively, can be written as

$$\dot{x}_1 = x_2, \tag{4.24}$$

$$\dot{x}_2 = \frac{c_0 H - d_0 P}{d_0 c_1 - c_0 d_1}, \tag{4.25}$$

$$\dot{x}_3 = x_4, \tag{4.26}$$

$$\dot{x}_4 = \frac{d_1 P - c_1 H}{d_0 c_1 - c_0 d_1} \tag{4.27}$$

where

$$P = c_2 x_4 + c_3 x_2 + c_4 x_3 + c_5 x_1 + \left(\frac{\overline{\omega}}{U^*}\right)^2 x_3, \tag{4.28}$$

$$H = d_2 x_2 + d_3 x_1 + d_4 x_4 + d_5 x_3 + \left(\frac{\overline{1}}{U^*}\right)^2 \left(x_1 + \beta_\alpha x_1^3\right), \tag{4.29}$$

and

$$\begin{cases} c_0 = 1 + \frac{1}{\mu}, & c_1 = x_\alpha - \frac{a_h}{\mu}, \\ c_2 = \frac{2}{\mu}, & c_3 = \frac{2}{\mu}\left(1 - a_h\right), \\ c_4 = 0, & c_5 = \frac{2}{\mu}, \\ d_0 = \frac{x_\alpha}{r_\alpha^2} - \frac{a_j}{\mu r_\alpha^2}, & d_1 = 1 + \frac{1}{\mu r_\alpha^2}\left(\frac{1}{8} + a_h\right), \\ d_2 = \frac{1}{\mu r_\alpha^2}\left(\left(\frac{1}{2} - a_h\right) - \left(\frac{1}{4} - a_h^2\right)\right), & d_3 = -\frac{1}{\mu r_\alpha^2}\left(1 + 2a_h\right), \\ d_4 = -\frac{1}{\mu r_\alpha^2}\left(1 + 2a_h\right), & d_5 = 0. \end{cases} \tag{4.30}$$

Here, μ, $\overline{\omega}$, U^* and r_α denote the airfoil to air mass ratio, natural frequency ratio, non-dimensional flow velocity and radius of gyration about elastic axis, respectively. Moreover, in Eq. 4.27 state variables are differentiated with respect to the non-dimensional time τ. For the chosen values of the parameters ($a_h = -0.5$, $x_\alpha = 0.25$, $r_\alpha = 0.75$, $\mu = 100$, $\overline{\omega} = 0.2$) the velocity at which the system becomes linearly unstable (Hopf bifurcation point) is determined (through numerical time integration) to be 5.29.

The initial conditional density presented in Eq. 4.23 is also assumed for this

problem. For $U^* = 5.43147$ (i.e. above the flow velocity at which the deterministic system becomes linearly unstable) the resulting Liouville equation is solved numerically on both fixed and time-adaptive grids along $N_p = 8$ Gauss-quadrature points in the ξ direction. The use of half time-step finite difference operators within the EAD method allows for stable computation with CFL ≤ 2 [124], and thus the maximum local CFL numbers in x_1, x_2, x_3 and x_4 directions are set to be 1.8, 1.8, 1.8 and 0.9, respectively.

Considering the Monte Carlo simulation with 2.25×10^6 realizations as the reference solution, the error in the first four moments of x_1 are computed and shown in Fig 4.17. As before, the results in this figure clearly demonstrate the excellent computational performance of the adaptive approach in comparison to the fixed grid solution. It should be noted that the relatively large errors in the odd moments for $t = 20$, as compared with the odd moments at $t = 10$ and even moments for both times, are likely due to the small values of these moments for $t = 20$.

4.3 Summary

In this chapter, through the extension of the adaptive moving domain/mesh algorithm, which was presented in Chapter 1, to multiple dimensions, an efficient computational tool was introduced to obtain the statistical quantities of interest for dynamical systems of moderate dimension with parametric uncertainty. The methodology formulates the UQ problem in the form of a hyperbolic PDE (Liouville equation) governing the time-evolution of the joint probability density of the random state (response) variables. As finding an analytical solution for this linear multidimensional partial differential equation is only feasible in select cases and its numerical solution can be computationally expensive, any enhancement in the computational performance of the numerical solution is crucial. In this chapter, such improvement is made through quadrature-based sampling in the random param-

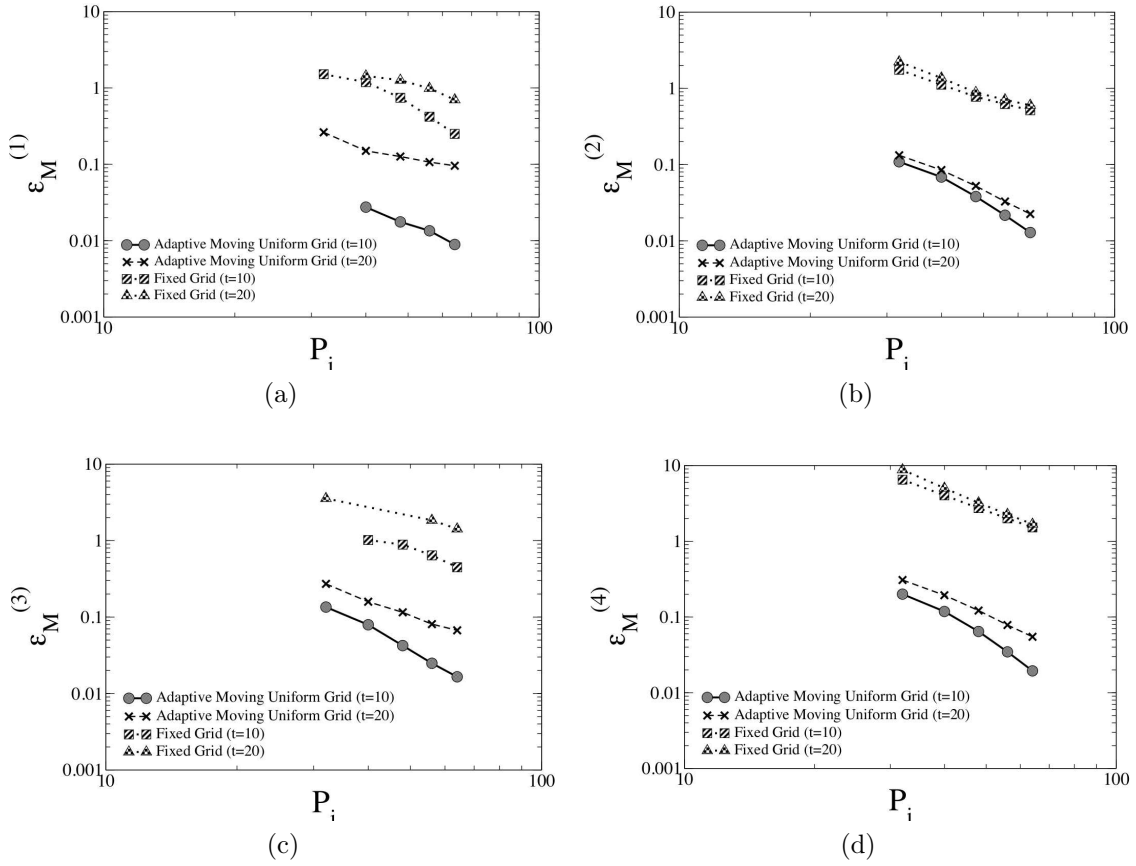

Figure 4.17: Error in the first four moments of the airfoil pitch displacement displacement (x_1), shown at $t = 10$ and 20, for Problem 4.4. Comparison is made between the finite difference solutions on fixed and adaptive grids ($N_P = 8$). In the computation of error, a Monte Carlo solution with 2.25×10^6 realizations is considered to be the reference solution.

eter space and the application of a novel time-varying grid adaptation technique in random state space. Solving the Liouville equation along only few number of Gauss-quadrature points, which can be extended to a parallel processing environment easily as it is perfectly parallel, reduces the computational costs drastically. Furthermore, solving the Liouville equation on a moving time-varying grid which is resized in each time-step in accordance with the conditional density function behavior increases the accuracy of the finite difference solution with respect to the number of grid points in the response space. Such reduction in the required number of grid points to maintain a high level of accuracy, allows for the efficient solution of UQ

problems with moderate (state) dimension. The results obtained from solution of the example problems studied in this chapter indicate that the proposed approach can accurately predict the long time behavior of the random response even when the dynamical system contains nonlinearities (test problems 4.2 and 4.4). Finally, the method presented gives the conditional density directly and accurately and there is no need for *a posteriori* analysis of the computed statistical data. Thus, it has the potential to be considered as an alternative to Monte Carlo simulation for uncertainty quantification of dynamical systems with moderate number of (random) states.

CHAPTER 5

Numerical Solution of Multidimensional PDEs Using Defect Correction on Adaptive Grids

In Chapter 3, we proposed a novel computational approach to obtain high order accurate, finite difference based numerical solutions of hyperbolic partial differential equations, through a combination of grid adaptation, non-iterative defect correction and remap with monotonicity preserving interpolation. This approach, which is the second grid adaptation method proposed in Chapter 3, is able to increase the formal order of accuracy of an underlying finite difference scheme while providing a numerical solution which minimizes non-physical numerical oscillations. Dimensional splitting techniques are used to extend the range of application of this method from single to multiple dimensions. Using the monotonicity preserving feature of this interpolant, finite difference schemes with high order of accuracy are developed for solving multidimensional, hyperbolic PDEs. In this chapter, for the proof of concept, three canonical problems including two-dimensional Liouville equations with spatially dependent drift coefficients as well as a two-dimensional nonlinear hyperbolic equation are solved. The results demonstrate four major features of the proposed methodology including: (1) the capability to improve the order of accuracy of difference schemes up to any desired level, (2) the ability to obtain the given level of accuracy at a lower computational cost (or time) when compared to some widely used standard finite difference schemes (3) accurate oscillation-free resolution of discontinuities and (4) the computational simplicity for application to multidimensional problems.

5.1 Extension to multiple dimensions

Operator splitting techniques are widely used techniques for dividing complex problems into several simpler subproblems in which sophisticated accurate numerical solutions are available [141, 142]. One particular use of this technique, as discussed in Chapter 4, is extending the application of high order accurate one-dimensional numerical methods to multidimensional problems [124]. The main feature of such a technique, typically referred to as dimension splitting, is the reduction of complex multidimensional problems into series of one-dimensional problems in each time-step. As one of the major issues in extending our approach to multiple dimensions is that the truncation error analysis of multidimensional discretization schemes results in highly nonlinear and complex expressions, it is almost impractical to completely remove irregularities by grid adaptation alone. As such dimension splitting, which benefits from the computational simplicity of one dimensional adaptive grid distribution, is an effective way of dealing with this issue.

The simplest version of this technique known as Lie-Trotter splitting was first applied by Bagrinovski and Godunov to solve PDE [143]. It approximates the N-dimensional PDEs solution as

$$f_j^{n+1} = \left(L_{\Delta t}^{(x_1)} L_{\Delta t}^{(x_2)} \dots L_{\Delta t}^{(x_{N-1})} L_{\Delta t}^{(x_N)} \right) \tilde{f}_j^n \quad , \tag{5.1}$$

where $L_{\Delta t}^{(x_i)}$ denotes a unidimensional numerical scheme applied for the jth dimension. This approximation is first order accurate in time. However, the accuracy also depends on the order of the sequence. Additive splitting is designed to remove such dependency [144]. Using this method for a two-dimensional problem the resultant sequence of one-dimensional numerical solution reads

$$f_j^{n+1} = \frac{1}{2} \left(L_{\Delta t}^{(x_1)} L_{\Delta t}^{(x_2)} + L_{\Delta t}^{(x_2)} L_{\Delta t}^{(x_1)} \right) \tilde{f}_j^n \quad , \tag{5.2}$$

where Eq. 5.2 is still first order accurate in time. Strang [145] constructed the second order equivalent of Lie-Trotter and additive splitting approaches by developing a symmetric combination of unidimensional numerical solutions.

$$f_j^{n+1} = \left(L_{\frac{\Delta t}{2}}^{(x_1)} L_{\frac{\Delta t}{2}}^{(x_2)} \dots L_{\frac{\Delta t}{2}}^{(x_{N-1})} L_{\Delta t}^{(x_N)} L_{\frac{\Delta t}{2}}^{(x_{N-1})} \dots L_{\frac{\Delta t}{2}}^{(x_2)} L_{\frac{\Delta t}{2}}^{(x_1)} \right) \tilde{f}_j^n \quad . \tag{5.3}$$

Higher order operator splitting methods have also been applied in the literature [146, 147, 141, 148]. A comprehensive table of splitting methods up to 8th order of accuracy can be found in the paper by Lee and Fornberg [149]. In this chapter, either Eq. 5.2 or Eq. 5.3 are used to extend the method presented in the previous section to higher dimensions. From an algorithmic prospective, in multiple dimensions steps 4 through 9 in Algorithm 1 are repeated N or $2N-1$ times depending on whether Eq. 5.2 or Eq. 5.3 is used. In addition Δt^n is now computed using the information from all N dimensions. Other than these two modifications no other changes to the structure of Algorithm 1 is necessary for application of the method to multiple dimensions.

5.2 Results and discussion

5.2.1 Problem 5.1: Two-dimensional Liouville equation with linearly varying coefficients

In order to demonstrate the capabilities of the proposed approach in enhancing the difference scheme's order of accuracy in multiple dimensions, three test problems are solved. The first one deals with the solution of the Liouville equation with linear spatially dependent coefficients:

$$\frac{\partial f}{\partial t} + \frac{\partial \left(y f \right)}{\partial x} - \frac{\partial \left(x f \right)}{\partial y} = 0, \tag{5.4}$$

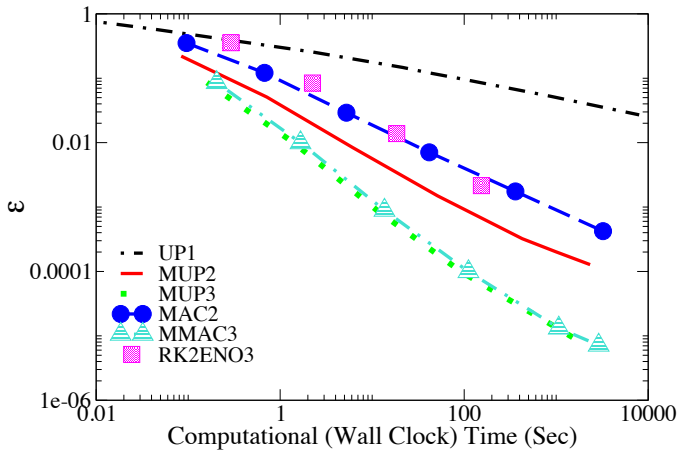

Figure 5.1: L2 Error in the computed solution for Problem 5.1 at t =0.75 versus computational (wall clock) time. Numerical solutions obtained from the standard first order upwind (UP1), the second order MacCormack (MAC2) and ENO (RK2ENO3) finite difference methods are compared with those obtained using grid adaptation and non-iterative defect correction (modified schemes) including the third order modified MacCormack (MMAC3) and second and third order modified upwind methods (MUP2, MUP3). In the computation of the error, the analytical solution is considered as the reference solution.

where the domain is defined as $x \in [-8.5, -0.5]$ and $y \in [-8, -1]$. Function f is assumed to be equal to zero at the domain boundaries and at $t = 0$ is given by:

$$f(x, y, 0) = \frac{1}{4\pi\sigma_x\sigma_y}\exp\left\{-\frac{(x-\mu_x)^2}{2\sigma_x^2} - \frac{(y-\mu_y)^2}{2\sigma_y^2}\right\}, \tag{5.5}$$

where $\mu_x = -2.5$, $\mu_y = -6.0$ and $\sigma_x = \sigma_y = 0.25$. The exact solution for Eq. 5.4 is obtained as

$$f(x, y, t) = \frac{1}{4\pi\sigma_x\sigma_y}\exp\left\{-\frac{(x\cos t - y\sin t - \mu_x)^2}{2\sigma_x^2} - \frac{(y\cos t + x\sin t - \mu_y)^2}{2\sigma_y^2}\right\}. \tag{5.6}$$

Equation 5.4 is solved using multiple standard finite difference schemes including first order upwind (UP1), MacCormack (MAC2) and third order ENO (RK2ENO3) methods as well as the schemes modified with the proposed approach. Applying defect corrections and solving the resultant discretized equations (modified upwind

and the MacCormack) on the adaptive grid leads to an improvement in the order of accuracy of numerical solution. Once again, the computational efficiency of the modified scheme with a higher order of accuracy is depicted in Fig. 5.1. While the splitting technique being used (Eq. 5.3) is second order accurate in time and therefore the improvement of accuracy to second order is straightforward, as shown in Figs. 5.2 and 5.3 the results using the defect correction expressions given as Eqs. 3.32 and C.1 for upwind and the MacCormack schemes respectively, exhibit third order accuracy in both space and time. This is due to the fact that spatial and temporal accuracy are tied together with characteristic equation $\Gamma^{(i)} = 0$ and any enhancement using the proposed methodology affects both. However, as the numbers of grid points increases the slope gradually decreases from 3 such that for instance it goes down to 2.74 in $800 \leq P_i \leq 1000$ for the modified upwind scheme. While in order to maintain third order accuracy the application of higher order splitting techniques appears necessary, for general practical problems in which a very large number of grid points is not needed, using the Strang splitting technique (Eq. 5.3) gives third order accuracy.

5.2.2 Problem 5.2: Two-dimensional Liouville equation with nonlinearly varying coefficients

The impact of applying a nonlinear grading function for resolving the singularities of the modified equation is investigated in the second test problem solved in this chapter. Equation 5.7 is a two-dimensional Liouville equation with nonlinear spatial dependencies in its coefficients

$$\frac{\partial f}{\partial t} + \frac{\partial \left(yf\right)}{\partial x} - \frac{\partial \left(\left(cy(1-x^2) - x\right) f\right)}{\partial y} = 0, \tag{5.7}$$

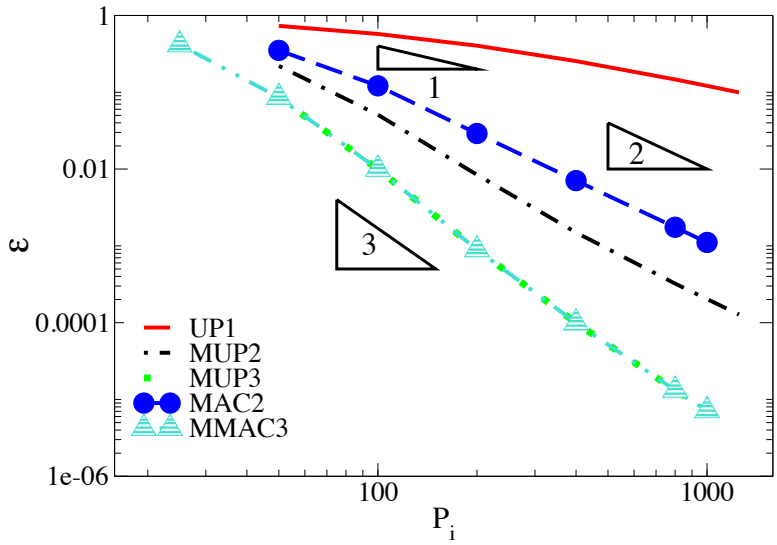

Figure 5.2: L2 Error in the computed solution for Problem 5.1 at t =0.75 versus the number of (uniform) grid points in each dimension, P_i. Numerical solutions obtained from the standard first order upwind (UP1) and the second order MacCormack (MAC2) finite difference methods are compared with those obtained using grid adaptation and non-iterative defect correction (modified schemes) including the third order modified MacCormack (MMAC3) and second and third order modified upwind methods (MUP2, MUP3). In the computation of the error, the analytical solution is considered as the reference solution.

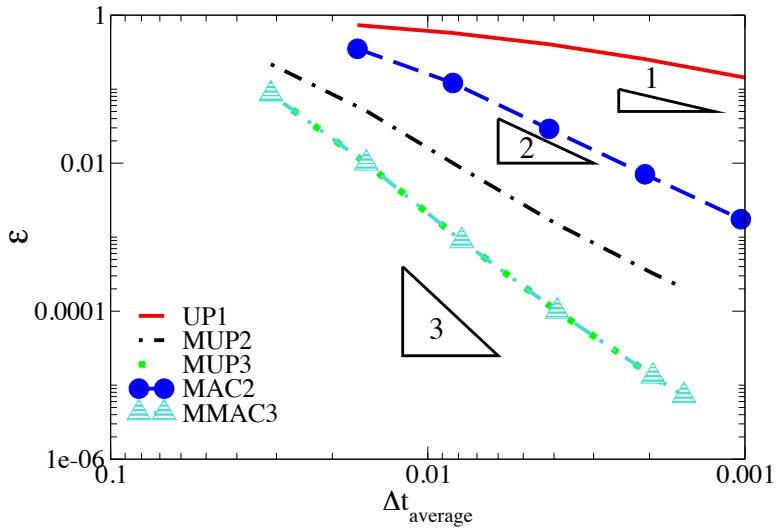

Figure 5.3: L2 Error in the computed solution for Problem 5.1 at t =0.75 versus average time-step, $\Delta t_{\text{average}}$. Numerical solutions obtained from the standard first order upwind (UP1) and the second order MacCormack (MAC2) finite difference methods are compared with those obtained using grid adaptation and non-iterative defect correction (modified schemes) including the third order modified MacCormack (MMAC3) and second and third order modified upwind methods (MUP2, MUP3). In the computation of the error, the analytical solution is considered as the reference solution.

where the domain is defined as $x \in [0.5, 2.5]$ and $y \in [0.05, 1.95]$ and $f = 0$ at the boundaries of the domain. This equation is used in the quantification of the uncertainties of a Van der Pol Oscillator with a random damping coefficient c. Here, we consider a case in which c is set equal to one and a bivariate Gaussian distribution (Eq. 5.5) is used as the initial condition for f with $\mu_x = 1.25$, $\mu = 1.5$ and $\sigma_x = \sigma_y = 0.1$. Unfortunately there is no exact solution available for this hyperbolic PDE. Therefore, the fully resolved solution obtained by the second order upwind scheme modified by the proposed approach on a domain with 3073 by 3073 grid points is considered as the reference solution for computing the L2 error using Eq. 3.46. After applying the defect correction terms to obtain second order accuracy for the upwind scheme, the following discretized equations are solved in the second order dimension

splitting sequence (if $D_{i,j}$ and $G_{i,j}$ are both positive):

$$\tilde{f}_{i,j}^{n+1,x} = \tilde{f}_{i,j}^{n} + \left(\Delta t^n / \left(2\Delta x_{i-\frac{1}{2},j}^{n}\right)\right)\left(D_{i-1,j}^{n}\tilde{f}_{i-1,j}^{n} - D_{i,j}^{n}\tilde{f}_{i,j}^{n}\right) + \frac{\left(\Delta t^n\right)^2}{8}\left(\tilde{f}_{i,j}^{n}\left(\left(D_x\right)_{i,j}^{n}\right)^2 + D_{i,j}^{n}\frac{-\alpha^2\tilde{f}_{i-1,j}^{n} + \tilde{f}_{i,j}^{n}\left(\alpha^2-1\right) + \tilde{f}_{i+1,j}^{n}}{\Delta x_{i-\frac{1}{2},j}^{n}\alpha\left(1+\alpha\right)}\left(D_x\right)_{i,j}^{n}\right), \tag{5.8}$$

$$\begin{aligned}\tilde{f}_{i,j}^{n+1,y} &= \tilde{f}_{i,j}^{n+1,x} + \left(\frac{\Delta t^n}{\Delta y_{i,j-\frac{1}{2}}^{n}}\right)\left(G_{i,j-1}^{n}\tilde{f}_{i,j-1}^{n+1,x} - G_{i,j}^{n}\tilde{f}_{i,j}^{n+1,x}\right) + \frac{\left(\Delta t^n\right)^2}{2}\times \\ &\left(\tilde{f}_{i,j}^{n+1,x}\left(\left(G_y\right)_{i,j}^{n}\right)^2 + G_{i,j}^{n}\frac{-\beta^2\tilde{f}_{i,j-1}^{n+1,x} + \tilde{f}_{i,j}^{n+1,x}\left(\beta^2-1\right) + \tilde{f}_{i,j+1}^{n+1,x}}{\Delta y_{i,j-\frac{1}{2}}^{n}\beta\left(1+\beta\right)}\times\right. \\ &\left.\left(G_y\right)_{i,j}^{n}\right),\end{aligned} \tag{5.9}$$

$$\begin{aligned}\tilde{f}_{i,j}^{n+1} &= \tilde{f}_{i,j}^{n+1,y} + \left(\frac{\Delta t^n}{2\Delta x_{i-\frac{1}{2},j}^{n}}\right)\left(D_{i-1,j}^{n}\tilde{f}_{i-1,j}^{n+1,y} - D_{i,j}^{n}\tilde{f}_{i,j}^{n+1,y}\right) + \frac{\left(\Delta t^n\right)^2}{8}\times \\ &\left(\tilde{f}_{i,j}^{n+1,y}\left(\left(D_x\right)_{i,j}^{n}\right)^2 + D_{i,j}^{n}\frac{-\alpha^2\tilde{f}_{i-1,j}^{n+1,y} + \tilde{f}_{i,j}^{n+1,y}\left(\alpha^2-1\right) + \tilde{f}_{i+1,j}^{n+1,y}}{\Delta x_{i-\frac{1}{2},j}^{n}\alpha\left(1+\alpha\right)}\times\right. \\ &\left.\left(D_x\right)_{i,j}^{n}\right),\end{aligned} \tag{5.10}$$

where $D(x,y) = -y$, $G(x,y) = cy(1-x^2) - x$, $\alpha = \Delta x_{i+\frac{1}{2},j}/\Delta x_{i-\frac{1}{2},j}$ and $\beta = \Delta y_{i,j+\frac{1}{2}}/\Delta y_{i,j-\frac{1}{2}}$. The discretized equation when $D_{i,j}$ and $G_{i,j}$ are negative can be obtained similarly. During the splitting sequence, it is necessary to perform interpolation six times not only to preserve the monotonicity but also to generate the singularity adaptive grid in an alternate direction process so that the same defect corrected discretization in one dimension can be applied to multiple dimensions. This might seem computationally costly, however comparison with the MacCormack

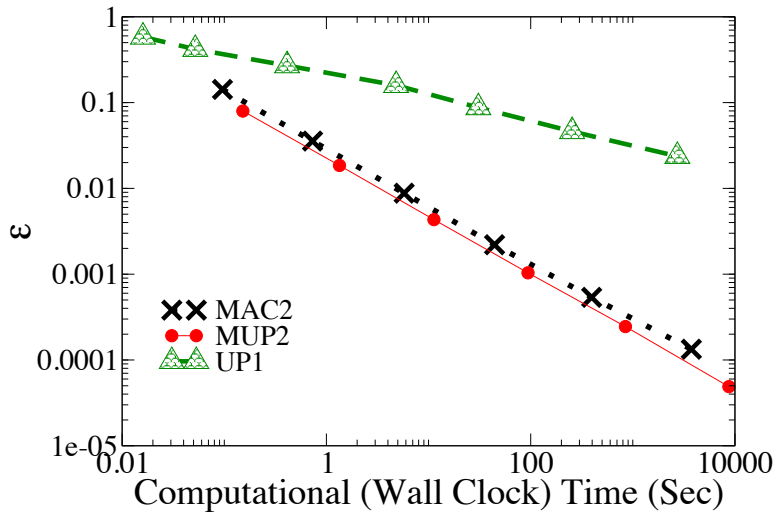

Figure 5.4: L2 Error in the computed solution for Problem 5.2 at t =0.5 versus computational (wall clock) time. Numerical solutions obtained from the standard first order upwind (UP1) and the second order MacCormack (MAC2) finite difference methods are compared with second order modified upwind method (MUP2). In the computation of the error, the fully resolved numerical solution is considered as the reference solution.

scheme in Fig. 5.4 demonstrates that the scheme has comparable computational efficiency for this particular problem. The results shown in Fig. 5.5 at $t = 0.5$ indicate the expected one order of accuracy improvement.

5.2.3 Problem 5.3: Two-dimensional nonlinear hyperbolic equation

One of distinctive features of hyperbolic PDEs is that their solution often contains discontinuities. These discontinuities occur typically in the form of a shock when a nonlinear hyperbolic conservation law such as Burgers equation is solved. Using a method of solution which eliminates or minimizes non-physical (spatial) oscillations is crucial in order to capture such discontinuities, which often rapidly propagates with time. The final canonical problem of this chapter is devoted to the study of the impact of the proposed methodology on the finite difference solutions of the model

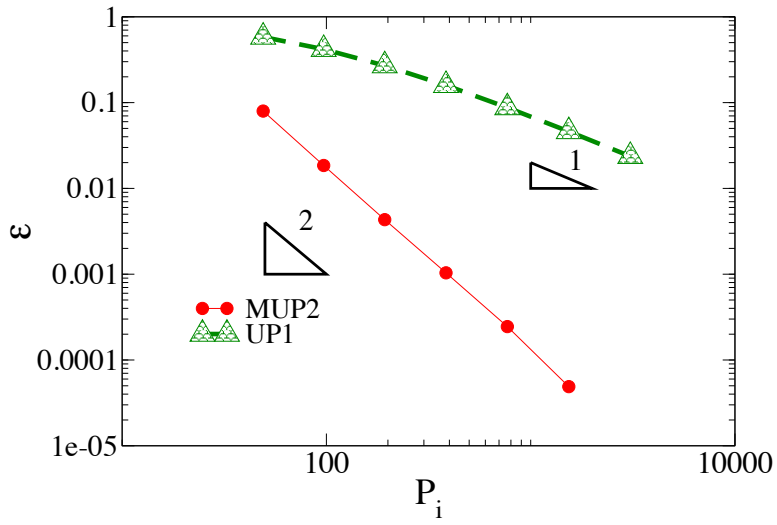

Figure 5.5: L2 Error in the computed solution for Problem 5.2 at t =0.5 versus the number of (uniform) grid points in each dimension, P_i. Numerical solutions obtained from the standard first order upwind (UP1) and the second order MacCormack (MAC2) finite difference methods are compared with second order modified upwind method (MUP2). In the computation of the error, the fully resolved numerical solution is considered as the reference solution.

nonlinear hyperbolic PDE:

$$\frac{\partial f}{\partial t} + f\frac{\partial f}{\partial x} + f\frac{\partial f}{\partial y} = 0. \tag{5.11}$$

Equation 5.11 has been used previously in the literature to investigate different schemes for the numerical solution of nonlinear hyperbolic PDEs in multiple dimensions [150, 151]. Also as discontinuity is involved in its solution, this problem can be used as a benchmark test problem to demonstrate the monotonicity preserving feature of a numerical method.

Here, Eq. 5.12 is considered as the initial condition for f:

$$f(x, y, 0) = 2 + \frac{1}{4\pi\sigma_x\sigma_y}\exp\left\{-\frac{(x-\mu_x)^2}{2\sigma_x^2} - \frac{(y-\mu_y)^2}{2\sigma_y^2}\right\}, \tag{5.12}$$

with $\mu_x = \mu_y = 12$ and $\sigma_x = \sigma_y = 1$. Equation 5.11 is solved on the domain defined as $x \in [0.5, 25.5]$ and $y \in [0.05, 25.05]$ where f is equal to 2 at its boundaries. Thus,

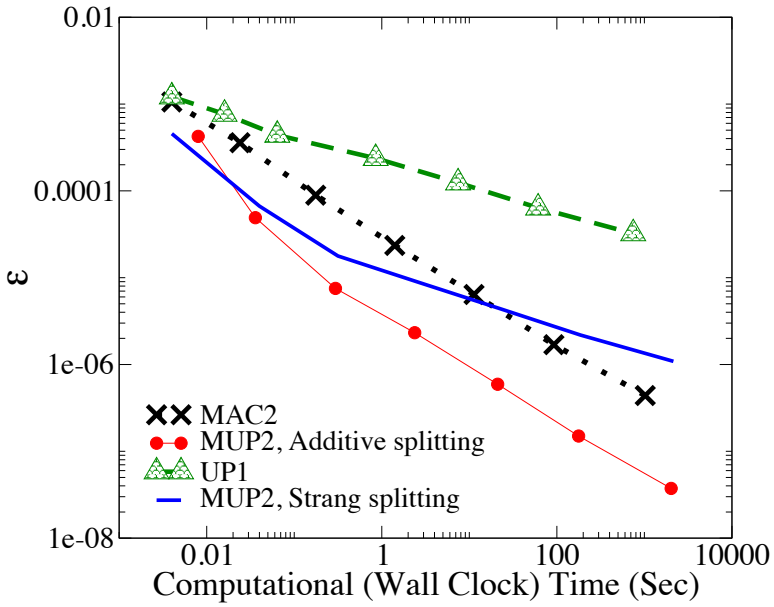

Figure 5.6: L2 Error in the computed solution for Problem 5.3 at t =2 versus computational (wall clock) time. Numerical solutions obtained from the standard first order upwind (UP1) and the second order MacCormack (MAC2) finite difference methods are compared with second order modified upwind methods (MUP2). In the computation of the error, the analytical solution is considered as the reference solution.

the exact solution of Eq. 5.11 with the initial condition given in Eq. 5.12 can be obtained by solving the following nonlinear algebraic equation:

$$f - 2 - \frac{1}{4\pi\sigma_x\sigma_y}\exp\left\{-\frac{(x - t\times f - \mu_x)^2}{2\sigma_x^2} - \frac{(y - t\times f - \mu_y)^2}{2\sigma_y^2}\right\} = 0. \tag{5.13}$$

If the first order upwind method is used to approximate the solution of Eq. 5.11, the truncation error expression for $L_{\Delta t}^{(x)}$ when $f \geq 0$ is given by

$$\text{TE} = \frac{f_{i,j}^n}{2}\left(\frac{\partial^2 f}{\partial x^2}\right)_{i,j}^n \left(\Delta x_{i-\frac{1}{2},j}^n - f_{i,j}^n \Delta t^n\right) + \left(\frac{\Delta x_{i-\frac{1}{2},j}^n}{2} - f_{i,j}^n \Delta t^n\right)\left(\left(\frac{\partial f}{\partial x}\right)_{i,j}^n\right)^2 + \mathcal{O}(\Delta t^n + \Delta x_{i-\frac{1}{2},j}^n)^2. \tag{5.14}$$

A similar expression can be obtained for the other dimension. From the heuristic

stability analysis put forth by Hirt [131], it is easy to distinguish the irregular perturbation, which is the first term of Eq. 5.14. Thus, the following grading function is used in order to generate the adaptive mesh, which automatically removes such irregularities:

$$x_{i-1,j} = x_{i,j} - f^n_{i,j}\Delta t^n \tag{5.15}$$

Applying the remaining terms of Eq. 5.14 in the non-iterative defect correction process to the original first order upwind approximation, the modified discretization is obtained:

$$L^{(x)}_{\Delta t} = \tilde{f}^n_{i,j} + \left(\Delta t^n / \left(2\Delta x^n_{i-\frac{1}{2},j}\right)\right)\left(\left(\tilde{f}^n_{i-1,j}\right)^2 - \left(\tilde{f}^n_{i,j}\right)^2\right) - \Delta t^n \left(\frac{-\alpha^2 \tilde{f}^n_{i-1,j} + \tilde{f}^n_{i,j}\left(\alpha^2 - 1\right) + \tilde{f}^n_{i+1,j}}{\Delta x^n_{i-\frac{1}{2},j}\alpha\left(1+\alpha\right)}\right)\left(\frac{\Delta x^n_{i-\frac{1}{2},j}}{2} - \tilde{f}^n_{i,j}\Delta t^n\right). \tag{5.16}$$

When Strang splitting is used, the solution sequence is in accordance with Eq. 5.3 and second order of accuracy is expected. However, as Crandall and Majda showed in their paper [151], such dimensional splitting does not give the expected order of accuracy due to the nonlinearities and discontinuities associated with the solution of Eq. 5.11. On the other hand, additive or Lie-Trotter dimension splitting techniques theoretically can give infinite order of accuracy for such problems [151] and therefore both can be used in this case to enhance the order of accuracy of the upwind scheme. The difference in the outcome of applying Strang and Additive splitting techniques is well illustrated in Figs. 5.6 and 5.7. These results confirm the results of Crandall and Majda. The resultant enhancement in the accuracy of unidimensional solutions is fully dominated by the order of accuracy of the alternate direction technique and such influence becomes more significant as the number of grid points increases. As shown in Fig. 5.6, the enhancement in the solution order of accuracy

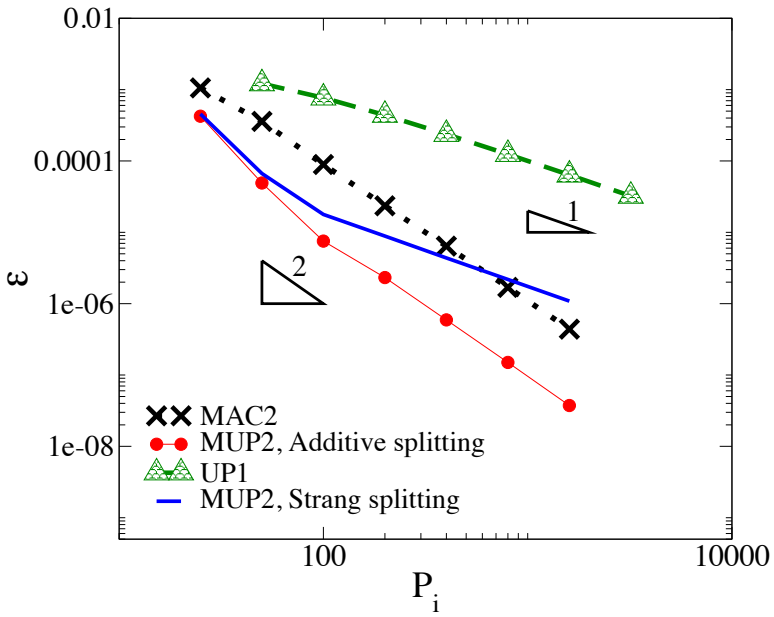

Figure 5.7: L2 Error in the computed solution for Problem 5.3 at t =2 versus the number of (uniform) grid points in each dimension, P_i. Numerical solutions obtained from the standard first order upwind (UP1) and the second order MacCormack (MAC2) finite difference methods are compared with second order modified upwind methods (MUP2). In the computation of the error, the analytical solution is considered as the reference solution.

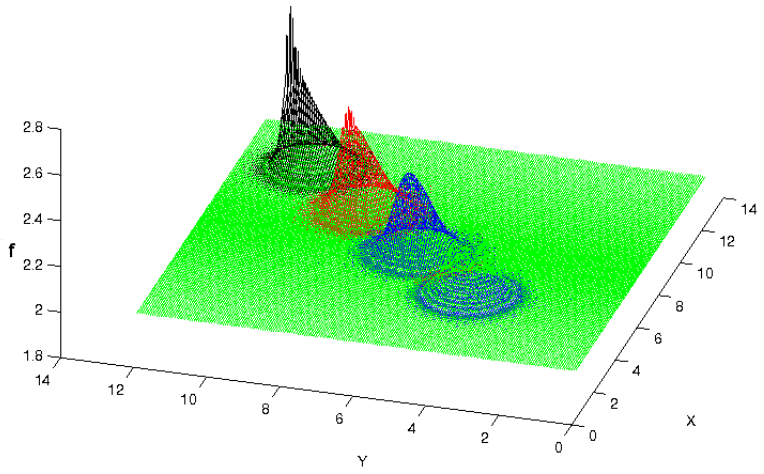

Figure 5.8: Illustration of shock formation in the finite difference solution of the model nonlinear hyperbolic PDE (Eq. 5.11); Response is shown at $t = 0$, 1.5, 2 and 3. The upwind scheme, which is modified by the proposed methodology in multiple dimensions, is used to solve the nonlinear PDE

of the modified upwind scheme is obtained with a significant computational time savings in comparison to the TVD MacCormack scheme. It is worth noting that as the response approaches the shock, the derivatives become undefined over the discontinuities. Therefore any enhancement in the order of accuracy of the solution gradually goes away and like other approaches the order of accuracy reduces to first order. However, as shown in Fig 5.8, the modified scheme is still able to accurately capture the shock and provide a solution which does not exhibit non-physical oscillations. Furthermore, as proved by Dougherty et al. [133], applying the monotonicity preservation constraints during the interpolation process does not reduce the order of accuracy to less than third if the local derivative values are at least second order accurate. Thus, the role of slope or flux limiters is performed automatically within the scheme without a significant degeneration of accuracy near local extrema as occurs when a TVD scheme is used.

5.3 Summary

As we noted earlier, Godunov's barrier theorem indicates impracticality of having a second or higher order linear monotonicity preserving finite difference solution. However, under certain conditions (for example, setting the local CFL number equal to one for the advection equation) such a scheme may exist. As an extension of the method presented in Chapter 3, in this chapter such a possibility was explored in multidimensional spaces through the application of an operator (dimension) splitting technique and a data remapping method (between adaptive non-uniform and uniform meshes) which uses monotonicity preserving interpolation. In this context, we developed a multi-dimensional, higher order accurate scheme which appears to not only preserve the monotonicity of the numerical solution but also benefit from the computational simplicity of linear finite difference schemes.

As the extension to multiple dimensions is achieved using a dimensional splitting technique, truncation error analysis is done in each dimension separately. In each dimension, irregular perturbations are identified using a heuristic stability analysis and the irregular perturbations are automatically eliminated using a grid adaptation method that is designed to remove the (leading order) singularities of the modified equation. The corresponding defect corrected discretized equation is obtained by the direct subtraction of the remaining terms in the modified equation up to the desired order of accuracy. As the irregularities are removed through grid adaptation, no iteration is necessary to establish the numerical stability of the resultant finite difference solution. In order to minimize non-physical spatial oscillations in high-gradient regions, as well as extend the grid adaptation to multidimensional space, a monotonicity preserving interpolation is used. Note that as the sequence of unidirectional solutions are obtained in accordance with the dimensional splitting technique being used, the grid adaptation is performed in an alternate direction fashion. The

outcome is a modified multidimensional difference scheme with a higher order of accuracy and reasonable computational speed.

Numerical results obtained using the proposed approach for three selected canonical problems (considered in this chapter) indicate the capability of the general approach to give the desired order of accuracy with less computational effort when compared with standard high-order finite difference methods.

CHAPTER 6

Conclusion

6.1 Overview

Novel finite difference (FD) based methods for numerical solution of hyperbolic partial differential equations (PDEs) using adaptive grids are proposed in this dissertation. While there are several challenges, especially due to complexity of implementation and high computational costs, associated with accurate numerical solution of PDEs based on high-order FD methods, the overall goal of this research is to seek improvements in accuracy and/or computational efficiency (in comparison to other approaches). In particular, we proposed a broad class of novel methods based on modifications to existing low-order finite difference schemes through the use of adaptive grids in order to further improve their order of accuracy. For the purpose of improving the order of accuracy and computational efficiency of numerical solutions of PDEs, it may be argued that the resultant modifications may be simpler to implement in an existing low-order finite-difference code (and leads to better performance) as opposed to the implementation of new code modules based on traditional high-order accurate finite-difference schemes. As such, the resultant modified methods can benefit from the computational simplicity and perhaps monotonicity preserving features of underlying low-order schemes.

The methods that we proposed based on adaptive grids can be grouped into two broad categories. In the first category, the methods that we proposed were based on modifications to a low-order finite difference scheme through the use of adaptive grid distribution alone. Some approaches for grid distribution considered include those

based on (i) a moving uniform mesh/domain, (ii) adaptive gradient based refinement (AGBR) and (iii) unit local Courant-Friedrich-Lewy (CFL) number. While these methods (in the first category) showed improvements in accuracy and computational efficiency, the formal order of accuracy could not always be improved considerably in comparison to the chosen base low-order finite-difference scheme. In the second category, the methods proposed in the first category were extended further using defect correction (or reduction of leading order terms of truncation error) in order to improve the formal order of accuracy and computational efficiency significantly (i.e. by at least one order or higher). While the first category of methods may be preferred in view of ease of implementation and lower computational complexity, the second category of methods may be preferred in view of greater accuracy and computational efficiency. In the second category of methods involving defect correction (or reduction of leading order terms of truncation error), we explored two different approaches for selection of adaptive grids, based on (i) optimal grid distribution using constrained minimization and (ii) remap with monotonicity preserving interpolation. The two broad categories of methods were also extended to multi-dimensional cases based on dimensional splitting approaches. The performance of these methods was demonstrated using several example problems in computational uncertainty quantification and computational mechanics. In some selected cases, the proposed adaptive grid based finite difference methods (in the second category) were shown to improve the computational efficiency by about three orders of magnitude.

6.2 Summary of proposed methods

As stated above, in the first category of methods, three different time-varying grid adaptation techniques for increasing the accuracy of an underlying finite difference scheme including adaptive uniform mesh, adaptive mesh based upon equidistribution (AGBR) and adaptive mesh based upon truncation error (CFLB) were studied

in one-dimensional spaces. In order to find the best technique among these three approaches, each of them was applied to solve a well-known hyperbolic PDE that is used to obtain statistical quantities of interest for dynamical systems with parametric uncertainties at a given time. For this purpose, the parameter (aleatory) uncertainty quantification (UQ) problem is formulated using a Liouville equation for the response conditional probability density.

A second order accurate MacCormack finite difference scheme with flux limiters is used to compute numerical solutions of the Liouville equation for a given sample of the conditioning variable. An improvement in the efficiency and a reduction in the computational costs of the numerical solution procedure is achieved in two steps. First, quadrature-based sampling of the conditioning variable is used which significantly reduces the number of samples required to obtain accurate moments. Second, the finite difference solution is computed on a mesh which has a domain and distribution of points which both vary in time. The results for all three different methods for mesh adaptation are compared with exact solutions and numerical solutions computed on a fixed grid. The comparison very well signifies the computational advantage of grid adaptation based upon truncation error over other two approaches.

Enhancement of accuracy by the implementation of these three adaptive FD approaches can not exceed further than the underlying scheme order of accuracy. Moreover, Godunov barrier theorem indicates impracticality of having a second or higher order linear monotonicity preserving finite difference solution. However, under certain conditions (for example, setting the local CFL number equal to one for the advection equation) such a scheme may exist. Thus, applying a combination of the CFLB grid adaptation with defect correction appears to be well-suited for this purpose. Similar to the third grid adaptation method (CFLB) proposed in Chapter 2, such an approach is based upon analysis of the truncation error of the

underlying finite difference equation. As the first step, using the modified equation technique, the modified differential equation for the original difference scheme is derived. Irregularities of this equation are found by a heuristic stability analysis. These irregular perturbations are automatically eliminated using grid adaptation designed to remove singularities of the modified equation. This step, which involves the determination of a computational grid, can be done either through a nonlinear, constrained minimization problem or through a mapping of the dependent variables from the non-uniform adaptive grids to uniform grids and vice versa using a monotonicity preserving interpolant. For the first approach, when a solution to this optimization problem exists, the result is the elimination of the leading order singular perturbation terms in the modified differential equation. On the other hand, when the hyperbolic PDE is solved on a moving domain or when the second grid adaptation technique is applied, the grid distribution problem is reduced to the solution of a system of linear equations. Therefore, a faster solution can be accomplished through application of the second proposed grid adaptation technique. In this approach in order to minimize non-physical spatial oscillations in high-gradient regions, and to make our our grid adaptation method amenable to a multidimensional space, a monotonicity preserving interpolation is used.

The construction of such a scheme can be described in two steps. In the first step, the corresponding defect corrected discretized equation is obtained by the direct subtraction of the remaining terms in the modified equation up to the desired order of accuracy. In the second step, the original low-order discretized equation is modified to include the leading terms in the truncation error expression corresponding to regular perturbations. As the irregularities are removed through grid adaptation, no iteration is necessary to establish the numerical stability of the resultant finite difference solution. The result of these two steps is a scheme which has (at least) one order higher accuracy than that given by the original finite difference equation.

In order to extend the first class of methods to multiple dimensions, a numerical method based upon the uniform grid adaptation technique proposed in Chapter 2, was first introduced in Chapter 4. A dimensional splitting technique is used to extend the range of application of this method from single to multiple dimensions. This approach is applied for uncertainty quantification to obtain the long-time statistical quantities for dynamical systems of moderate dimension in the presence of parametric uncertainties. In this approach, the uncertainty quantification problem is formulated in the form of the multidimensional Liouville equation which governs the time-evolution of the multivariate joint probability density function associated with system states and parameters. No *a priori* assumption about the measure of the random variables corresponding to system states is made, allowing for the accurate simulation of problems with sufficiently smooth nonlinear state dynamics. Moreover, this approach can admit any form of continuous probability distribution for random variables corresponding to uncertain parameters including uniform, lognormal and normal distributions.

Similar to one dimensional cases studied in Chapter 2, Gauss-quadrature nodes are used for sampling in the space of random variables corresponding to uncertain parameters which allows for the solution of relatively few (order 10) Liouville equations for the conditional density. This sampling is perfectly parallel and as such is easily extended to a parallel processing environment. Also, additional improvement in the efficiency of the numerical solution is gained by redefining, at each time-step, the computational domain in state space over which the Liouville equation for the conditional density is solved. This re-sizing of the (hyper-rectangular) computational domain is accomplished in accordance with the time-evolution (convection) of the conditional density function. Grid points are then redistributed uniformly within the redefined domain. For problems in which the joint probability density function becomes irregular, a more sophisticated grid redistribution approaches such

as a combination of truncation error based grid adaptation and defect correction can be implemented within the proposed framework of adaptive moving meshes in the response space.

Finally as an extension to the second proposed approach in Chapter 3, the possibility of developing a method based upon such a combination of grid adaptation, non-iterative defect correction and remap with monotonicity preserving interpolation methods was explored in Chapter 5. In addition to the remap with monotonicity preserving interpolation used previously for one-dimensional spaces, in order to easily extend the method to multiple dimensions, an operator (dimensional) splitting technique is utilized. In this approach, truncation error analysis is done in each dimension separately. Hence as the sequence of unidirectional solutions proceeds in accordance with the dimensional splitting technique being used, the grid adaptation is performed in an alternate direction method. The outcome is a modified multidimensional difference scheme with a higher order of accuracy and reasonable computational speed.

6.3 Summary of results for canonical problems

In order to evaluate the utility of the proposed methods, we investigate their performance using benchmark test problems relevant to computational uncertainty quantification and computational mechanics. In Chapter 2, three grid adaptation methodologies were applied to two problems, each of which contained one (random) parameter and one state (response). The first problem examined was a decay problem (population balance) while the second involved a system with nonlinear deterministic dynamics with multiple fixed points. For each of these example problems, comparison with exact solutions demonstrated the ability of the Liouville formulation to accurately predict both the conditional density and resulting moments. Comparison of the numerical solutions showed that those computed on a

time-varying mesh partition were most often at least an order of magnitude more accurate for a given number of grid points used to discretize the response domain. In particular, a method which is based upon distributing the grid such that a local CFL=1 condition is imposed showed significant improvement over a fixed grid solution due to a reduction in the numerical dispersion and diffusion errors (by about an order of magnitude).

The method presented has potential application in uncertainty quantification problems which have low to moderate state dimension and which require highly accurate estimates of the conditional density. Unlike many current methods for uncertainty quantification based upon Galerkin projection, no *a priori* assumption is made about the form of the response measure in our method. This allows for the accurate estimation of the statistics for problems whose response densities show significant changes in time. In addition, as the problem is formulated directly in terms of a conditional density, the accuracy of the conditional density can be assessed directly without the need for reconstruction using response surface methods or methods based upon moment reconstruction. Also, as each Liouville equation is solved independently for a given sample of the random parameters (conditioning variable), the method can easily be extended to a parallel processing environment thus allowing for efficient solution for problems with many random variables.

Next, the adaptive grid adaptation method based upon truncation error discussed in Chapter 2 (CFLB method) was applied in combination with defect correction method. In order to demonstrate the resultant method, three one-dimensional hyperbolic PDEs are solved. In Chapter 3, the first order upwind and MacCormack schemes both are used as original low-order schemes. The first and second test problems in this chapter were concerned with enhancing the accuracy of finite difference solutions of homogeneous and non-homogeneous nonlinear advection equations. The third problem examined was the numerical solution of the Liouville equation which

is a linear PDE. For this problem, cases with linear and nonlinear spatially dependent drift functions were studied. This problem also involves the propagation of an initial square wave through the solution of a one-dimensional Liouville equation with a spatially dependent drift coefficient. The results for this problem demonstrate the desired increase in order of accuracy and numerical solutions using the second proposed approach are free from oscillations. Moreover, comparison with the exact solution for these example problems indicates that at least an order of accuracy enhancement in the results is obtained when any of two proposed adaptive approach is used. Due to the elimination of the regular perturbation term, the modified upwinding scheme has low numerical diffusion with the result that the formal increase in order is achieved even for low resolution solutions. The results indicate computational benefits of using the solution of a system of linear equations instead of constrained optimization to redistribute the grid point on an adaptive mesh. This grid adaptation approach not only can deal properly with the issue of very small drift function values, but also is very well extendable to multiple dimension.

While only one-dimensional problems were studied in Chapters 2 and 3, proposed adaptive finite difference methodologies can be extended to multidimensional problems through the application of dimensional splitting finite difference schemes. This was investigated in the following two chapters. In Chapter 4, with an emphasis on its application in uncertainty quantification, a novel adaptive finite difference method of solution was proposed for multidimensional Liouville equation. To demonstrate the method which is based upon adaptive uniform grid distribution on hyper-rectangular domains, various example problems were studied, including a) single spring-mass system, b) Van der Pol oscillator, c) double spring-mass system and d) a nonlinear aeroelastic problem consisting of a typical section airfoil in an incompressible flow. The results from these example problems indicate that the proposed approach can accurately predict long-time statistical behavior of states for

both linear and nonlinear dynamical systems. Furthermore, these results demonstrate significantly higher accuracy of the proposed adaptive finite difference solution compared with a standard fixed mesh/domain solution. For the single spring-mass oscillator problem (Problem 4.1), for which an analytical solution was determined, numerical experiments showed that for a given level of accuracy the adaptive grid solution was more computationally efficient (time) when compared to Monte Carlo simulation. As the method presented solves for the conditional density directly (without the need for reconstruction of the PDF based on moments), it would appear to have potential application in analyses where direct, and accurate, knowledge of the probability function is needed. One such application could be in the analysis of failure probabilities for the reliability assessment of engineering systems.

Finally in Chapter 5, the proposed methodology for finite difference solution of multidimensional hyperbolic PDEs using defect correction on adaptive grids, which had been discussed in Chapter 3, was extended to multiple dimensions. In order to demonstrate this methodology in multidimensional spaces, three canonical test problems dealing with the numerical solutions of hyperbolic PDEs are studied. First, the proposed approach is investigated by solving a Liouville equation with linear and nonlinear spatially dependent coefficients. The results indicate the superiority of the modified schemes over both the underlying scheme (by about three orders of magnitude) and standard high order solution approaches with regards to computational (wall clock) time for a given accuracy. When a nonlinear hyperbolic equation is solved (as Problem 5.3), the choice of splitting sequence proves to be crucial in enhancing the order of accuracy. In such cases when additive splitting is used (as opposed to Strang splitting), the proposed approach is again shown to be highly effective in increasing both temporal and spatial order of accuracy of finite difference schemes as well as preserving the monotonicity of the numerical solution in regions of discontinuity. Moreover, such features are obtained while taking ad-

vantage of the computational simplicity of the underlying lower order scheme. The proposed methodology provides a possible path toward faster and more accurate finite difference solutions of high-dimensional PDEs such as Fokker-Planck equations and problems relevant to computational fluid dynamics such as the shallow water and Euler equation.

6.4 Potential areas for future research

The proposed framework for solving hyperbolic PDEs can be extended into different interesting areas in computational physics and uncertainty quantification. An immediate extension of this research can be the application of our proposed approach for enhancing the accuracy of finite difference scheme to the other types of partial differential equations including parabolic and elliptic PDEs. The resultant approach can be used to obtain better accuracy and computational performance for low-order finite difference schemes especially near the singularities. For this purpose, the proposed concept of moving mesh and rezoning approach can be well adopted into the finite difference solution of parabolic and elliptic PDEs as an alternative for the standard moving mesh methods [152, 153, 154, 155].

From a different prospective, similar framework can be developed for both finite element [156] and finite volume [12] solutions of PDEs. In such cases, available local or global error estimation strategies can be used for a more efficient adaptation of elements with regard to discretization accuracy. Similarly, defect correction have been applied in finite element computations as a mean for enhancing both numerical stability and increasing the accuracy of the solution [157, 158, 159]. As an example, one-step and two-step defect correction methods by adding an artificial viscosity with an anti-diffuser was implemented in the finite element solution of incompressible Navier-Stokes equations [158]. Using such an approach results in higher accuracy on a very coarse mesh. This enhancement was shown to be up to one order in the

formal accuracy of the underlying finite element method. A similar defect correction approach was used by Si and He for a stationary conduction problem [159]. Again they applied an artificial viscosity as a form of defect correction and obtained a numerical solution with a higher accuracy.

Also the methods based on truncation error analysis as another type of defect correction have been implemented within the framework of finite element solution. A localized truncation error analysis (LTEA) was used by Hagen et al. to generate a mesh based upon the flow variables and their derivatives for a one-dimensional wave continuity equation [160]. In comparison with the mesh generated with either topographic length scale criterion or wave length to grid size ratio criterion, it was shown that the resultant grid is more coupled with the physics of the problem, which leads to a more accurate and computationally efficient solution for one-dimensional problems [160]. Hence, it appears that the implementation of a similar grid adaptation methodology to the approach we have applied in this dissertation can enhance finite element solutions accuracy.

Moreover, operator splitting has been previously applied to develop efficient finite element approach especially for solving hyperbolic PDEs [161, 162]. Therefore, extension of the application of such an approach to multidimensional finite element computations can be achieved using a combination of non-iterative defect correction and time-varying grid adaptation in conjunction with a dimension splitting technique. In this regard, application of the rezoning approach and the moving mesh strategies used in this dissertation might be computationally beneficial when it is compared with standard moving finite element methods [163, 164].

One other possible interesting extension of the approach proposed in this dissertation is developing a novel stochastic finite difference methodology based upon a combination of the proposed dimensional grid adaptation technique and particle tracking methods [165, 166, 167]. The exact solution of one-dimensional linear

hyperbolic PDEs such as the Liouville equation can be obtained through the characteristic analysis. By considering the result of particle tracking approaches as a form of grid adaptation in the framework of a dimension splitting technique these unidimensional solutions can be numerically integrated into the solution of multidimensional hyperbolic PDEs. More details on the formulation of this methodology along with preliminary results are discussed in Appendix E.

Finally, it may be possible to construct a more computationally efficient methodology by adding a proper sub-grid model, which is derived from a data driven approach, to the defect corrected discretization. Recently, Optimal Spatiotemporal Reduced Order Modeling (OPSTROM) has been developed and applied to enhance the efficiency of PDEs numerical solutions with respect to both required spatial and temporal step sizes for a given level of accuracy [168, 169, 170, 171]. Therefore, embedding sub-grid models which accounts for unresolved spatial and temporal scales (coarse grids) into the defect corrected discretization and solving the resultant equation on an adaptive grid may reduce the computational costs even further. For potential application of such an approach in computational uncertainty quantification, a smooth scaling with respect to the system dynamics appears to be possible due to the similarity of the boundary condition used for the evolutions of JPDFs. Hence, bridging between macro scale dynamics and micro scale dynamics might be performed perfectly and as a result sub-grid models for one UQ problem might be applicable to a group of UQ problems.

Bibliography

[1] J. Li and J. Chen. The principle of preservation of probability and the generalized density evolution equation. *Structural Safety*, 30(1):65–77, 2008.

[2] J. Li and J. Chen. *Stochastic dynamics of structures*. John Wiley & Sons, 2009.

[3] S. Benzoni-Gavage and D. Serre. *Multi-dimensional hyperbolic partial differential equations*. Clarendon Press Oxford, 2007.

[4] T. Nishida. *Nonlinear hyperbolic equations and related topics in fluid dynamics*. Université de Paris-Sud, Département de Mathématique, 1978.

[5] U. Harlander and L. R. Maas. Two alternatives for solving hyperbolic boundary value problems of geophysical fluid dynamics. *Journal of Fluid Mechanics*, 588:331, 2007.

[6] Y. Ren, Q. Liu, S. Wang, and M. Shen. A high order accurate, non-oscillating finite volume scheme using spline interpolation for solving hyperbolic conservation laws (computational fluid dynamics). *Acta Aerodynamica Sinica*, 14(3):281–287, 1996.

[7] G. Avalos. The exponential stability of a coupled hyperbolic/parabolic system arising in structural acoustics. In *Abstract and Applied Analysis*, volume 1, pages 203–217, 1996.

[8] J. Hunter. Hyperbolic waves and nonlinear geometrical acoustics. In *Trans. 6th Army Conference on Applied Mathematics and Computing*, volume 2, pages 527–569, 1989.

[9] A. Majda and M. Taylor. Inverse scattering problems for transparent obstacles, electromagnetic waves, and hyperbolic systems. *Communications in Partial Differential Equations*, 2(4):395–438, 1977.

[10] W. Kaminski. Hyperbolic heat conduction equation for materials with a nonhomogeneous inner structure. *Journal of Heat Transfer*, 112(3), 1990.

[11] Gilbert Strang and George J Fix. *An analysis of the finite element method*, volume 212. Prentice-Hall Englewood Cliffs, NJ, 1973.

[12] R. J. LeVeque. *Finite Volume Methods for Hyperbolic Problems*. Cambridge Texts in Applied Mathematics. Cambridge University Press, 2002.

[13] Joel H Ferziger and Milovan Perić. *Computational methods for fluid dynamics*, volume 3. Springer Berlin, 2002.

[14] F. G. Blottner. Finite difference methods of solution of the boundary-layer equations. *AIAA Journal*, 8(2):193–205, 1970.

[15] S. W. Armfield. Finite difference solutions of the Navier-Stokes equations on staggered and non-staggered grids. *Computers & Fluids*, 20(1):1–17, 1991.

[16] J. C. Tannehill, D. D. A. Anderson, and H. Pletcher, R. *Computational fluid mechanics and heat transfer*. Taylor & Francis, 1997.

[17] J. D. Hoffman. *Numerical methods for engineers and scientists*. McGraw-Hill, New York, USA, 1992.

[18] A. Bermudez and M. E. Vazquez. Upwind methods for hyperbolic conservation laws with source terms. *Computers & Fluids*, 23(8):1049–1071, 1994.

[19] J. L. Steger. Implicit finite-difference simulation of flow about arbitrary two-dimensional geometries. *AIAA Journal*, 16(7):679–686, 1978.

[20] J. F. Thompson, B. K. Soni, and N. P. Weatherill. *Handbook of Grid Generation*. Taylor & Francis, 1998.

[21] F. Bade and P. Haldenwang. High order scheme for thermally driven flows in an open channel. *Computers & Fluids*, 27(2):273–290, 1998.

[22] T. P. Loc and R. Bouard. Numerical solution of the early stage of the unsteady viscous flow around a circular cylinder: A comparison with experimental visualization and measurements. *Journal of Fluid Mechanics*, 160(1):93–117, 1985.

[23] X. Zhong and M. Tatineni. High-order non-uniform grid schemes for numerical simulation of hypersonic boundary-layer stability and transition. *Journal of Computational Physics*, 190(2):419–458, 2003.

[24] W. Cai. High-order hybrid numerical simulations of two-dimensional detonation waves. *AIAA Journal*, 33(7):1248–1255, 1995.

[25] A. Rezgui, P. Cinnella, and A. Lerat. Third-order accurate finite volume schemes for Euler computations on curvilinear meshes. *Computers & Fluids*, 30(7):875–901, 2001.

[26] S. K. Lele. Compact finite difference schemes with spectral-like resolution. *Journal of Computational Physics*, 103(1):16–42, 1992.

[27] P. R. Eiseman. Adaptive grid generation. *Computer Methods in Applied Mechanics and Engineering*, 64(1):321–376, 1987.

[28] M. J. Berger and J. Oliger. Adaptive mesh refinement for hyperbolic partial differential equations. *Journal of Computational Physics*, 53(3):484–512, 1984.

[29] S. A. Richards. Completed Richardson extrapolation in space and time. *Communications in Numerical Methods in Engineering*, 13(7):573–582, 1997.

[30] W. Kress. Error estimates for deferred correction methods in time. *Applied Numerical Mathematics*, 57(3):335–353, 2007.

[31] B. Gustafsson and L. Hemmingsson-Frändén. Deferred correction in space and time. *Journal of Scientific Computing*, 17(1-4):541–550, 2002.

[32] B. Gustafsson and L. Hemmingsson-Frändén. Implicit high-order difference methods and domain decomposition for hyperbolic problems. *Applied Numerical Mathematics*, 33(1):493–500, 2000.

[33] K. T. Chu. Boosting the accuracy of finite difference schemes via optimal time step selection and non-iterative defect correction. *Applied Mathematics and Computation*, 218(7):3596–3614, 2011.

[34] Parviz Moin. *Fundamentals of engineering numerical analysis*. Cambridge University Press, 2010.

[35] P. Wesseling. *Principles of Computational Fluid Dynamics*. Springer, 2009.

[36] Sergei Konstantinovich Godunov. A difference method for numerical calculation of discontinuous solutions of the equations of hydrodynamics. *Matematicheskii Sbornik*, 89(3):271–306, 1959.

[37] G. Jiang and C. Shu. Efficient implementation of weighted ENO schemes. *Journal of Computational Physics*, 126(1):202–228, 1996.

[38] A. Harten. High resolution schemes for hyperbolic conservation laws. *Journal of Computational Physics*, 49(3):357–393, 1983.

[39] A. Marquina. Local piecewise hyperbolic reconstruction of numerical fluxes for nonlinear scalar conservation laws. *SIAM Journal on Scientific Computing*, 15(4):892–915, 1994.

[40] P. Colella and P. R. Woodward. The piecewise parabolic method (PPM) for gas-dynamical simulations. *Journal of Computational Physics*, 54(1):174–201, 1984.

[41] Chi-Wang Shu and Stanley Osher. Efficient implementation of essentially non-oscillatory shock-capturing schemes. *Journal of Computational Physics*, 77(2):439–471, 1988.

[42] C. Shu and S. Osher. Efficient implementation of essentially non-oscillatory shock-capturing schemes, II. *Journal of Computational Physics*, 83(1):32–78, 1989.

[43] X. Liu, S. Osher, and T. Chan. Weighted essentially non-oscillatory schemes. *Journal of Computational Physics*, 115(1):200–212, 1994.

[44] Chi-Wang Shu. *Essentially non-oscillatory and weighted essentially non-oscillatory schemes for hyperbolic conservation laws*. Springer, 1998.

[45] A. Harten and J. M. Hyman. Self-adjusting grid methods for one-dimensional hyperbolic conservation laws. *Journal of Computational Physics*, 50:235–269, 1981.

[46] J. M. Stockie, J. A. Mackenzie, and R. D. Russell. A moving mesh method for one-dimensional hyperbolic conservation laws. *SIAM Journal of Scientific Computing*, 22:1791–1813, 2001.

[47] I. Babuška and W. C. Rheinboldt. A-posteriori error estimates for the finite element method. *International Journal of Numerical Methods in Engineering*, 12:1597–1615, 1978.

[48] A. B. White. On selection of equidistributing meshes for two-point boundary problems. *SIAM Journal on Numerical Analysis*, 16:472–502, 1979.

[49] H. A. Dwyer. Grid adaptation for problems in fluid dynamics. *AIAA Journal*, 22:1705–1712, 1984.

[50] M. Letini and V. Pereyra. An adaptive finite difference solver for nonlinear two-point boundary problems with mild boundary layers. *SIAM Journal on Numerical Analysis*, 4:91–111, 1977.

[51] G. H. Klopfer and D. S. McRae. The nonlinear modified equation approach to analyzing finite difference scheme. Paper no. 81–1029, AIAA, 1981.

[52] V. E. Denny and R. B. Landis. A new method for solving two-point boundary-value problems using optimal node distribution. *Journal of Computational Physics*, 9:120–137, 1972.

[53] B. Pierson and P. Kutler. Optimal nodal point distribution for improved accuracy in computational fluid dynamics. *AIAA Journal*, 18:49–54, 1980.

[54] N. K. Yamaleev. Minimization of the truncation error by grid adaptation. Report no. 99–461999, ICASE, 1999.

[55] G. F. Carey and H. T. Dinh. Grading functions and mesh redistribution. *SIAM Journal on Numerical Analysis*, 22(5):1028–1040, 1985.

[56] A. Sidi. *Practical extrapolation methods: Theory and applications*. Cambridge University Press, 2003.

[57] W. Shyy, M. Garbey, A. Appukuttan, and J. Wu. Evaluation of Richardson extrapolation in computational fluid dynamics. *Numerical Heat Transfer: Part B: Fundamentals*, 41(2):139–164, 2002.

[58] C. F. Gerald and P. O. Wheatley. *Applied numerical analysis*. Addison-Wesley, 2004.

[59] R. D. Skeel. A theoretical framework for proving accuracy results for deferred corrections. *SIAM Journal on Numerical Analysis*, 19(1):171–196, 1982.

[60] R. F. Warming and B. J. Hyett. The modified equation approach to the stability and accuracy analysis of finite-difference methods. *Journal of Computational Physics*, 14(2):159–179, 1974.

[61] S. Chang. A critical analysis of the modified equation technique of Warming and Hyett. *Journal of Computational Physics*, 86(1):107–126, 1990.

[62] F. R. Villatoro and J. I. Ramos. On the method of modified equations. I: Asymptotic analysis of the Euler forward difference method. *Applied Mathematics and Computation*, 103(2):111–139, 1999.

[63] W. F. Spotz and G. F. Carey. High-order compact finite difference methods. In *Preliminary Proceedings International Conference on Spectral and High Order Methods, Houston, TX*, 1995.

[64] W. F. Spotz and G. F. Carey. Extension of high-order compact schemes to time-dependent problems. *Numerical Methods for Partial Differential Equations*, 17(6):657–672, 2001.

[65] D. A. Jones. Modified-truncation finite difference schemes. *Journal of Computational Physics*, 209(1):322–339, 2005.

[66] A. Christlieb, B. Ong, and J. Qiu. Integral deferred correction methods constructed with high order Runge-Kutta integrators. *Mathematics of Computation*, 79(270):761–783, 2010.

[67] G. H. Klopfer and D. S. McRae. Nonlinear truncation error analysis of finite difference scheme for the Euler equation. *AIAA Journal*, 21(4):487–494, 1983.

[68] T. Nilsen and T. Aven. Models and model uncertainty in the context of risk analysis. *Reliability Engineering & System Safety*, 79:309–317, 2003.

[69] H. N. Najm. Uncertainty quantification and polynomial chaos techniques in computational fluid dynamics. *Annual Review of Fluid Mechanics*, 41:35–52, 2009.

[70] H. N. Najm, B. J. Debusschere, Y. M. Marzouk, S. Widmer, and O. P. Le MaÃőtre. Uncertainty quantification in chemical systems. *International Journal of Numerical Methods in Engineering*, 80:789–814, 2009.

[71] C. J. Roy and W. L. Oberkampf. A comprehensive framework for verification, validation, and uncertainty quantification in scientific computing. *Computational Methods in Applied Mechanics & Engineering*, 200:2131 – 2144, 2011.

[72] G. Schuëller. On the treatment of uncertainties in structural mechanics and analysis. *Computers and Structures*, 85:235–243, 2007.

[73] A. T. Beck and W. J. Gomes. Stochastic fracture mechanics using polynomial chaos. *Probabilistic Engineering Mechanics*, 34:26–39, 2013.

[74] C. L. Pettit. Uncertainty quantification in aeroelasticity: Recent results and research challenges. *Journal of Aircraft*, 41:1217–1229, 2004.

[75] J. S. Witteveen and H. Bijl. A TVD uncertainty quantification method with bounded error applied to transonic airfoil flutter. *Communication in Computational Physics*, 6:406–432, 2009.

[76] M. Lamorte, B. Glaz, P. P. Friedmann, A. J. Culler, A. R. Crowell, and J. J. McNamara. Uncertainty propagation in hypersonic aerothermoelastic analysis. Aiaa 2010–2964, 51st AIAA/ASME/ASCE/AHS/ASC Structures, Structural Dynamics, and Materials Conference, Orlando,Florida, 12 - 15 April, 2010.

[77] M. D. Brandyberry. Uncertainty quantification in 3D rocket simulation. Aiaa 2006–4586, 42nd AIAA/ASME/SAE/ASEE Joint Propulsion Conference and Exhibit, Sacramento, California, 9 - 12 July, 2006.

[78] C. L. Pettit, M. R. Hajj, and P. S. Beran. A stochastic approach for modeling incident gust effects on flow quantities. *Probabilistic Engineering Mechanics*, 25:153–162, 2010.

[79] R. E. Melchers. *Structural reliability analysis and prediction*. John Wiley & Sons, New York, USA, 1999.

[80] L. P. Swiler and A. A. Giunta. Aleatory and epistemic uncertainty quantification for engineering applications. Sandia technical report no. sand2007–2670c, Sandia National Laboratories, Livermore, USA, 2007.

[81] P. Pettersson, G. Iaccarino, and J. Nordström. An intrusive hybrid method for discontinuous two-phase flow under uncertainty. *Computers & Fluids*, 86:228–239, 2013.

[82] J. Tryoen, O. Le Maître, M. Ndjinga, and A. Ern. Intrusive Galerkin methods with upwinding for uncertain nonlinear hyperbolic systems. *Journal of Computational Physics*, 229(18):6485–6511, 2010.

[83] M. S. Eldred, C. G. Webster, and P. Constantine. Evaluation of non-intrusive approaches for Wiener-Askey generalized polynomial chaos. In *Proceedings of the 10th AIAA Non-Deterministic Approaches Conference, number AIAA-2008-1892, Schaumburg, IL*, volume 117, page 189, 2008.

[84] D. Zhang, H. Li, H. Chang, and G. Yan. Non-intrusive stochastic approaches for efficient quantification of uncertainty associated with reservoir simulations. In *11th European Conference on the Mathematics of Oil Recovery*, 2008.

[85] R. Ghanem and P. Spanos. *Stochastic finite elements*. Dover Publications, New York, USA, 2003.

[86] P. J. Attar and P. Vedula. Direct quadrature method of moments solution of the fokker-planck equation. *Journal of Sound and Vibration*, 317:265–272, 2008.

[87] R. E. Caflisch. Monte carlo and quasi-monte carlo methods. *Acta Numerica*, 7:1–49, 1998.

[88] D. Xiu and G. E. Karniadakis. The Wiener-Askey polynomial chaos for stochastic differential equations. *SIAM Journal of Scientific Computing*, 42:619–644, 2002.

[89] R. Ghanem and P. Spanos. *Stochastic finite elements: a spectral approach*. Springer-Verlag, New York, USA, 1991.

[90] D. Xiu and J. S. Hesthaven. High-order collocation methods for differential equations with random inputs. *SIAM Journal of Scientific Computing*, 27:1118–1139, 2005.

[91] F. Nobile, R. Tempone, and C. G. Webster. A sparse grid stochastic collocation method for partial differential equations with random input data. *SIAM Journal on Numerical Analysis*, 46:2309–2345, 2008.

[92] M. Eldred and J. Burkardt. Comparison of non-intrusive polynomial chaos and stochastic collocation methods for uncertainty quantification. Paper no. 2009-0976, AIAA, 2009.

[93] T. Crestaux, O. Le Matre, and J. Martinez. Polynomial chaos expansion for sensitivity analysis. *Reliability Engineering & System Safety*, 94:1161–1172, 2009.

[94] O. Le Maître, P. Olivier, and O. M. Knio. *Spectral methods for uncertainty quantification: With applications to computational fluid dynamics*. Springer, 2010.

[95] R. Ghanem and P. D. Spanos. A stochastic Galerkin expansion for nonlinear random vibration analysis. *Probabilistic Engineering Mechanics*, 8:255–264, 1993.

[96] S. Sakamoto and R. Ghanem. Simulation of multi-dimensional non-Gaussian non-stationary random fields. *Probabilistic Engineering Mechanics*, 17:167–176, 2002.

[97] D. Xiu. Fast numerical methods for stochastic computations: a review. *Communications in Computational Physics*, 5:242–272, 2009.

[98] S. A. Orszag. Dynamical properties of truncated Wiener-Hermite expansions. *The Physics of Fluids*, 10:2603–2613, 1967.

[99] M. Gerritsma, J. Van der Steen, P. Vos, and G. Karniadakis. Time-dependent polynomial chaos. *Journal of Computational Physics*, 229:8333–8363, 2010.

[100] C. L. Pettit and P. S. Beran. Spectral and multiresolution wiener expansions of oscillatory stochastic processes. *Journal of Sound and Vibration*, 294:752–779, 2006.

[101] M. Ghommem, M. R. Hajj, and A. H. Nayfeh. Uncertainty analysis near bifurcation of an aeroelastic system. *Journal of Sound and Vibration*, 329:3335–3347, 2010.

[102] D. Millman, P. I. King, and P. Beran. Airfoil pitch-and-plunge bifurcation behavior with Fourier chaos expansions. *Journal of Aircraft*, 42:376–384, 2005.

[103] D. Millman, P. I. King, R. C. Maple, P. Beran, and L. K. Chilton. Uncertainty quantification with B-spline stochastic projection. *AIAA Journal*, 44:1845–1853, 2006.

[104] X. Wan and G. E. Karniadakis. An adaptive multi-element generalized polynomial chaos method for stochastic differential equations. *Journal of Computational Physics*, 209:617–642, 2005.

[105] J. A. S. Witteveen, A. Loeven, and H. Bijl. An adaptive stochastic finite elements approach based on Newton-Cotes quadrature in simplex elements. *Computers & Fluids*, 38:1270–1288, 2009.

[106] A. C. Yucel, H. Bagci, and E. Michielssen. An adaptive multi-element probabilistic collocation method for statistical EMC/EMI characterization. *IEEE Transactions on Electromagnetic Compatibility.*, 99:1–15, 2013.

[107] J. Foo and G. E. Karniadakis. Multi-element probabilistic collocation method in high dimensions. *Journal of Computational Physics*, 229:1536–1557, 2010.

[108] D. Venturi and G. E. Karniadakis. Convolutionless Nakajima–Zwanzig equations for stochastic analysis in nonlinear dynamical systems. *Proceedings of the Royal Society A: Mathematical, Physical and Engineering Science*, 470(2166):20130754, 2014.

[109] David Montgomery. A bbgky framework for fluid turbulence. *Physics of Fluids (1958-1988)*, 19(6):802–810, 1976.

[110] G. Lin and G. E. Karniadakis. Stochastic simulations and sensitivity analysis of plasma flow. Aiaa 2010–1073, 46th AIAA Aerospace Sciences Meeting and Exhibit, Reno ,Nevada, 7 - 10 January, 2008.

[111] B. M. Ayyub. *Risk Analysis in Engineering and Economics*. CRC Press, Florida, USA, 2003.

[112] I. Elishakoff. *Probability methods in the theory of structures*. John Wiley, New York, USA, 1983.

[113] A. M. Hasofer and N. C. Lind. Exact and invariant second-moment code format. *Journal of Engineering Mechanics*, 100:111–121, 1974.

[114] H. Cho, D. Venturi, and G. E. Karniadakis. Adaptive discontinuous Galerkin method for response-excitation PDF equations. *SIAM Journal on Scientific Computing*, 35(4):B890–B911, 2013.

[115] M. Razi, P. J. Attar, and P. Vedula. Adaptive finite difference solutions of Liouville equations in computational uncertainty quantification. *Submitted to Reliability Engineering & System Safety*, 2013.

[116] J. Chen and J. Li. Dynamic response and reliability analysis of non-linear stochastic structures. *Probabilistic Engineering Mechanics*, 20(1):33–44, 2005.

[117] J. Li, J. Chen, W. Sun, and Y. Peng. Advances of the probability density evolution method for nonlinear stochastic systems. *Probabilistic Engineering Mechanics*, 28:132–142, 2012.

[118] J. Chen and J. Li. A note on the principle of preservation of probability and probability density evolution equation. *Probabilistic Engineering Mechanics*, 24(1):51–59, 2009.

[119] J. Chen and J. Li. Joint probability density function of the stochastic responses of nonlinear structures. *Earthquake Engineering and Engineering Vibration*, 6:35–47, 2007.

[120] P. E. Gill and F. Miller. An algorithm for the integration of unequally spaced data. *The Computer Journal*, 15:80–83, 1972.

[121] w. Huang and R. D. Russell. *Adaptive moving mesh methods*. Springer, New York, USA, 2011.

[122] C. J. Budd, W. Huang, and R. D. Russell. Adaptivity with moving grids. *Acta Numerica*, 18:111–241, 2009.

[123] J. M. Hyman. Accurate monotonicity preserving cubic interpolation. *SIAM Journal of Scientific Computing*, 4:645–654, 1983.

[124] V. Guinot. *Wave propagation in fluids: models and numerical techniques*. John Wiley & Sons, Hoboken, New Jersey, USA, 2010.

[125] R.J. LeVeque. *Numerical methods for conservation laws*. Birkhaüser, Basel, Switzerland, 1990.

[126] S. O. Unverdi and G. Tryggvason. A front-tracking method for viscous, incompressible, multi-fluid flows. *Journal of Computational Physics*, 100:25–37, 1992.

[127] V. D. Liseikin. *Grid Generation Methods*. Scientific Computation. Springer, 2009.

[128] G. F. Carey. *Computational Grids: Generations, Adaptation & Solution Strategies*. Series in Computational and Physical Processes in Mechanics. Taylor & Francis, 1997.

[129] M. Razi, P. J. Attar, and P. Vedula. Grid adaptation and non-iterative defect correction for improved accuracy of numerical solutions of PDEs. *Submitted to Applied Mathematics and Computation*, 2014.

[130] A. R. Conn, N. I. M. Gould, and P. L. Toint. *Trust Region Methods*. Society for Industrial and Applied Mathematics, 2000.

[131] C. W. Hirt. Heuristic stability theory for finite-difference equations. *Journal of Computational Physics*, 2(4):339–355, 1968.

[132] C. de Boor and B. Swartz. Piecewise monotone interpolation. *Journal of Approximation Theory*, 21(4):411–416, 1977.

[133] R. L. Dougherty, A. S. Edelman, and J. M. Hyman. Nonnegativity-, monotonicity-, or convexity-preserving cubic and quintic Hermite interpolation. *Mathematics of Computation*, 52(186):471–494, 1989.

[134] K. Lika and T. G Hallam. Traveling wave solutions of a nonlinear reaction–advection equation. *Journal of Mathematical Biology*, 38(4):346–358, 1999.

[135] M. Razi, P. J. Attar, and P. Vedula. Uncertainty quantification of multidimensional dynamical systems based on adaptive numerical solutions of the Liouville equation. *Submitted to Probabilistic Engineering Mechanics*, 2013.

[136] S. Jin and X. Wen. Hamiltonian-preserving schemes for the Liouville equation with discontinuous potentials. *Communications in Mathematical Sciences*, 3(3):285–315, 2005.

[137] S. Jin and X. Wen. Computation of transmissions and reflections in geometrical optics via the reduced Liouville equation. *Wave Motion*, 43(8):667–688, 2006.

[138] J. A. S. Witteveen, A. Loeven, S. Sarkar, and H. Bijl. Probabilistic collocation for period-1 limit cycle oscillations. *Journal of Sound and Vibration*, 311(1):421–439, 2008.

[139] E. H. Dowell, R. Clark, D. Cox, H. C. Curtiss Jr, J. W. Edwards, K. C. Hall, D. A. Peters, R. Scanlan, E. Simiu, F. Sisto, and T. W. Strganac. *A modern course in aeroelasticity*. Kluwer Academic Publisher, Dordrecht, The Netherlands, 2004.

[140] B. H. k. Lee, S. J. Price, and Y. S. Wong. Nonlinear aeroelastic analysis: Bifurcation and chaos. *Progress in Aerospace Sciences*, 35:205–334, 1999.

[141] R. I. McLachlan and G. R. W. Quispel. Splitting methods. *Acta Numerica*, 11:341–434, 2002.

[142] E. Hairer, C. Lubich, and G. Wanner. *Geometric numerical integration: structure-preserving algorithms for ordinary differential equations*, volume 31. Springer, 2006.

[143] K. A. Bagrinovski and S. K. Godunov. Difference schemes for multidimensional problems. *Doklady Akademii Nauk SSSR*, 115:431–1433, 1957.

[144] H. Holden, K. H. Karlsen, K. Lie, and N. H. Risebro. *Splitting methods for partial differential equations with rough solutions*. European Mathematical Society, Zurich, Switzerland, 2010.

[145] G. Strang. On the construction and comparison of difference schemes. *SIAM Journal on Numerical Analysis*, 5(3):506–517, 1968.

[146] S. Blanes and P. C. Moan. Practical symplectic partitioned Runge–Kutta and Runge–Kutta–Nyström methods. *Journal of Computational and Applied Mathematics*, 142(2):313–330, 2002.

[147] W. Kahan and R. Li. Composition constants for raising the orders of unconventional schemes for ordinary differential equations. *Mathematics of Computation of the American Mathematical Society*, 66(219):1089–1099, 1997.

[148] H. Yoshida. Construction of higher order symplectic integrators. *Physics Letters A*, 150(5):262–268, 1990.

[149] J. Lee and B. Fornberg. A split step approach for the 3-d Maxwell's equations. *Journal of Computational and Applied Mathematics*, 158(2):485–505, 2003.

[150] W. D. Gropp. A test of moving mesh refinement for 2-d scalar hyperbolic problems. *SIAM Journal on Scientific and Statistical Computing*, 1(2):191–197, 1980.

[151] M. Crandall and A. Majda. The method of fractional steps for conservation laws. *Numerische Mathematik*, 34(3):285–314, 1980.

[152] D. Bai and A. Brandt. Local mesh refinement multilevel techniques. *SIAM Journal on Scientific and Statistical Computing*, 8(2):109–134, 1987.

[153] K. Debrabant and J. Lang. On asymptotic global error estimation and control of finite difference solutions for semilinear parabolic equations. *Computer Methods in Applied Mechanics and Engineering*, 2014.

[154] H. A. Dwyer, R. J. Kee, and B. R. Sanders. Adaptive grid method for problems in fluid mechanics and heat transfer. *AIAA Journal*, 18(10):1205–1212, 1980.

[155] J. A. Mackenzie and W. R. Mekwi. An analysis of stability and convergence of a finite-difference discretization of a model parabolic pde in 1d using a moving mesh. *IMA Journal on Numerical Analysis*, 2006.

[156] O. C. Zienkiewicz and R. L. Taylor. *The Finite Element Method: Solid mechanics*. Butterworth-Heinemann, 2000.

[157] C. Düsterhöft, D. Heinemann, and D. Kolb. Dirac–Fock–Slater calculations for diatomic molecules with a finite element defect correction method (FEM-DKM). *Chemical Physics Letters*, 296(1):77–83, 1998.

[158] W. Layton, H. K. Lee, and J. Peterson. A defect-correction method for the incompressible Navier–Stokes equations. *Applied Mathematics and Computation*, 129(1):1–19, 2002.

[159] Z. Si and Y. He. A defect-correction mixed finite element method for stationary conduction-convection problems. *Mathematical Problems in Engineering*, 2011, 2011.

[160] S. C. Hagen, J. J. Westerink, and R. L. Kolar. One-dimensional finite element grids based on a localized truncation error analysis. *International Journal for Numerical Methods in Fluids*, 32(2):241–261, 2000.

[161] L. Demkowicz, J. T. Oden, and W. Rachowicz. A new finite element method for solving compressible Navier-Stokes equations based on an operator splitting method and h-p adaptivity. *Computer Methods in Applied Mechanics and Engineering*, 84(3):275–326, 1990.

[162] S. Yu, S. Zhao, and G. W. Wei. Local spectral time splitting method for first-and second-order partial differential equations. *Journal of Computational Physics*, 206(2):727–780, 2005.

[163] S. Adjerid and J. E. Flaherty. A moving finite element method with error estimation and refinement for one-dimensional time dependent partial differential equations. *SIAM Journal on Numerical Analysis*, 23(4):778–796, 1986.

[164] R. J. Gelinas, S. K. Doss, and K. h. Miller. The moving finite element method: applications to general partial differential equations with multiple large gradients. *Journal of Computational Physics*, 40(1):202–249, 1981.

[165] B. Engquist and T. Y. Hou. Particle method approximation of oscillatory solutions to hyperbolic differential equations. *SIAM Journal on Numerical Analysis*, 26(2):289–319, 1989.

[166] P. K. Kitanidis. Particle-tracking equations for the solution of the advection-dispersion equation with variable coefficients. *Water Resources Research*, 30(11):3225–3227, 1994.

[167] A. Chertock and D. Levy. Particle methods for dispersive equations. *Journal of Computational Physics*, 171(2):708–730, 2001.

[168] A. LaBryer, P. J. Attar, and P. Vedula. An optimal prediction method for underresolved time-marching and time-spectral. *International Journal for Multiscale Computational Engineering*, 11(2), 2013.

[169] A. LaBryer, P. J. Attar, and P. Vedula. Optimal spatiotemporal reduced order modeling, part i: proposed framework. *Computational Mechanics*, 52(2):417–431, 2013.

[170] A. LaBryer, P. J. Attar, and P. Vedula. Characterization of subgrid-scale dynamics for a nonlinear beam. *Computers & Structures*, 129:13–29, 2013.

[171] A. LaBryer, P. J. Attar, and P. Vedula. Optimal spatiotemporal reduced order modeling of the viscous Burgers equation. *Finite Elements in Analysis and Design*, 79:40–52, 2014.

[172] R. C. Fetecau and T. Y. Hou. A modified particle method for semilinear hyperbolic systems with oscillatory solutions. *Methods and Applications of Analysis*, 11(4):573–604, 2004.

[173] E. G. Puckett. Convergence of a random particle method to solutions of the kolmogorov equation. *Mathematics of Computation*, 52(186):615–645, 1989.

[174] P. Bernard, D. Talay, and L. Tubaro. Rate of convergence of a stochastic particle method for the Kolmogorov equation with variable coefficients. *Mathematics of Computation*, 63(208):555–587, 1994.

[175] S. Roberts. Convergence of a random walk method for the burgers equation. *Mathematics of Computation*, 52(186):647–673, 1989.

[176] M. Bossy and D. Talay. A stochastic particle method for some one-dimensional nonlinear pde. *Mathematics and Computers in Simulation*, 38(1):43–50, 1995.

[177] Y. Zhang, M. M. Meerschaert, and B. Baeumer. Particle tracking for time-fractional diffusion. *Physical Review E*, 78(3):036705, 2008.

[178] KE Hyland, S McKee, and MW Reeks. Exact analytic solutions to turbulent particle flow equations. *Physics of Fluids*, 11(5):1249–1261, 1999.

[179] S. Suh. A hybrid approach to particle tracking and eulerian–lagrangian models in the simulation of coastal dispersion. *Environmental Modelling & Software*, 21(2):234–242, 2006.

[180] W. Zhang. Analytical solution of general one-dimensional Fokker-Planck equation. *International Journal of Control*, 49(6):2085–2091, 1989.

[181] M. Grzywiński and A. Służalec. Stochastic convective heat transfer equations in finite differences method. *International Journal of Heat and Mass Transfer*, 43(21):4003–4008, 2000.

[182] M. Kamiński. A generalized version of the perturbation-based stochastic finite difference method for elastic beams. *Journal of Theoretical and Applied Mechanics*, 47(4):957–975, 2009.

[183] M. Kamiński. Stochastic perturbation approach to engineering structure vibrations by the finite difference method. *Journal of Sound and Vibration*, 251(4):651–670, 2002.

[184] C. Wang, Z. Qiu, and D. Wu. Numerical analysis of uncertain temperature field by stochastic finite difference method. *Science China Physics, Mechanics and Astronomy*, 57(4):698–707, 2014.

[185] M. Kamiński. Reaction-diffusion problems with random parameters using the generalized stochastic finite difference method. *Journal of Applied Computer Science*, 19(2):31–45, 2011.

[186] A. V. Wouwer, P. Saucez, and W. E. Schiesser. *Adaptive Method of Lines*. CRC Press, 2001.

APPENDIX A

Derivation of Liouville equation for evolution of conditional density

Similar to the derivation of Li and Chen [2], one can derive the Liouville equation for evolution of conditional probability density function. The equations governing the evolution of the system states read

$$\dot{\mathbf{x}} = H(\mathbf{x}, \boldsymbol{\xi}, t). \tag{A.1}$$

where $\mathbf{x} = (x_1, x_2, ..., x_M)$ is an M-dimensional vector of random variables corresponding to system states and $\boldsymbol{\xi} = (\xi_1, \xi_2, ..., \xi_N)$ is an N-dimensional vector of random variables corresponding to model input parameters. Also, H denotes the vector of drift terms or $(h_1, h_2, ..., h_M)$.

Considering an arbitrary fixed domain A in state space, the variation of conditional probability within the time interval $[t_1, t_2]$ (conditioned on $\boldsymbol{\xi} = Y$; where $Y = (y_1, y_2, ..., y_N)$) in A can be simply written as

$$\begin{aligned} \Delta_A P(\mathbf{x}; Y, [t_1, t_2]) &= \int_A f(\mathbf{x}; Y, t_2) dX - \int_A f(\mathbf{x}; Y, t_1) dX \\ &= \int_A \int_{t_1}^{t_2} \frac{\partial f(\mathbf{x}; Y, t)}{\partial t} dt dX \end{aligned} \tag{A.2}$$

where

$$dX = \prod_{i=1}^{M} d\mathbf{x}_i. \tag{A.3}$$

On the other hand, the conditional probability flux passing over the boundaries of

A (B_A) during the time interval $[t_1, t_2]$ can be obtained as

$$\Delta_{B_A} P(\mathbf{x}; Y, [t_1, t_2]) = -\int_{t_1}^{t_2} \int_{B_A} f(\mathbf{x}; Y, t)(vdt) \cdot nds \tag{A.4}$$

where v represents the velocity (vector) field in state space. This velocity field according to Eq. A.1 is H and n is the unit outward vector that is normal to boundary surface, B_A. Thus,

$$\Delta_{B_A} P(\mathbf{x}; Y, [t_1, t_2]) = -\int_{t_1}^{t_2} \int_{B_A} (f(\mathbf{x}; Y, t) H(\mathbf{x}, \boldsymbol{\xi}, t)) \cdot nds dt \tag{A.5}$$

Using the divergence theorem, one can further simplify Eq. A.5.

$$\begin{aligned} \Delta_{B_A} P(\mathbf{x}; Y, [t_1, t_2]) &= -\int_{t_1}^{t_2} \int_{A} \nabla . \left(f(\mathbf{x}; Y, t) H(\mathbf{x}, \boldsymbol{\xi}, t)\right) dV dt \\ &= -\int_{A} \int_{t_1}^{t_2} \sum_{i=1}^{M} \frac{\partial \left(f(\mathbf{x}; Y, t) h_i(\mathbf{x}, \boldsymbol{\xi}, t)\right)}{\partial \mathbf{x}_i} dt dX \end{aligned} \tag{A.6}$$

where, V is the volume bounded by B_A.

The principle of preservation of probability states that the probability must be conserved within an arbitrary time interval $[t_1, t_2]$ in state space and as a result the conditional probability transiting through the boundary, B_A, is equal to the conditional probability variation within A. Thus, from Eqs. A.6 and A.2 one can deduce

$$\int_{A} \int_{t_1}^{t_2} \frac{\partial f(\mathbf{x}; Y, t)}{\partial t} dt dX = -\int_{A} \int_{t_1}^{t_2} \sum_{i=1}^{M} \frac{\partial \left(f(\mathbf{x}; Y, t) h_i(\mathbf{x}, \boldsymbol{\xi}, t)\right)}{\partial \mathbf{x}_i} dt dX \tag{A.7}$$

which finally simplifies as a Liouville equation

$$\frac{\partial f_{\mathbf{x}|\boldsymbol{\xi}}}{\partial t} = \sum_{i=1}^{M} -\frac{\partial}{\partial x_i} [h_i(\mathbf{x}, \boldsymbol{\xi}, t) f_{\mathbf{x}|\boldsymbol{\xi}}] \quad , \tag{A.8}$$

APPENDIX B

Boundary point arrangement for the AGBR scheme

In the adaptive gradient based refinement (AGBR) scheme, the boundary points are obtained by first determining, through interpolation, the conditional PDF value $\tilde{f}^n_{x|\xi}$ at points η_1 and η_{P-6} and then applying the rule:

$$x^{n+1}_{i-1} = x^{n+1}_i - \left|\frac{x^{n+1}_{i+1} - x^{n+1}_i}{2}\right| \times \max\left[H(\tilde{f}^n_{x|\xi}(\eta_1) - \varepsilon) + H(\tilde{f}^n_{x|\xi}(x_i) - \varepsilon), 1\right]$$
$$i = 2, 3, .., N_1$$
$$x^{n+1}_{i+1} = x^{n+1}_i - \left|\frac{x^{n+1}_i - x^{n+1}_{i-1}}{2}\right| \times \max\left[H(\tilde{f}^n_{x|\xi}(\eta_{P-6}) - \varepsilon) + H(\tilde{f}^n_{x|\xi}(x_i) - \varepsilon), 1\right]$$
$$i = P-1, P-2, .., N_2. \tag{B.1}$$

where $H(x)$ is the Heaviside step function and ε is a designated small value used as a criteria for setting the number of auxiliary grid points in each tail (N_1 and N_2). If both $\tilde{f}^n_{x|\xi}(\eta_{P-6})$ and $\tilde{f}^n_{x|\xi}(\eta_1)$ are smaller or larger than this value, N_1 and N_2 will set to be 4 and $P-3$, respectively to have equally three auxiliary grid points on both tails. Otherwise, 4 points are allocated to the tail in which $\tilde{f}_{x|\xi}$ has a value larger than ε and the rest will be arranged on the other response curve tale. By choosing the location of these points in this way, the grid adaptation depends upon both the PDF tail values and PDF gradients. Moreover, by using this approach, we avoid a non-smooth grid distribution in regions of small PDF gradients which can reduce the accuracy of the finite difference scheme up to one order of magnitude.

APPENDIX C

Defect correction for MacCormack scheme

Truncation error analysis of the MacCormack scheme (Eq. 3.36) using the method of modified equation [60] followed by a heuristic numerical stability analysis [131] gives $D_i\Delta t - \Delta x_{i-\frac{1}{2}} = 0$ as the characteristic equation for the singular perturbations to the modified differential equation. Therefore in order to obtain the expression for non-iterative defect correction (DC), the spatial increments $\Delta x_{i-\frac{1}{2}}$ and $\Delta x_{i+\frac{1}{2}}$ should be considered spatially dependent variables. Using the method of modified equation, the expression for the defect correction (DC) term can be obtained as:

$$
\begin{aligned}
\mathrm{DC} \;=\; & \frac{\Delta t}{2}\left(D_{i+1}-D_i\right)\left(\frac{\partial^2(Df)}{\partial x^2}\right)_i + \Delta t^2\Bigg(f_i\Bigg(\frac{(D_i')^3}{6} + \\
& \frac{1}{4}\left(\frac{dD}{dx}\right)_{i+1}\left(D\frac{d^2D}{dx^2}\right)_i + D_{i+1}\left(\frac{dD}{dx}\frac{d^2D}{dx^2}\right)_i - \frac{1}{12}\left(D\frac{dD}{dx}\frac{d^2D}{dx^2}\right)_i - \\
& \frac{1}{6}\left(D\right)^2_{i+1}\left(\frac{d^3D}{dx^3}\right)_i + \frac{1}{2}D_{i+1}\left(D\frac{d^3D}{dx^3}\right)_i + \frac{1}{3}\left(D^2\frac{d^3D}{dx^3}\right)_i\Bigg) + \\
& \frac{\partial f}{\partial x}\Bigg(\frac{1}{2}\left(\frac{dD}{dx}\right)_{i+1}\left(D\frac{dD}{dx}\right)_i + \frac{3}{2}D_{i+1}\left(\frac{dD}{dx}\right)^2_i - \frac{1}{3}\left(D\left(\frac{dD}{dx}\right)^2\right)_i - \\
& \frac{1}{2}D^2_{i+1}\left(\frac{d^2D}{dx^2}\right)_i + \frac{7}{4}D_{i+1}\left(D\frac{d^2D}{dx^2}\right)_i - \frac{5}{6}\left(D^2\frac{d^2D}{dx^2}\right)_i\Bigg) + \\
& \frac{\partial^2 f}{\partial x^2}\Bigg(\frac{1}{4}D_i^2\left(\frac{dD}{dx}\right)_{i+1} - \frac{1}{2}D^2_{i+1}\left(\frac{dD}{dx}\right)_i + \frac{9}{4}D_{i+1}\left(D\frac{dD}{dx}\right)_i - \\
& \frac{5}{4}\left(D^2\frac{dD}{dx}\right)_i\Bigg) + \frac{\partial^3 f}{\partial x^3}\Bigg(-\frac{1}{6}D_i\left(D\right)^2_{i+1} + \frac{1}{2}D_{i+1}\left(D\right)_i - \\
& \frac{1}{3}D_i^3\Bigg) + \mathcal{O}(\Delta x^3_{i-\frac{1}{2}} + \Delta x^3_{i+\frac{1}{2}} + \Delta t^3). \qquad \text{(C.1)}
\end{aligned}
$$

APPENDIX D

Impact of scaling on the overall accuracy of the numerical solution

For solution of UQ related problems in this dissertation, the numerical solution is re-scaled at each time step. Here, the scaling factor is given by

$$K = \frac{1}{1 + I_1}, \tag{D.1}$$

where I_1 denotes the computed zeroth moment of conditional density and can be obtained as

$$I_1 = \int_{\Re^{\mathbf{M}}} f_{\mathbf{x}|\mathbf{Y}}(\mathbf{x}, \mathbf{Y}, t) d\mathbf{x}. \tag{D.2}$$

Since the exact value of the zeroth moment is always equal to 1 and the quadrature used for performing the numerical integration to compute I_1 is second order accurate, one can write

$$K = \frac{1}{1 + \mathcal{O}(\sum_{i=1}^{M} \Delta x_i^2)}, \tag{D.3}$$

where M is the number of system states. Here, one can reasonably argue that $\mathcal{O}(\sum_{i=1}^{M} \Delta x_i^2)$ can be assumed to be small. Therefore, using the Taylor series to approximate K (Eq. D.1) about $\mathcal{O}(\sum_{i=1}^{M} \Delta x_i^2) = 0$ gives

$$K = 1 - \mathcal{O}(\sum_{i=1}^{M} \Delta x_i^2), \tag{D.4}$$

and

$$\tilde{f}^* = \tilde{f}^n - \mathcal{O}(\sum_{i=1}^{M} \Delta x_i^2) \tilde{f}^n. \tag{D.5}$$

Consequently the re-scaling process should preserve the formal second order accuracy of the numerical solution.

APPENDIX E

Potential application of the proposed framework for stochastic particle tracking method

In this appendix, a proposal for future research is presented based on the framework proposed in this dissertation to develop a novel stochastic particle tracking approach for uncertainty quantification of dynamical systems. The appendix starts with an introduction to particle tracking methods in Section E.1. In the next section, through implementation of a Lagrangian approach in our proposed framework, we develop a novel methodology for uncertainty quantification of dynamical systems. In Section E.3, preliminary results for low-dimensional UQ problems are discussed. Finally, in Section E.4, we propose the implementation of this stochastic particle tracking method for stochastic finite difference solution of PDEs.

E.1 Background on particle tracking method

Particle tracking methods have been developed to avoid the numerical errors produced by grid based numerical solutions. Advection-dominated PDEs are the best candidates for application of these approaches. While the presence of wide range of scales in the solution of PDEs is one of the major difficulties in obtaining their solutions, small scales can be resolved by using relatively small number of particles when a particle tracking method is used. Moreover by an accurate treatment of advection, particle tracking methods do not produce dissipative or dispersive errors. Such advantages has made particle tracking a popular approach for solving different computational problems such as numerical solution of dispersive equa-

tions [167], hyperbolic PDEs [172, 165], Kolmogorov equation [173, 174], Burgers equation [175, 176], advection-dispersion equation [166], time-fractional diffusion equation [177] and Navier-Stokes equations [178].

Random walk particle has been shown to be very computationally beneficial for transport problems. Using this approach, Kitanidis [166] solved dispersion-advection equation. In his paper, a set of moving particles were convected in the field by the flow and Brownian motion. The laws of motion was obtained by integration by part rather than stochastic calculus which is used by Roberts for Burgers equation [175]. In his work, he used fractional steps to solve the one-dimensional Burgers equation. After the particles advected under the influence of the velocity field in the first step, diffusion is simulated by adding an appropriate random perturbation. In his work, the gradient of solution is approximated by finite series of weighted Dirac delta functions. This approach was proved to be an efficient tool for analyzing compressible fluid flow. In a similar approach with a definition of an operational time, Zhang et al. used a Lagrangian framework that can track particles dynamics along with stochastic calculus to solve time-fractional diffusion equation [177]. They showed an enhancement in computational efficiency for both large-scale flow and sharp discontinuities when particle tracking method is used. However, their algorithm outputs the solution on irregular temporal grid which makes the application of an interpolation method necessary.

Suh considered such a drawback which demands large amount of memory and computational time due to its requirement for saving and tracking the history of each particle movements [179]. He only applied this approach in the vicinity of the source point of contamination for the simulation of coastal dispersion. Also, non-smooth solution of these approaches is a major drawback [166]. This problem significantly affects the particle tracking method solution for dynamical systems which display more complex (irregular) dynamics and are exhibiting chaotic states and strange

attractors. A good example of such cases can be found when a dynamical system exhibits limit cycle oscillations (LCO). Under this circumstance commonly used particle tracking approaches are unable to give the full picture of bifurcation and limit cycle oscillation in the solutions.

In this dissertation, we have applied dimensional splitting along with explicit finite difference approaches to solve PDEs. By switching our frame of reference from Eulerian to Lagrangian, application of the same framework in the context of particle tracking method is possible. We believe that splitting the problem into different pieces and using a fractional approach to solve PDEs along with the grid movement control implemented with our proposed framework can enhance the feasibility of particle tracking method for solving PDEs. The Liouville equation solution, which is used to quantify the uncertainties of a dynamical system with parametric randomness, due to its extensive applications is an excellent benchmark test problem for the new methodology which we propose here. The resultant computational savings might pave the way to present a new framework for stochastic finite difference solutions of PDEs.

E.2 Stochastic particle tracking method for uncertainty quantification of dynamical systems with parametric randomness

As mentioned in Chapter 2, the Liouville equation is an advection-reaction equation with variable coefficients. Analytical solutions for this PDE are available only for rare low-dimensional cases and obtaining numerical solutions for the Liouville equations corresponding to dynamical systems with a large number of (random) states using available methods is hardly possible due to their large computational costs. On the other hand when dimension splitting is used (for example Eq. 4.1),

the solution of large multidimensional Liouville equation can be broken into several one-dimensional PDEs with an advection velocity dependent on a random states. Such a measure greatly simplifies the computations in the sense that theoretically the coupling between (random) states can be broken in a very small time span. Moreover, with such an assumption the solution of each of these series of split PDEs can be obtained using characteristic analysis.

In order to demonstrate the concept, consider the general form for each of theses equations as follows:

$$f_t + u\left(\mathbf{x}, \boldsymbol{\xi}\right) f_{x_i} = r\left(\mathbf{x}\right) f \qquad i = 1, 2, ..., M. \tag{E.1}$$

where $\mathbf{x} = (x_1, x_2, ..., x_M)$ is a M-dimension vector of random states and $\boldsymbol{\xi} = (\xi_1, \xi_2, ..., \xi_N)$ is an N-dimensional vector of random parameters of a dynamical system. Similar to our proposed approach in this dissertation, for each sampled parameter ξ_j we can have an initial hyper-rectangular box of particles which is tailored for the joint probability density initial distribution ($f_{\mathbf{x},\boldsymbol{\xi}}(\mathbf{X}; \boldsymbol{\xi}, t = 0)$) by grid adaptation rules discussed in Chapter 4. Choosing Strang splitting technique (Eq. 4.1) as the sequence of consecutive fractional solution for the Liouville equation, the movement of each particle is determined in fractional steps. Based on the notion of particle tracking method the equations obtained from the characteristic analysis of Eq. E.1 describes each particle dynamics within a fractional steps. Hence, the characteristic equation for the lth particle for jth (random) state in qth fractional step of the solution sequence is derived as:

$$\left(\frac{dX_l^j}{d\tau}\right)_q = -u\left(\mathbf{x}, \boldsymbol{\xi}\right). \tag{E.2}$$

Solving Eq. E.2 gives $\left(X_l^j(\tau)\right)_q$. The value of the probability density associated with

lth particle at qth fractional step of nth time-step can be found as:

$$f_l^{n+\frac{q}{s}} = f_l^{n+\frac{q-1}{s}} \left(\exp \left\{ \int_0^{\sigma} r\left(\mathbf{x}\right) d\sigma \right\} \right). \tag{E.3}$$

Setting $\tau = 0$ gives the foot of the characteristic line or $\left(X_l^j(0)\right)_q$ and consequently new locations of the lth particle in response space for the qth fractional step. The final evolution of particle location in probability space and its associated probability density value in time span Δt is determined by repeating this process until the solution reaches the end of the splitting sequence (Eq. 4.1). The solution process is performed independently for any particle and based upon the splitting sequence and the assumption of lack of coupling in a small time span, the solution converges as Δt goes to zero.

As the characteristic solution is highly accurate within a small time-step, one major advantage of this intrusive CUQ approach is removing the solution dependencies in response space as the inaccuracy or accuracy of the solution for one particle has no effect on other particles solutions. Also, there is no need to save the time history of particles movements and solution or re-scaling of the solution. As such, this UQ simulation is "embarrassingly parallelizable" which makes it a powerful alternative for Monte Carlo simulation.

Integration of the resultant solution with different parameters in excitation space, as we proposed in this dissertation, gives statistical quantities of corresponding dynamical system. Initial adaptive "boxing" of particles provides enough samples for obtaining a complete picture of joint probability density evolution even with few particles. Although the probability density values associated with these particles can be determined very accurately independent of their number, integration in response space demands sufficient resolution of particles. Irregular PDF shapes, which can occur due to the presence of strange attractors or lack of smoothness in system

dynamics, makes it much more difficult to use grid based integration schemes. To address this issue, application of a high order accurate coordinate transformation scheme is suggested. Application of such a scheme appears to reduce the required number of particles for an accurate estimation of random variable moments.

Another way of addressing this issue is to use an approach similar to that of the proposed framework for finite difference solution of hyperbolic PDEs. In this case, an adaptive moving grid algorithm (similar to Algorithm 1) can be applied here by replacing truncation error based grid redistribution and finite difference computations with a grid redistribution and solution obtained from the stochastic particle tracking method in a fractional time-step. In a similar manner, in this algorithm grid points are mapped back and froth from uniform to adaptive mesh and vice versa and the integration is performed on a uniform hyper-rectangular mesh. Moreover, application of the monotonicity preserving interpolation used in this dissertation guarantees the monotonicity of the solution. However, in this case the accuracy of the solution in response space is tied to interpolation scheme accuracy.

Choosing either of these two approaches, it is quite reasonable to expect far better computational efficiency compared to adaptive finite difference solutions due to high accuracy of the stochastic particle tracking method as the underlying numerical scheme of both. The major advantage of application of the second approach is the computational simplicity of numerical integration over uniform meshes and its major drawback is the requirement for performing interpolation in each fractional solution step, which limits high performance computing. Both proposed approaches will be investigated for future works. It might be also possible to use the same solution methodology for other PDEs with available one-dimensional analytical solution such as the Fokker-Planck equation [180].

E.3 Preliminary results

In order to demonstrate the computational efficiency of the stochastic particle tracking method in accurate prediction of joint probability density evolution for dynamical systems, we apply this approach without grid redistribution to the two first test problems of Chapter 4 (including Problems 4.1 and 4.2). First, a spring-mass with parametric uncertainty in its stiffness is studied. The Liouville equation for this system as discussed in Chapter 2 (Eq. 2.3) can be written as:

$$\frac{\partial f}{\partial t} + y\frac{\partial f}{\partial x} - k(\xi)x\frac{\partial f}{\partial y} = 0. \tag{E.4}$$

Thus, the unidimensional PDEs to be solved for the time-step Δt are:

$$\begin{aligned} \frac{\partial f}{\partial t} + y\frac{\partial f}{\partial x} &= 0, \\ \frac{\partial f}{\partial t} - k(\xi)x\frac{\partial f}{\partial y} &= 0. \end{aligned} \tag{E.5}$$

This is a divergence-free system and the sequence of the stochastic particle tracking solution proceeds based upon the selected splitting technique. Here we choose to use Strang splitting (Eq. 4.1) which is second order accurate in time. As such, first fractional step for the lth particle becomes:

$$\begin{aligned} x_l^{n+\frac{1}{3}} &= x_l^n + y_l^n\left(\frac{\Delta t}{2}\right), \\ y_l^{n+\frac{1}{3}} &= y_l^n, \\ f_l^{n+\frac{1}{3}} &= f_l^n. \end{aligned} \tag{E.6}$$

The next step gives:

$$\begin{aligned} x_l^{n+\frac{2}{3}} &= x_l^{n+\frac{1}{3}}, \\ y_l^{n+\frac{2}{3}} &= y_l^{n+\frac{2}{3}} - k(\xi) x_l^{n+\frac{1}{3}} \Delta t, \\ f_l^{n+\frac{2}{3}} &= f_l^{n+\frac{1}{3}}. \end{aligned} \tag{E.7}$$

And finally at the end of each temporal increment the solution is completed with the third fractional step.

$$\begin{aligned} x_l^{n+1} &= x_l^{n+\frac{2}{3}} + y_l^{n+\frac{2}{3}} \left(\frac{\Delta t}{2} \right), \\ y_l^{n+1} &= y_l^{n+\frac{2}{3}}, \\ f_l^{n+1} &= f_l^{n+\frac{2}{3}}. \end{aligned} \tag{E.8}$$

This procedure is repeated until the system reaches to a desired time. As shown in Fig. E.1, comparison between the computational time obtained from this approach with computational time of finite difference computations and Monte Carlo simulation indicates a significant enhancement. In other words, up to seven orders of magnitude in computational time is saved for a given accuracy when the proposed stochastic particle tracking approach is used. Comparison of the the stochastic particle tracking results with Monte Carlo simulation results even gives more insight on the outstanding accuracy of this approach. Such an impressive accuracy is due to the implementation of fractional analytical solution of the Liouville equation.

Another interesting fact about the stochastic particle tracking method is the dependency of its accuracy on temporal grid alone. As shown in Fig. E.2, the only contributing factor to overall error of the computations is splitting error. Here, slope of 2 of the error line in a logarithmic graph (Fig. E.2) exhibits the expected second order of accuracy of Strang splitting method independent of number of particles.

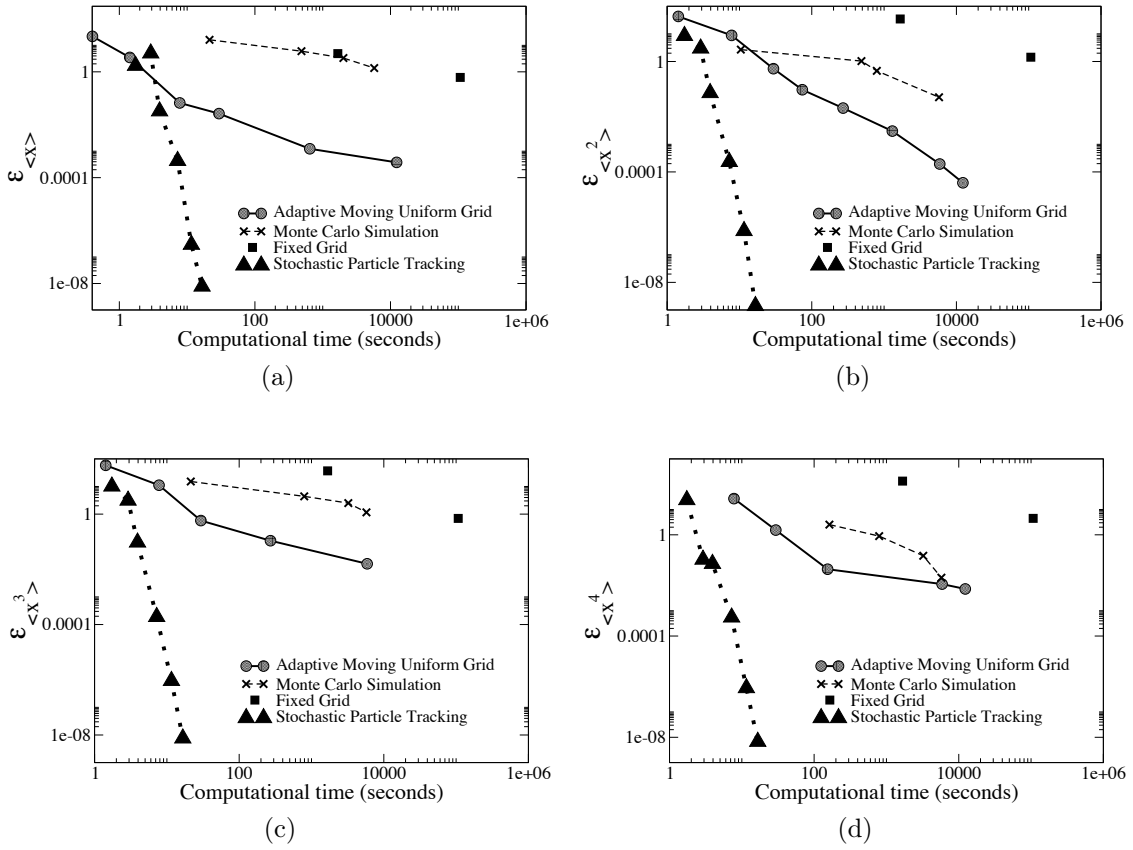

Figure E.1: Percent error ($\varepsilon_{\langle x_1^n \rangle}$), for $t = 40$, in the first four moments of mass displacement (x_1) versus the computational time for Problem 4.1, with a unimodal initial distribution. Comparison is made between Monte Carlo simulation results, finite difference solutions on fixed and adaptive grids and the stochastic particle tracking method with $N_P = 10$. In the computation of errors, the analytical solution is considered to be the reference solution.

Based on availability of analytical solutions for one-dimensional ODEs representing the fractional movement of particles within a time-step, this approach appears to be effective for any dynamical system including the systems which suffer from lack of smoothness in their dynamics. One good example of such systems is the Van der Pol oscillator, which we studied using the proposed finite difference scheme in Problem 4.2. This system can undergo limit cycle oscillations (LCO). From Eqs. 4.18, the corresponding Liouville equation for a Van der Pol oscillator is derived as:

$$\frac{\partial f}{\partial t} + y\frac{\partial f}{\partial x} + \frac{\partial \left(C(\xi)y\left(1-x^2\right)-x\right)f}{\partial y} = 0. \tag{E.9}$$

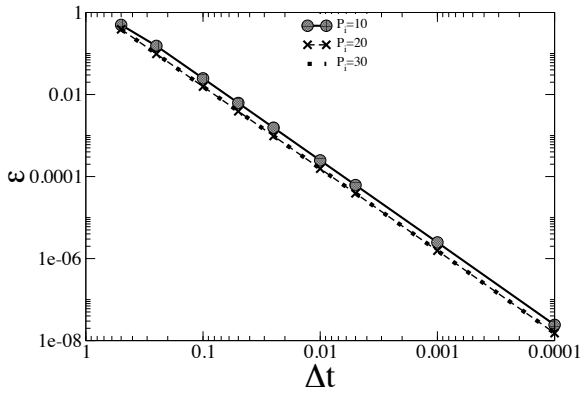

Figure E.2: Error in the computed conditional density for Problem 4.1, with a unimodal initial distribution, with 10×10, 20×20 and 30×30 particles for each excitation parameter (ξ)versus temporal increment, Δt; $N_p = 10$. In the computation of error, the analytical solution is considered to be the reference solution.

Based on operator splitting, the solution of the Eq. E.9 can be obtained as a combination of solutions of two one-dimensional PDEs in the time span Δt.

$$\begin{aligned} \frac{\partial f}{\partial t} + y\frac{\partial f}{\partial x} &= 0, \\ \frac{\partial f}{\partial t} + \frac{\partial \left(C(\xi) y \left(1 - x^2\right) - x\right) f}{\partial y} &= 0. \end{aligned} \tag{E.10}$$

Hence, particle tracking algorithm applied to Strang splitting sequence gives the particles dynamics in the following steps:

$$\begin{aligned} x_l^{n+\frac{1}{3}} &= x_l^n + y_l^n \left(\frac{\Delta t}{2}\right), \\ y_l^{n+\frac{1}{3}} &= y_l^n, \\ f_l^{n+\frac{1}{3}} &= f_l^n, \end{aligned} \tag{E.11}$$

$$x_l^{n+\frac{2}{3}} = x_l^{n+\frac{1}{3}},$$

$$y_l^{n+\frac{2}{3}} = \frac{\left(x_l^{n+\frac{1}{3}} + C(\xi) y_l^{n+\frac{2}{3}} \left(1 - \left(x_l^{n+\frac{1}{3}}\right)^2\right) - x_l^{n+\frac{1}{3}}\right) e^{C(\xi)\left(1-\left(x_l^{n+\frac{1}{3}}\right)^2\right)\Delta t}}{C(\xi)\left(1 - \left(x_l^{n+\frac{1}{3}}\right)^2\right)}, \quad x_l^{n+\frac{1}{3}} \neq 1,$$

$$y_l^{n+\frac{2}{3}} = y_l^{n+\frac{1}{3}} - x_l^{n+\frac{1}{3}} \Delta t, \quad x_l^{n+\frac{1}{3}} = 1,$$

$$f_l^{n+\frac{2}{3}} = f_l^{n+\frac{1}{3}} \exp\left\{-C(\xi)\left(1 - \left(x_l^{n+\frac{1}{3}}\right)^2\right)\Delta t\right\}, \tag{E.12}$$

$$\begin{aligned} x_l^{n+1} &= x_l^{n+\frac{2}{3}} + y_l^{n+\frac{2}{3}} \left(\frac{\Delta t}{2}\right), \\ y_l^{n+1} &= y_l^{n+\frac{2}{3}}, \\ f_l^{n+1} &= f_l^{n+\frac{2}{3}}, \end{aligned} \tag{E.13}$$

While an accurate representation of JPDF can be obtained with very few particles, 10125 particles are required for an accurate estimation of statistical quantities for this complex system. The irregular shape of JPDF as shown in Fig. E.3 demands the application of highly accurate grid transformation scheme for the numerical integration of data. In order to obtain these results an 8th order accurate finite difference compact estimate of derivatives derived by Lele [26] is used. As shown in Fig E.4, using this accurate transformation the computed results for the fourth moment of the oscillator displacement (x) agrees well with Monte Carlo simulation data.

As shown in Fig. E.5, if we use similar initial distribution as the one used for spring-mass system ($C(\xi) \in [0.4, 0.6]$), a clear map of LCO can be observed in the solution obtained from the stochastic particle tracking methods at $t = 40$. This very complex geometry of JPDF, makes multidimensional numerical integration very difficult. We have used 72000 particles in order to obtain the moments of random

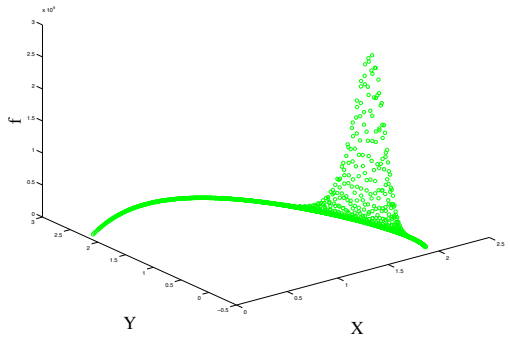

Figure E.3: Joint probability density function for Van der Pol oscillator with uniformly distributed damping coefficient between 0 and 1 ($C(\xi) \in [0, 1]$; Problem 4.2) at $t = 20$, solution is obtained with 10125 particles; $\xi = 0.90618$

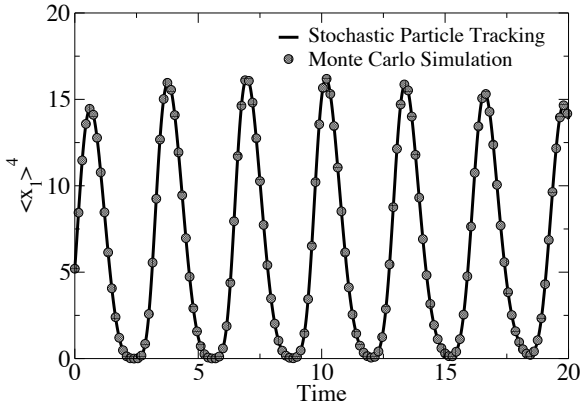

Figure E.4: Evolution of the displacement fourth moment $\langle x_1 \rangle^4$ in a Van der Pol oscillator (Problem 4.2) computed using the stochastic particle tracking method and a Monte Carlo simulation with 7.5×10^5 realizations.

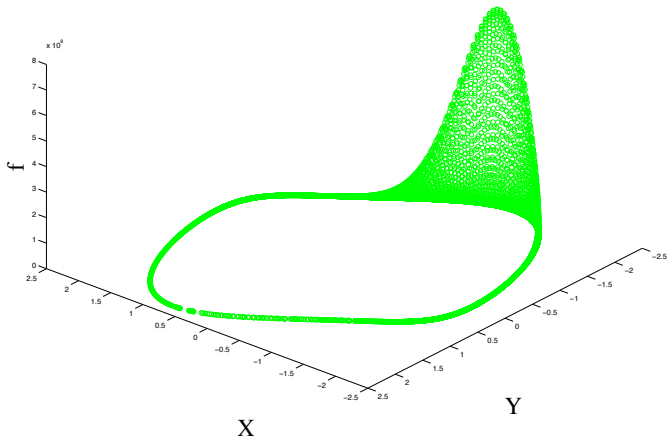

Figure E.5: Joint probability density function for Van der Pol oscillator with uniformly distributed damping coefficient between 0.4 and 0.6 ($C(\xi) \in [0.4, 0.6]$) at $t = 40$, solution is obtained with 72000 particles; $\xi = 0.90618$

variables correctly in this case. The evolution of the mean displacement of a Van der Pol oscillator is illustrated in Fig. E.6. This figure confirms the periodic behavior of the system due to limit cycle oscillations.

In closing, it appears that application of our proposed framework with an alternate adaptive grid distribution to the proposed stochastic tracking method may reduce the required number of particles for obtaining system statistics as numerical integration is performed on a uniform hyper-rectangular mesh. Further studies on the computational benefits of using the stochastic particle tracking method will be conducted in future to more thoroughly investigate this proposed approach.

E.4 Stochastic particle tracking finite difference method

Finite difference schemes are some of most common tools to solve PDEs due to their simplicity of implementation. For a dynamical system with parametric uncertainties, statistical evolution of the state variables is governed by the Liouville equation and can be obtained using computational uncertainty quantification (CUQ) approaches.

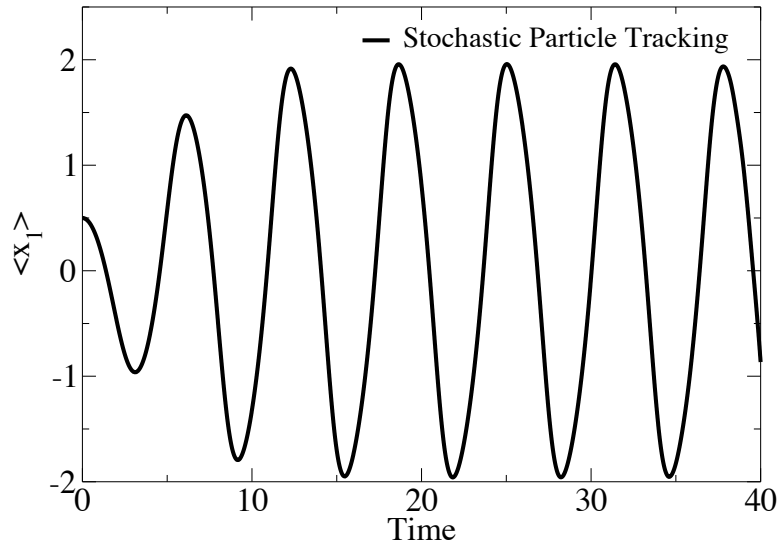

Figure E.6: Evolution of the displacement mean $\langle x_1 \rangle$ in a Van der Pol oscillator with $C(\xi) \in [0.4, 0.6]$ computed using the stochastic particle tracking method

One possible approach is performing finite difference discretization and applying an intrusive UQ approach to modify the discretized equations for an accurate estimation of the systems statistics. In this context, Grzywiński and Służalec used a finite series of basis functions to obtain random function of uncertain parameters which then were expanded about the mean using Taylor series up to the second order term [181]. Plugging in the resultant expression, a system of equations for estimating temperature mean and variance based upon the convection heat transfer equation was derived.

For other approaches applied in the area of stochastic finite difference methods, stochastic perturbation technique is used to derive the equations for statistical analysis of dynamical systems. Such approaches were used for uncertainty quantification of beams [182, 183], plates [183], heat conduction [184] and reaction-diffusion problems [185]. On the other hand, the application of these methods are usually limited to Gaussian form of parametric uncertainty distribution. These approaches are applicable mostly for finite difference based solution of linear PDEs. Although these approaches may be appropriate for estimation of low-order statistical mo-

ments, computational cost of obtaining high order moments grows exponentially. Furthermore, these stochastic numerical solutions usually are hardly computationally parallelizable.

In order to address some of the abovementioned issues, a UQ method based upon a combination of excitation space sampling and particle tracking solution of the Liouville equation is proposed for future research. It is well known that by applying the method of lines to PDEs and using finite difference approximations of spatial derivatives, a system of first order ODEs is derived [186]. As mentioned in Chapter 2, this system can then be integrated into one large multidimensional PDE known as the Liouville equations. Here, the number of random states is equal to the number of unknowns.

One-dimensional advection equation is a good example for the purpose of demonstrating the proposed approach for future work. This PDE can be written as:

$$\frac{\partial u}{\partial t} + C\frac{\partial u}{\partial x} = 0. \tag{E.14}$$

Using the method of lines along with applying central differencing for the spatial derivative, we have:

$$\frac{\partial u}{\partial t} = C\frac{u_{i-1} - u_{i+1}}{2\Delta x}, \qquad i = 2, 3, ..., M-1, \tag{E.15}$$

where M is number of finite difference one-dimensional grid points. Thus assuming Dirichlet boundary condition on both ends, the corresponding Liouville equation can be derived as Eq. E.16.

$$\frac{\partial f}{\partial t} + C\sum_{i=2}^{M-1}\frac{\partial}{\partial u_i}\left(\left(\frac{u_{i-1} - u_{i+1}}{2\Delta x}\right)f\right) = 0. \tag{E.16}$$

Applying particle tracking along with a dimension splitting technique, this equation

can be solved for any number of grid points, M.

Depending on the particle redistribution method, different high performance computing strategies can be considered to accelerate the speed of computations. For instance, if the pure stochastic particle tracking, which was discussed in Section E.3, is used the computations lend themselves nicely to parallelization in an MPI environment. However, application of domain decomposition algorithms appears necessary for performing the numerical integration to obtain the systems statistics from the resultant solution.

This approach can be applied to finite difference discretization on both regular and irregular grids. Moreover, in the context of CUQ, random parameters of PDEs can be associated with any type of probability density distribution such as uniform, normal, log-normal and etc. Finally, this approach appears to be numerically stable as the solutions of ODEs representing the stochastic dynamics of a system exist for any type of drift functions. As the first step to verify these claims, we will apply this approach to one-dimensional advection and heat conduction equations with parametric uncertainties in our future research.

Nomenclature

Roman letters

CFL	CFL number
D	Drift function
$\tilde{\mathbf{F}}^n$	Vector of interpolated solution at nth time-step
$\tilde{f}^*$	Scaled value of the conditional density
$\tilde{f}_i^n$	Elements of interpolated solution vector at nth time-step
f	Response or conditional probability density
$f_{\mathbf{x},\boldsymbol{\xi}}(\mathbf{X};\boldsymbol{\xi},t)$	joint probability density function (JPDF)
f_{e}	Fully resolved solution
f_ξ	Probability distribution of random parameter ξ
$\boldsymbol{G}(x)$	Indicator function
$\mathbf{h}$	M-dimensional vector of drift function
h_i	Elements of $\mathbf{h}$
I_1	Computed zeroth moment
L_i	Domain length
$L_{\Delta t}^{(x_{i,j})}$	Numerical scheme which solves the Liouville equation in the x_i direction over time-step Δt

$M^{(n)}$ Computed value of the nth moment

$m^{(n)}$ Reference value of the nth moment

M_i Number of grid points, for the ith dimension on the adaptive mesh

$M_x^{(n)}(t)$ nth moment of the (random) output variable x

N_p Number of Gauss-quadrature points

δ_t the upper bound for Δt^n in the constrained minimization process

P Number of grid points

P_i Number of grid points in ith direction

S Reaction function

$S_\Gamma(t)$ Boundary of the time-varying mesh partition

Δt^n the nth time-step

$\mathcal{T}_A$ Adaptive mesh

$\mathcal{T}_F$ uniform grid

TE Expression for non-iterative defect correction

T Desired time

t time

TR Truncation error expression

w_{j_k} quadrature weights

$< x_i^n >$ The nth raw moment of the random variable x_i

Δx_1 The spatial interval to the left of the grid point i

Δx_2 The spatial interval to the right of the grid point i

$\Delta x_{i+\frac{1}{2}}$ The spatial interval to the right of the grid point i

$\Delta x_{i-\frac{1}{2}}$ The spatial interval to the left of the grid point i

$\mathbf{x}$ M-dimensional vector of random states

TE Expression for non-iterative defect correction

x_i Random variables or grid point

$x_{i,l}(t^n)$ Lower bound of the hyper-rectangular domain

$x_{i,u}(t^n)$ Upper bound of the hyper-rectangular domain

Y_{j_k} quadrature abscissas

Greek letters

δ Forward difference

δ_- Backward difference

$\epsilon(t)$ the normalized L2 error

ϵ_L Local error

ε normalized L2 error

ε_c Contraction indices

ε_g Growth indices

$\varepsilon_M^{(n)}$ Statistical moment error

$\varepsilon_{\langle x_1^n \rangle}$ Percent error in $\langle x_1^n \rangle$

Γ grading or objective function for irregular perturbation

$\Gamma(t)$ Time-varying mesh partition

$< \mu >$ Joint Probability distribution mean

μ Gaussian distribution mean

$\mu(\xi)$ Coefficient of a dynamical system with parametric uncertainty

μ_i Mean of initial Gaussian distribution in ith dimension

$\eta(x)$ Mesh grading function

$\psi^n_{j+\frac{1}{2}}$ Flux limiter at nth time-step

μ_x Mean of initial Gaussian distribution in x direction

μ_y Mean of initial Gaussian distribution in y direction

σ Gaussian distribution standard deviation; CFL number

σ_i Standard deviation of initial Gaussian distribution in ith dimension

σ_x Standard deviation of initial Gaussian distribution in x direction

σ_y Standard deviation of initial Gaussian distribution in y direction

$\theta^n_{i+\frac{1}{2}}$ Monotonicity indicator

$\boldsymbol{\xi}$ N-dimensional vector of random parameters

ξ Random parameter